

## THE UCSD HIRES/KECK I DAMPED Ly $\alpha$ ABUNDANCE DATABASE. I. THE DATA

JASON X. PROCHASKA,<sup>1,2</sup> ARTHUR M. WOLFE,<sup>1,3</sup> DAVID TYTLER,<sup>1,3</sup> SCOTT BURLES,<sup>1,4</sup> JEFF COOKE,<sup>1,3</sup> ERIC GAWISER,<sup>1,3</sup>  
DAVID KIRKMAN,<sup>1,3</sup> JOHN M. O'MEARA,<sup>1,3</sup> AND LISA STORRIE-LOMBARDI<sup>1,5</sup>

Received 2001 April 27; accepted 2001 June 14

### ABSTRACT

We present new chemical abundance measurements of 16 damped Ly $\alpha$  systems at  $z > 1.5$  and update our previous abundance analyses. The entire database presented here was derived from HIRES observations on the Keck I telescope, reduced with the same software package, and analyzed with identical techniques. Altogether, we present a large, homogeneous database of chemical abundance measurements for protogalaxies in the early universe, ideal for studying a number of important aspects of galaxy formation. In addition, we have established an on-line directory for this database and will continuously update the results.

*Subject headings:* galaxies: abundances — galaxies: evolution —  
nuclear reactions, nucleosynthesis, abundances — quasars: absorption lines

*On-line material:* color figures, machine-readable table

### 1. INTRODUCTION

Since their discovery nearly 20 years ago (Wolfe et al. 1986), the damped Ly $\alpha$  (DLA) systems have provided an extraordinary means for probing the properties of high-redshift galaxies. For example, Wolfe and his collaborators have lead a number of observing programs to trace the universal neutral baryonic content, a study made possible by the fact that the DLA systems are the dominant neutral gas reservoirs at every epoch (e.g., Wolfe et al. 1995; Lanzetta, Wolfe, & Turnshek 1995; Storrie-Lombardi, Irwin, & McMahon 1996; Storrie-Lombardi & Wolfe 2000). Through accurate metallicity measurements, DLA studies also provide an examination of the chemical enrichment history of the universe (Pettini et al. 1994, 1997; Prochaska & Wolfe 2000; Prochaska, Gawiser, & Wolfe 2001, hereafter PGW01). In addition, the advent of high-resolution echelle spectrographs on 10 m class telescopes has enabled researchers to trace the relative chemical abundances of these systems, measurements that provide direct insight into processes of nucleosynthesis and dust depletion in the early universe (Lu et al. 1996, hereafter L96; Prochaska & Wolfe 1999, hereafter PW99; Pettini et al. 2000).

In this paper we build on previous observations of the chemical abundances of DLA systems. In particular, we introduce new measurements of over 15 DLA systems and revise the measurements of our previously analyzed systems (PW99). The principle goal of this paper is to provide the community with a uniform, homogeneous database of  $z > 1.5$  DLA abundances. To this end, we have created a

Web site<sup>6</sup> where we will continuously update our observations and possibly include measurements from throughout the community. Our new observations include spectra with wavelength coverage extending blueward of Ly $\alpha$  where elements like Ar, P, S, N, and O can be examined. In the second paper in this series (Prochaska & Wolfe 2001, hereafter Paper II), we address the implications of the complete data set on chemical evolution, dust depletion, dust obscuration, and nucleosynthesis. In several companion papers, we address the N/O abundance of the DLA systems, examine the kinematic characteristics of the full sample (J. X. Prochaska & A. M. Wolfe 2001, in preparation), infer the star formation rate of the DLA systems (Wolfe, Prochaska, & Gawiser 2001), and investigate the observational evidence for photoionization in these systems.

### 2. OBSERVATIONS AND ANALYSIS

All of the observations presented in this paper were acquired with the High Resolution Echelle Spectrometer (HIRES; Vogt et al. 1994) on the Keck I 10 m telescope. The HIRES spectrograph is mounted at the Nasmyth focus of Keck I and is equipped with an image rotator, two collimators (red and blue sensitive), and a Tektronix 2048  $\times$  2048 CCD. For each observation, we implemented either a 1".1 or a 0".8 slit, which provides a resolution of FWHM  $\approx$  8.4 and 6.3 km s<sup>-1</sup>, respectively. The HIRES spectrograph affords  $\approx$  2500 Å of wavelength coverage per setting with continuous coverage below  $\lambda \approx$  5100 Å. Table 1 summarizes all of the new observations; refer to PW99 for previous observations.

All of the data were reduced with the MAKEE package as tailored for HIRES observations by T. Barlow.<sup>7</sup> This package flat-fields the exposures, optimally extracts the spectra from the two-dimensional images traced by a standard star or pinhole image, removes cosmic rays, and wavelength calibrates the spectra by cross-correlating each object's Th-Ar calibrations with a large database of calibrated HIRES data. We then continuum fitted each spectrum with an in-house routine similar to the IRAF task

<sup>1</sup> Visiting Astronomer, W. M. Keck Telescope. The Keck Observatory is a joint facility of the University of California and the California Institute of Technology.

<sup>2</sup> The Observatories of the Carnegie Institute of Washington, 813 Santa Barbara Street, Pasadena, CA 91101.

<sup>3</sup> Department of Physics and Center for Astrophysics and Space Sciences, University of California, San Diego, C-0424, La Jolla, CA 92093-0424.

<sup>4</sup> Experimental Astrophysics Department, Fermi National Accelerator Laboratory, MS 127, P.O. Box 500, 500 Wilson Road, Batavia, IL 60637-1433.

<sup>5</sup> SIRTF Science Center, California Institute of Technology, MS 100-22, Pasadena, CA 91125.

<sup>6</sup> <http://kingpin.ucsd.edu/~hiresdla>.

<sup>7</sup> <http://spider.ipac.caltech.edu/staff/tab/makee>.

TABLE 1  
JOURNAL OF NEW OBSERVATIONS

QSO	$z_{\text{em}}$	Wavelength (Å)	Date	Exposure (s)	Resolution (km s <sup>-1</sup> )	S/N (pixel <sup>-1</sup> )
J0255+00 .....	4.02	5100–8160	F99, F00	20200	6.3	15
Q0336–01 .....	3.22	3940–6390	F99	5400	8.2	10
Q0347–38 .....	3.23	3600–5900	F98	4500	8.2	6
HS 0741+4741 .....	3.20	3600–5900	F98, S00	10800	8.2	25
		5050–7470	F00	5400	6.3	30
BRI 0951–04 .....	4.37	5720–8150	F99	7200	8.2	10
BRI 0952–0115 .....	4.43	5700–8150	S99	28800	8.2	15
PSS 0957+33 .....	4.25	6440–8760	F00	7200	6.3	15
BRI 1108–0747 .....	3.92	5950–8340	F98, F99	12600	8.2	20
Q1210+17 .....	2.54	3760–6170	S00	7200	8.2	20
Q1223+17 .....	2.92	4780–7160	S98	19600	8.2	30
		3560–5900	S98	5000	8.2	7
BRI 1346–0322 .....	3.99	4280–6600	S00	7200	8.2	4
PSS 1443+27 .....	4.41	6070–8500	S99	25200	8.2	20
		6790–9180	S00	11000	8.2	15
Q1759+75 .....	3.05	3500–5800	S00	22200	8.2	30
Q1946+7658 .....	2.99	3470–5055	F98	47970	8.2	50
Q2344+12 .....	4.30	3400–4985	F98	4000	8.2	12
Q2348–01 .....	3.01	5060–7480	F99, F00	16200	8.2	15

CONTINUUM. For quasars with multiple exposures, the individual spectra were co-added (weighting by signal-to-noise ratio [S/N] and rejecting bad pixels) to produce a single one-dimensional spectrum with 2 km s<sup>-1</sup> pixels.

### 3. IONIC COLUMN DENSITIES

In this section we present ionic column density measurements for all of the new systems as well as a number of transitions excluded in PW99. All of the ionic column densities were derived with the apparent optical depth method (AODM; Savage & Sembach 1991). This technique corrects for hidden saturation by comparing the apparent column density,  $N_a$ , for multiple transitions from a single ion. This technique also gives an efficient means of calculating total column densities for each ion. The analysis involves calculating  $N_a(v)$  for each pixel from the optical depth equation

$$N_a(v) = \frac{m_e c \tau_a(v)}{\pi e^2 f \lambda}, \quad (1)$$

where  $\tau_a(v) = \ln [I_i(v)/I_a(v)]$ ,  $f$  is the oscillator strength,  $\lambda$  is the rest wavelength (see Table 2), and  $I_i$  and  $I_a$  are the incident and measured intensities. By summing over the velocity profile of a given transition, one calculates the total column density,

$$N_T = \sum N_a(v) \Delta v, \quad (2)$$

and a 1  $\sigma$  error on the column density through standard error propagation

$$\sigma^2(N_T) = \sum \left( \frac{m_e c}{\pi e^2 f \lambda} \right)^2 \frac{\sigma^2[I_a(v)]}{I_a^2(v)} \Delta v^2. \quad (3)$$

In previous papers (Wolfe et al. 1994; Prochaska & Wolfe 1996, 1997), we showed that the DLA profiles are not contaminated by hidden saturation. Furthermore, we demonstrated that the total column densities derived with the AODM agree very well with line profile fitting, which should give a more accurate measure of the ionic column densities when hidden saturation is negligible. As the

AODM is easier to apply to a large data set, we have chosen to use this technique to measure the ionic column densities for the DLA sample.

Tables 3–40 present the results of the abundance measurements including an estimate of the 1  $\sigma$  error. For those transitions where the profile saturates, i.e.,  $I_a/I_i < 0.05$  in at least 1 pixel, the column densities are listed as lower limits. The values reported as upper limits are 3  $\sigma$  limits except in the cases in which we set an upper limit due to significant line blending. We have ignored continuum error in our analysis that may dominate the measurements of very weak transitions, especially those blueward of Ly $\alpha$  emission. We estimate a systematic error of  $\approx 10\%$  in most cases. The 3  $\sigma$  statistical limits are conservative, however, and are likely to account for the continuum error in all but the noisiest and/or crowded absorption regions. In the following subsections we comment briefly on each DLA system, plot the metal line profiles, and tabulate column densities for each profile. We adopt ionic column densities from these measurements by calculating the weighted mean. In the velocity plots,  $v = 0$  is chosen arbitrarily and corresponds to the redshift listed in the figure caption. We indicate regions of blending, primarily through blends with other metal line systems or the Ly $\alpha$  forest, by plotting with dotted lines. For those systems previously analyzed in PW99, we report only upon the changes made since publication. For completeness, when we include the measurement of a new transition (e.g., Ni II  $\lambda 1317$ ), we report other measurements of the same ion and the new adopted ionic column density.

Throughout the paper we adopt the wavelengths and oscillator strengths presented in Table 2. When possible, we have adopted laboratory values for the oscillator strengths. Since PW99 there have been several new measurements of  $f$ -values that impact the abundances of the DLA systems, including new Ni II and Ti II oscillator strengths, which have significantly revised the abundances of these elements. Most importantly, however, is the adoption of new oscillator strengths for the majority of Fe II transitions and in particular the Fe II  $\lambda\lambda 1608, 1611$  transitions. In this paper we adopt  $f(1608) = 0.0580$  from the laboratory measurement of Ber-

TABLE 2  
ATOMIC DATA

Transition	$\lambda$	$f$	Reference
H I-19 $\lambda$ 914	914.0390	0.00019700	1
H I-18 $\lambda$ 914	914.2860	0.00023000	1
H I-17 $\lambda$ 914	914.5760	0.00027000	1
H I-16 $\lambda$ 914	914.9190	0.00032100	1
H I-15 $\lambda$ 915	915.3290	0.00038600	1
N II $\lambda$ 915	915.6120	0.14490000	1
H I-14 $\lambda$ 915	915.8240	0.00046900	1
H I-13 $\lambda$ 916	916.4290	0.00057700	1
P III $\lambda$ 917	917.1180	0.40490000	1
H I-12 $\lambda$ 917	917.1806	0.00072260	1
H I-11 $\lambda$ 918	918.1294	0.00092100	1
H I-10 $\lambda$ 919	919.3514	0.00120000	1
H I-9 $\lambda$ 920	920.9631	0.00160500	1
O I $\lambda$ 921	921.8600	0.00117300	2
O I $\lambda$ 922	922.2000	0.00242000	2
H I-8 $\lambda$ 923	923.1504	0.00221600	1
O I $\lambda$ 924	924.9520	0.00153400	2
O I $\lambda$ 925	925.4420	0.00350000	2
H I-7 $\lambda$ 926	926.2257	0.00318300	1
O I $\lambda$ 929	929.5168	0.00226370	2
O I $\lambda$ 930	930.2566	0.00532000	2
H I-6 $\lambda$ 930	930.7483	0.00481400	1
S VI $\lambda$ 933	933.3780	0.44140000	1
O I $\lambda$ 936	936.6295	0.00373500	1
H I-5 $\lambda$ 937	937.8035	0.00779900	1
S VI $\lambda$ 944	944.5230	0.21810000	1
O I $\lambda$ 948	948.6855	0.00644600	1
H I-4 $\lambda$ 949	949.7431	0.01394000	1
O I $\lambda$ 950	950.8846	0.00157100	1
P II $\lambda$ 963	963.8010	1.45800000	1
N I $\lambda$ 963	963.9903	0.01837000	1
N I $\lambda$ 964	964.6256	0.01180000	1
N I $\lambda$ 965	965.0413	0.00580100	1
O I $\lambda$ 971	971.7380	0.01480000	1
H I-G $\lambda$ 972	972.5368	0.02900000	1
O I $\lambda$ 976	976.4481	0.00330000	1
C III $\lambda$ 977	977.0200	0.76200000	1
O I $\lambda$ 988a	988.5778	0.00051460	1
O I $\lambda$ 988b	988.6549	0.00771200	1
O I $\lambda$ 988	988.7734	0.04318000	1
N III $\lambda$ 989	989.7990	0.10660000	1
Si II $\lambda$ 989	989.8731	0.13300000	1
S III $\lambda$ 1012	1012.5020	0.03550000	1
Si II $\lambda$ 1020	1020.6989	0.02828000	1
H I-B $\lambda$ 1025	1025.7223	0.07912000	1
O I $\lambda$ 1025	1025.7620	0.02030000	1
O VI $\lambda$ 1031	1031.9261	0.13290000	1
C II $\lambda$ 1036	1036.3367	0.12310000	1
O VI $\lambda$ 1037	1037.6167	0.06609000	1
O I $\lambda$ 1039	1039.2304	0.00919700	1
Ar I $\lambda$ 1048	1048.2199	0.24410000	1
Fe II $\lambda$ 1055	1055.2617	0.00751400	3
Fe II $\lambda$ 1062	1062.1520	0.00380000	1
S IV $\lambda$ 1062	1062.6620	0.03999000	1
Fe II $\lambda$ 1063	1063.1760	0.06000000	1
Fe II $\lambda$ 1064	1063.9718	0.00371800	3
Ar I $\lambda$ 1066	1066.6600	0.06652000	1
Fe II $\lambda$ 1081	1081.8748	0.01400000	1
N II $\lambda$ 1083	1083.9900	0.10310000	1
Fe II $\lambda$ 1096	1096.8769	0.03240000	3
Fe II $\lambda$ 1106	1106.3596	0.00150000	1
Fe II $\lambda$ 1112	1112.0480	0.00629000	3
P V $\lambda$ 1117	1117.9770	0.47320000	1
Fe II $\lambda$ 1121	1121.9748	0.02020000	3
Fe III $\lambda$ 1122	1122.5260	0.16200000	4
Fe II $\lambda$ 1125	1125.4478	0.01600000	3

TABLE 2—Continued

Transition	$\lambda$	$f$	Reference
P V $\lambda$ 1128	1128.0080	0.23450000	1
Fe II $\lambda$ 1133	1133.6650	0.00550000	3
N I $\lambda$ 1134	1134.1653	0.01342000	1
N I $\lambda$ 1134	1134.4149	0.02683000	1
N I $\lambda$ 1134	1134.9803	0.04023000	1
C I $\lambda$ 1139	1139.7930	0.01410000	1
Fe II $\lambda$ 1142	1142.3656	0.00420000	3
Fe II $\lambda$ 1143	1143.2260	0.01770000	3
Fe II $\lambda$ 1144	1144.9379	0.10600000	3
P II $\lambda$ 1152	1152.8180	0.23600000	1
C I $\lambda$ 1157	1157.1857	0.02440000	1
S III $\lambda$ 1190	1190.2080	0.02217000	1
Si II $\lambda$ 1190	1190.4158	0.25020000	1
Si II $\lambda$ 1193	1193.2897	0.49910000	1
Mn II $\lambda$ 1197	1197.1840	0.15660000	1
Mn II $\lambda$ 1199	1199.3910	0.10590000	1
N I $\lambda$ 1199	1199.5496	0.13280000	1
N I $\lambda$ 1200	1200.2233	0.08849000	1
N I $\lambda$ 1200	1200.7098	0.04423000	1
Si III $\lambda$ 1206	1206.5000	1.66000000	1
H I-A $\lambda$ 1215	1215.6701	0.41640000	1
N V $\lambda$ 1238	1238.8210	0.15700000	1
N V $\lambda$ 1242	1242.8040	0.07823000	1
S II $\lambda$ 1250	1250.5840	0.00545300	1
S II $\lambda$ 1253	1253.8110	0.01088000	1
S II $\lambda$ 1259	1259.5190	0.01624000	1
Si II $\lambda$ 1260	1260.4221	1.00700000	1
Fe II $\lambda$ 1260	1260.5330	0.02500000	1
C I $\lambda$ 1277	1277.2450	0.09665000	1
P II $\lambda$ 1301	1301.8740	0.01730000	1
O I $\lambda$ 1302	1302.1685	0.04887000	1
Si II $\lambda$ 1304	1304.3702	0.09400000	5
Ni II $\lambda$ 1317	1317.2170	0.07786000	6
C I $\lambda$ 1328	1328.8333	0.05804000	1
C I $\lambda$ 1334	1334.5323	0.12780000	1
C II* $\lambda$ 1335	1335.7077	0.11490000	1
O I $\lambda$ 1355	1355.5977	0.00000124	1
Ni II $\lambda$ 1370	1370.1310	0.07690000	6
Si IV $\lambda$ 1393	1393.7550	0.52800000	1
Si IV $\lambda$ 1402	1402.7700	0.26200000	1
Ga II $\lambda$ 1414	1414.4020	1.80000000	2
Ni II $\lambda$ 1454	1454.8420	0.03230000	7
Co II $\lambda$ 1466	1466.2120	0.03100000	8
Ni II $\lambda$ 1467	1467.2590	0.00990000	7
Ni II $\lambda$ 1467	1467.7560	0.00630000	7
Si II $\lambda$ 1526	1526.7066	0.12700000	9
C IV $\lambda$ 1548	1548.1950	0.19080000	1
C IV $\lambda$ 1550	1550.7700	0.09522000	1
C I $\lambda$ 1560	1560.3092	0.08041000	1
C I* $\lambda$ 1560	1560.6822	0.06030000	1
Co II $\lambda$ 1574	1574.5503	0.02500000	8
Ge II $\lambda$ 1602	1602.4863	1.35000000	1
Fe II $\lambda$ 1608	1608.4511	0.05800000	10
Fe II $\lambda$ 1611	1611.2005	0.00136000	11
C I $\lambda$ 1656	1656.9283	0.14050000	1
C I* $\lambda$ 1657a	1657.3792	0.03512000	1
C I* $\lambda$ 1657b	1657.9068	0.04681000	1
Al II $\lambda$ 1670	1670.7874	1.88000000	1
Ni II $\lambda$ 1703	1703.4050	0.00600000	7
Ni II $\lambda$ 1709	1709.6000	0.03240000	7
Ni II $\lambda$ 1741	1741.5490	0.04270000	7
Ni II $\lambda$ 1751	1751.9100	0.02770000	7
Si II $\lambda$ 1808	1808.0126	0.00218000	12
Si I $\lambda$ 1845	1845.5200	0.22900000	1
Al III $\lambda$ 1854	1854.7164	0.53900000	1
Al III $\lambda$ 1862	1862.7895	0.26800000	1

TABLE 2—Continued

Transition	$\lambda$	$f$	Reference
Fe II $\lambda$ 1901 .....	1901.7730	0.00010090	1
Ti II $\lambda$ 1910a .....	1910.6000	0.20200000	13
Ti II $\lambda$ 1910b .....	1910.9700	0.09800000	13
Co II $\lambda$ 1941 .....	1941.2852	0.03400000	8
Co II $\lambda$ 2012 .....	2012.1664	0.03679000	8
Zn II $\lambda$ 2026 .....	2026.1360	0.48900000	14
Cr II $\lambda$ 2026 .....	2026.2690	0.00471000	2
Mg I $\lambda$ 2026 .....	2026.4768	0.11200000	1
Cr II $\lambda$ 2056 .....	2056.2539	0.10500000	14
Cr II $\lambda$ 2062 .....	2062.2340	0.07800000	14
Zn II $\lambda$ 2062 .....	2062.6640	0.25600000	14
Cr II $\lambda$ 2066 .....	2066.1610	0.05150000	14
Fe II $\lambda$ 2249 .....	2249.8768	0.00182100	15
Fe II $\lambda$ 2260 .....	2260.7805	0.00244000	15
Fe II $\lambda$ 2344 .....	2344.2140	0.11400000	4
Fe II $\lambda$ 2374 .....	2374.4612	0.03130000	4
Fe II $\lambda$ 2382 .....	2382.7650	0.32000000	4
Mn II $\lambda$ 2576 .....	2576.8770	0.35080000	1
Fe II $\lambda$ 2586 .....	2586.6500	0.06910000	4
Mn II $\lambda$ 2594 .....	2594.4990	0.27100000	1
Fe II $\lambda$ 2600 .....	2600.1729	0.23900000	4
Mn II $\lambda$ 2606 .....	2606.4620	0.19270000	1
Mg II $\lambda$ 2796 .....	2796.3520	0.61230000	16
Mg II $\lambda$ 2803 .....	2803.5310	0.30540000	16
Mg I $\lambda$ 2852 .....	2852.9642	1.81000000	1
Ti II $\lambda$ 3073 .....	3073.8770	0.10910000	1
Ti II $\lambda$ 3230 .....	3230.1310	0.05860000	1
Ti II $\lambda$ 3242 .....	3242.9290	0.18320000	1
Ti II $\lambda$ 3384 .....	3384.7400	0.34000000	1

NOTE.—Table 2 is also available in machine-readable form in the electronic edition of the *Astrophysical Journal Supplement*.

REFERENCES.—(1) Morton 1991. (2) Verner, Barthel, & Tytler 1994. (3) Howk et al. 2000. (4) D. C. Morton 2001, in preparation. (5) Tripp, Lu, & Savage 1996. (6) Fedchak & Lawler 1999. (7) Fedchak, Wiese, & Lawler 2000. (8) Mullman et al. 1998. (9) Schectman, Povolny, & Curtis 1998. (10) Bergeson et al. 1996. (11) Raassen & Uylings 1998. (12) Bergeson & Lawler 1993a. (13) Wiese, Fedchak, & Lawler 2001. (14) Bergeson & Lawler 1993b. (15) Bergeson, Mullman, & Lawler 1994. (16) Verner 1996.

geson et al. (1996) and  $f(1611) = 0.00136$  from Raassen & Uylings (1998). In general, these values revise the abundance of  $\text{Fe}^+$  downward by  $\approx 0.1$  dex. Finally, we adopt solar meteoritic abundances from Grevesse, Noels, & Sauval (1996).

To assess the accuracy of our measurements and the reliability of the error analysis, one can compare the column density measurements from two transitions for the same ion with very accurately known relative oscillator strengths. The majority of our DLA systems exhibit absorption from the high-ion  $\text{C}^{3+}$  (Wolfe & Prochaska 2000), which exhibits a pair of resonance absorption lines at  $\lambda \approx 1550 \text{ \AA}$  as a result of the spin-orbit coupling of the  $2p$  electronic level. Because the physics of spin-orbit coupling is well understood, we have high confidence that the relative oscillator strengths of the  $\lambda\lambda 1548, 1550$  transitions have a ratio of 2:1. Figure 1 plots the  $N(1550)$  value versus  $N(1548)$  for all of the DLA systems where the transitions are unsaturated and unblended. One notes that the agreement in the values is excellent even out to  $N(\text{C}^{3+}) \approx 14.5$  where saturation could affect the stronger  $\text{C IV } \lambda 1548$  transition. In short, Figure 1 demonstrates that the AODM provides a reasonably accurate measure of the column densities and  $1 \sigma$  errors for our analysis.

We now comment on the individual systems noting revisions from previous works where applicable.

### 3.1. Q0000–26, $z = 3.390$

We presented metal abundances for this system in PW99 but missed the  $\text{Ni II } \lambda 1454$  profile (Fig. 2 and Table 3). Furthermore, we have identified a telluric blend with the  $\text{Ni II } \lambda 1751$  profile, which led to an overestimate of Ni for this system. The  $\text{Ni II } \lambda 1454$  column density is in excellent agreement with the Ni abundance derived by Molaro et al. (2000) and further clouds the nucleosynthetic interpretation of this system (Molaro et al. 2001). Owing to the higher S/N of the UVES spectrum, we now adopt the  $\text{Fe}^+$  column density from Molaro et al. (2000) but revise it downward to

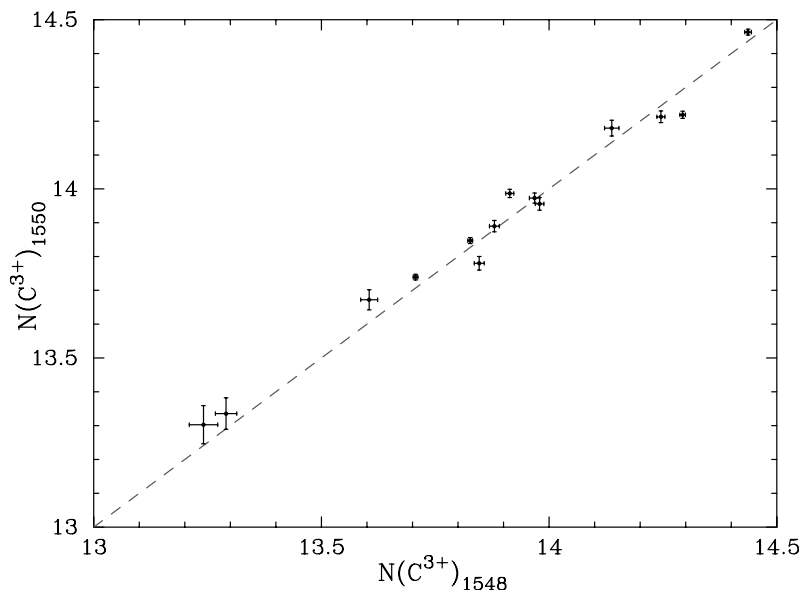


FIG. 1.—Comparison of  $\text{C}^{3+}$  column densities measured independently from  $\text{C IV } \lambda\lambda 1548$  and  $1550$  in the same system using the AODM. The dashed line traces the line of equality. The good agreement between the two values over a large range in  $N(\text{C}^{3+})$  indicates that the AODM is an accurate method for measuring column densities in unblended transitions.

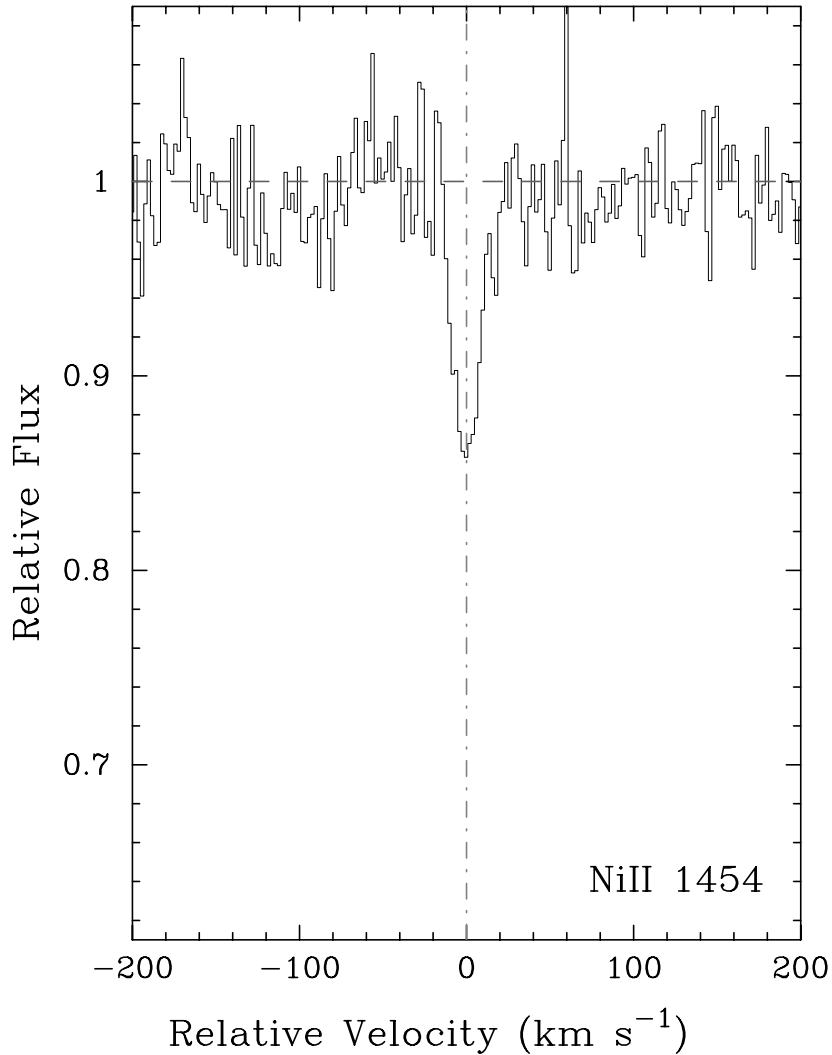


FIG. 2.—Velocity plot of the new metal line transition for the DLA system at  $z = 3.390$  toward Q0000–26. The vertical line at  $v = 0$  corresponds to  $z = 3.3901$ . [See the electronic edition of the Journal for a color version of this figure.]

$N(\text{Fe}^+) = 14.75 \pm 0.03$  as a result of the new Fe II  $\lambda 1611$  oscillator strength. This places the  $\text{Fe}^+$  column density in reasonably good agreement with the  $N(\text{Ni}^+)$  measurement and further supports the notion that the  $\alpha$ -elements (O, Si) are enhanced in this system. We note in passing that the  $N(\text{Fe}^+)$  value derived from our HIRES spectrum of Fe II  $\lambda 1611$  still significantly exceeds the UVES measurement for reasons we do not fully appreciate.

### 3.2. BR 0019–15, $z = 3.439$

This system was analyzed in PW99. Since publication, we have identified the C II\*  $\lambda 1335$  profile (Fig. 3 and Table 4)

and revised the Fe II  $\lambda 1608$  column density to a lower limit because the profile is mildly saturated. This revision accounts for the large Ni/Fe ratio reported in PW99.

### 3.3. PH 957, $z = 2.309$

This system was carefully studied in Wolfe et al. (1994) and subsequently in PW99. We present new limits on  $N(\text{Co}^+)$  and  $N(\text{Ti}^+)$ , the latter of which places a tight constraint on the Ti/Fe ratio ( $[\text{Ti}/\text{Fe}] < -2.04$  dex). We also present a measurement of  $N(\text{Mg}^0)$  from the Mg I  $\lambda 2026$  transition. Figure 4 presents the new profiles as well as several Zn II and Cr II transitions that provide clarification

TABLE 3  
IONIC COLUMN DENSITIES: Q0000–2619,  $z = 3.390$

Ion	$\lambda$	AODM	$N_{\text{adopt}}$	[X/H]
H I .....	1215	$21.410 \pm 0.080$	...	...
Ni II .....	1454	$13.365 \pm 0.045$	$13.365 \pm 0.045$	$-2.295 \pm 0.092$
Ni II .....	1751	$< 13.689$	...	...

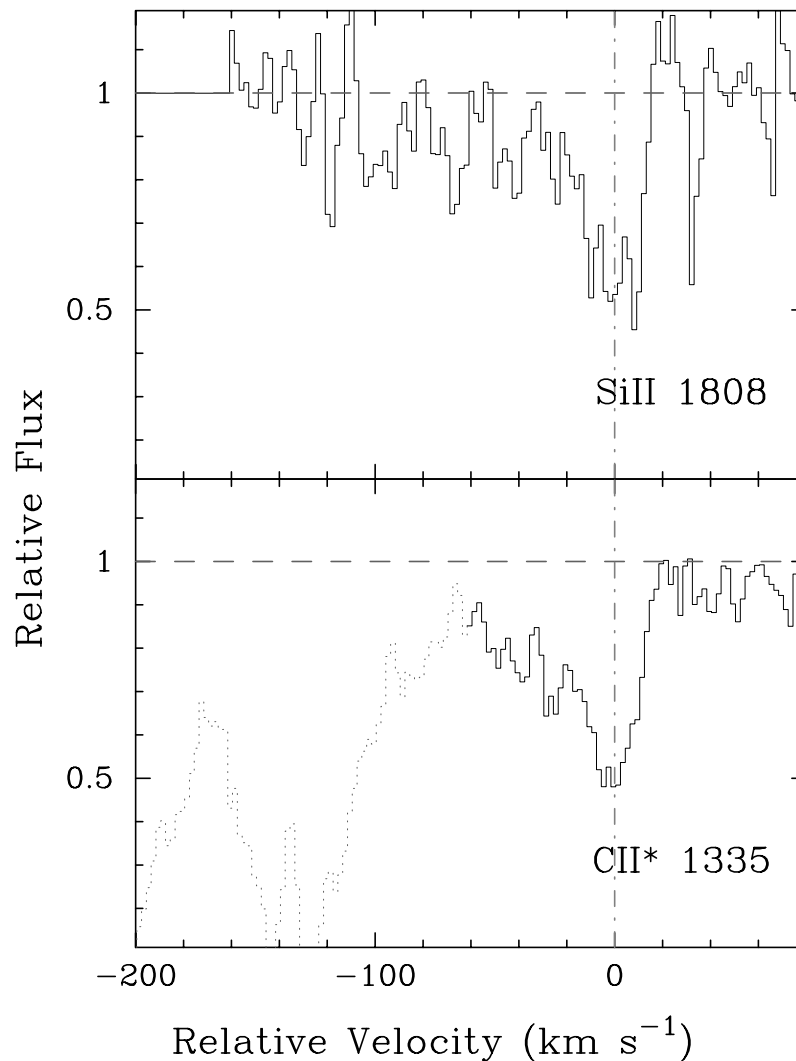


FIG. 3.—Velocity plot of the C II\*  $\lambda 1335$  profile for the DLA system at  $z = 3.439$  toward BR 0019–15. The Si II  $\lambda 1808$  profile is shown for comparison. The vertical line at  $v = 0$  corresponds to  $z = 3.4388$ . [See the electronic edition of the *Journal* for a color version of this figure.]

with respect to the identification of Mg I  $\lambda 2026$ . Table 5 lists the new values.

### 3.4. Q0149+33, $z = 2.140$

We have several changes to report on this system since PW99. Figure 5 and Table 6 present the Ni II  $\lambda 1317$  and Ti II  $\lambda 1910$  profiles that were overlooked in PW99. We have also revised the Si II  $\lambda 1304$  and Si II  $\lambda 1526$  column densities to lower limits and base the Si abundance solely on the unsaturated Si II  $\lambda 1808$  profile. For Cr, we now include the Cr II  $\lambda 2062$  profile in our analysis. Finally, we warn that the

Fe II  $\lambda 1608$  column density might be considered a lower limit for  $N(\text{Fe}^+)$ , which would explain its underabundance relative to Cr and Ni. As noted in PW99, this system exhibits a supersolar Cr/Zn ratio ( $[\text{Cr}/\text{Zn}] = 0.22 \pm 0.1$ ). Because of its low  $[\text{Zn}/\text{H}]$  and  $N(\text{H I})$  values, this system has special significance in terms of dust depletion (Paper II, § 3).

### 3.5. Q0201+36, $z = 2.463$

This system was studied at length in Prochaska & Wolfe (1996), and we now include an upper limit on the Ti II  $\lambda 1910$

TABLE 4  
IONIC COLUMN DENSITIES: BR 0019–15,  $z = 3.439$

Ion	$\lambda$	AODM	$N_{\text{adopt}}$	[X/H]
H I .....	1215	$20.920 \pm 0.100$	...	...
C II .....	1335	$13.838 \pm 0.018$	...	...
Fe II .....	1608	$> 14.789$	$> 14.789$	$> -1.631$
Ni II .....	1709	$13.607 \pm 0.105$	$13.683 \pm 0.040$	$-1.487 \pm 0.108$
Ni II .....	1741	$13.701 \pm 0.043$	...	...

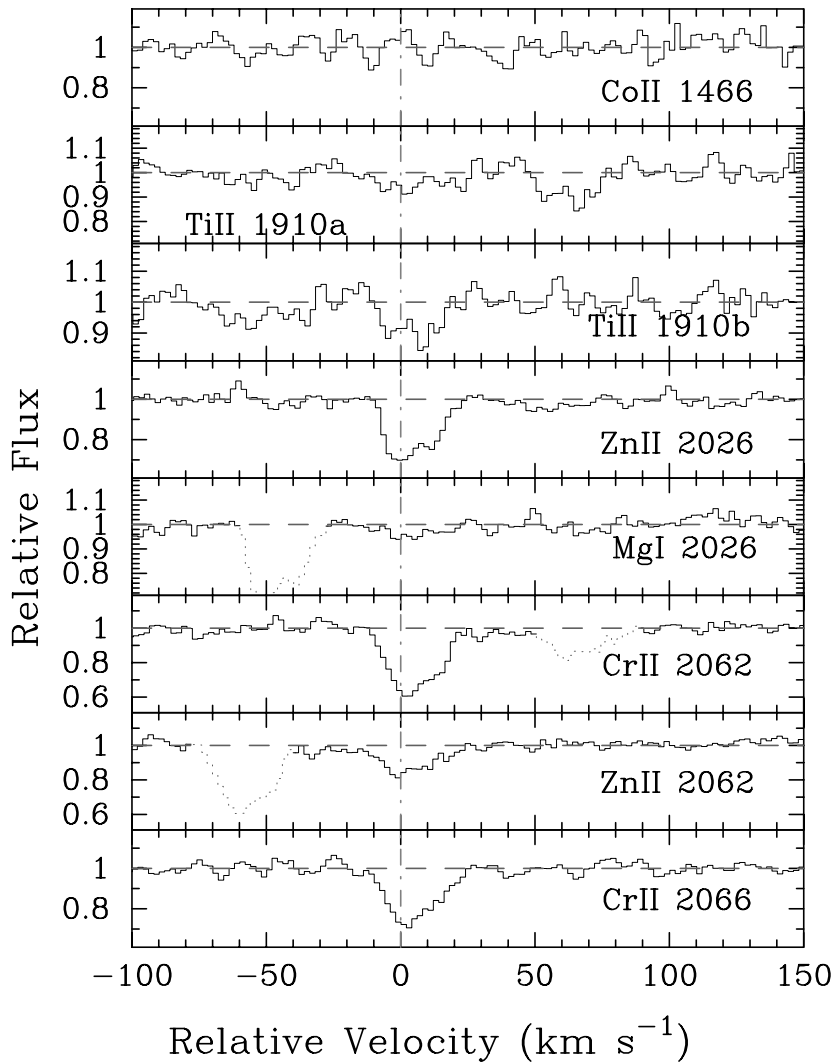


FIG. 4.—Velocity plot of several new metal line transitions for the DLA system at  $z = 2.309$  toward PH 957. The vertical line at  $v = 0$  corresponds to  $z = 2.309$ . [See the electronic edition of the *Journal* for a color version of this figure.]

transition and a measurement for the Ni II  $\lambda 1454$  profile (Fig. 6). To provide the best comparison with other objects in the complete sample, we adopt AODM column densities for all of the transitions (Table 7).

### 3.6. J0255+00, $z = 3.253$ and 3.915

The two DLA systems observed toward this faint Sloan Digital Sky Survey (SDSS) quasar ( $r = 19.1$ ; Fan et al. 1999) were identified as part of a program designed to survey  $z > 3$  DLA systems (A. M. Wolfe et al. 2001, in preparation). We measured the  $N(\text{H I})$  column densities of the two systems with a Low Resolution Imaging Spectrometer (LRIS) spectrum and then acquired HIRES obser-

vations at wavelengths redward of the Ly $\alpha$  forest. Figures 7 and 8 present the metal line profiles for the two systems, and Tables 8 and 9 list the ionic column densities. For the system at  $z = 3.915$ ,  $N(\text{Fe}^+)$  is well constrained by the lower and upper limits from the Fe II  $\lambda 1608$  and Fe II  $\lambda 1611$  transitions, respectively, and we have adopted a column density by averaging the two limits:  $\log N(\text{Fe}^+) = 14.75 \pm 0.08$  dex.

### 3.7. Q0336-01, $z = 3.062$

This Large Bright Quasar Survey (LBQS) quasar is one of the few DLA systems at  $z > 3$  with  $N(\text{H I}) > 10^{21} \text{ cm}^{-2}$ .

TABLE 5  
IONIC COLUMN DENSITIES: PH 957,  $z = 2.309$

Ion	$\lambda$	AODM	$N_{\text{adopt}}$	[X/H]
H I.....	1215	$21.400 \pm 0.050$	...	...
Mg I.....	2026	$12.344 \pm 0.126$	...	...
Ti II.....	1910	$< 12.207$	$< 12.207$	$< -2.133$
Co II.....	1466	$< 13.164$	$< 13.164$	$< -1.146$

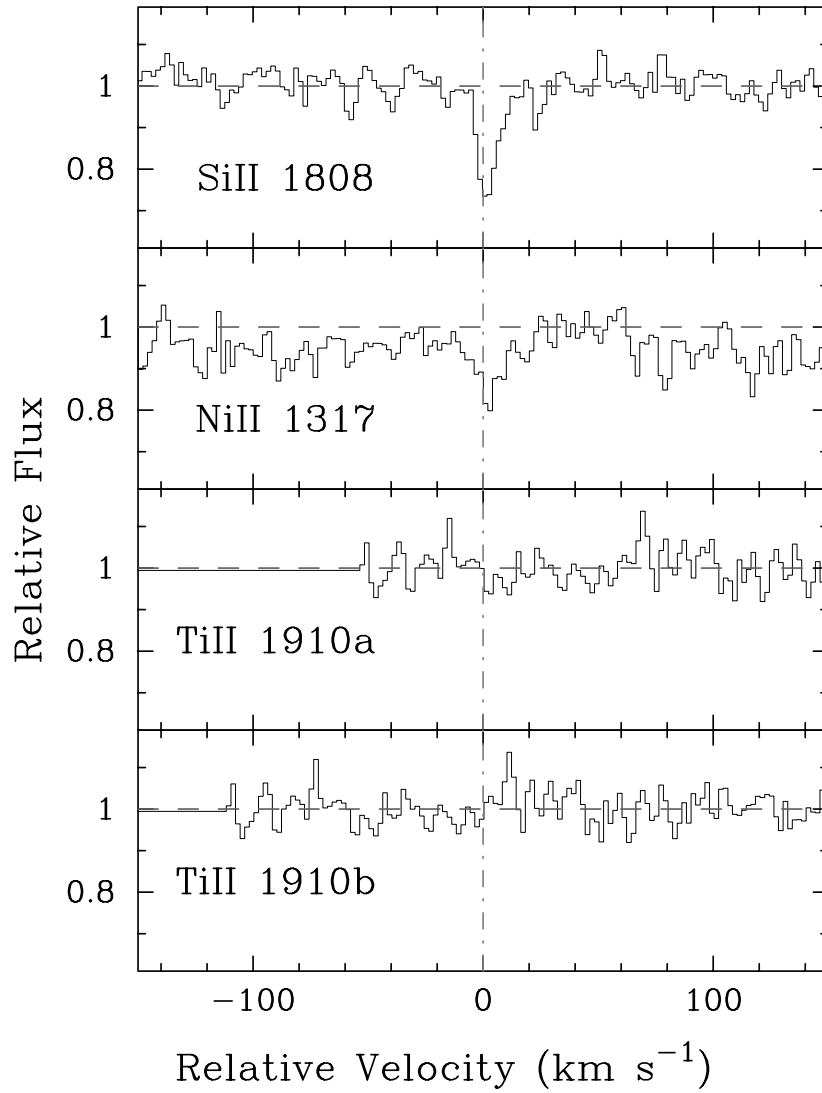


FIG. 5.—Velocity plot of several new metal line transitions for the DLA system at  $z = 2.141$  toward Q0149+33. For comparison, we also plot the Si II  $\lambda 1808$  profile. The vertical line at  $v = 0$  corresponds to  $z = 2.140755$ . [See the electronic edition of the *Journal* for a color version of this figure.]

TABLE 6  
IONIC COLUMN DENSITIES: Q0149+33,  $z = 2.141$

Ion	$\lambda$	AODM	$N_{\text{adopt}}$	[X/H]
H I .....	1215	$20.500 \pm 0.100$	...	...
Si II .....	1304	$> 14.432$	$14.572 \pm 0.047$	$-1.488 \pm 0.110$
Si II .....	1526	$> 14.339$	...	...
Si II .....	1808	$14.572 \pm 0.047$	...	...
Ti II .....	1910	$< 12.169$	$< 12.169$	$< -1.271$
Cr II .....	2056	$12.793 \pm 0.044$	$12.720 \pm 0.035$	$-1.450 \pm 0.106$
Cr II .....	2062	$12.520 \pm 0.090$	...	...
Cr II .....	2066	$12.841 \pm 0.062$	...	...
Ni II .....	1317	$13.092 \pm 0.071$	$13.169 \pm 0.036$	$-1.581 \pm 0.106$
Ni II .....	1370	$13.192 \pm 0.103$	...	...
Ni II .....	1703	$< 13.885$	...	...
Ni II .....	1709	$13.184 \pm 0.088$	...	...
Ni II .....	1741	$13.250 \pm 0.064$	...	...
Ni II .....	1751	$13.179 \pm 0.090$	...	...



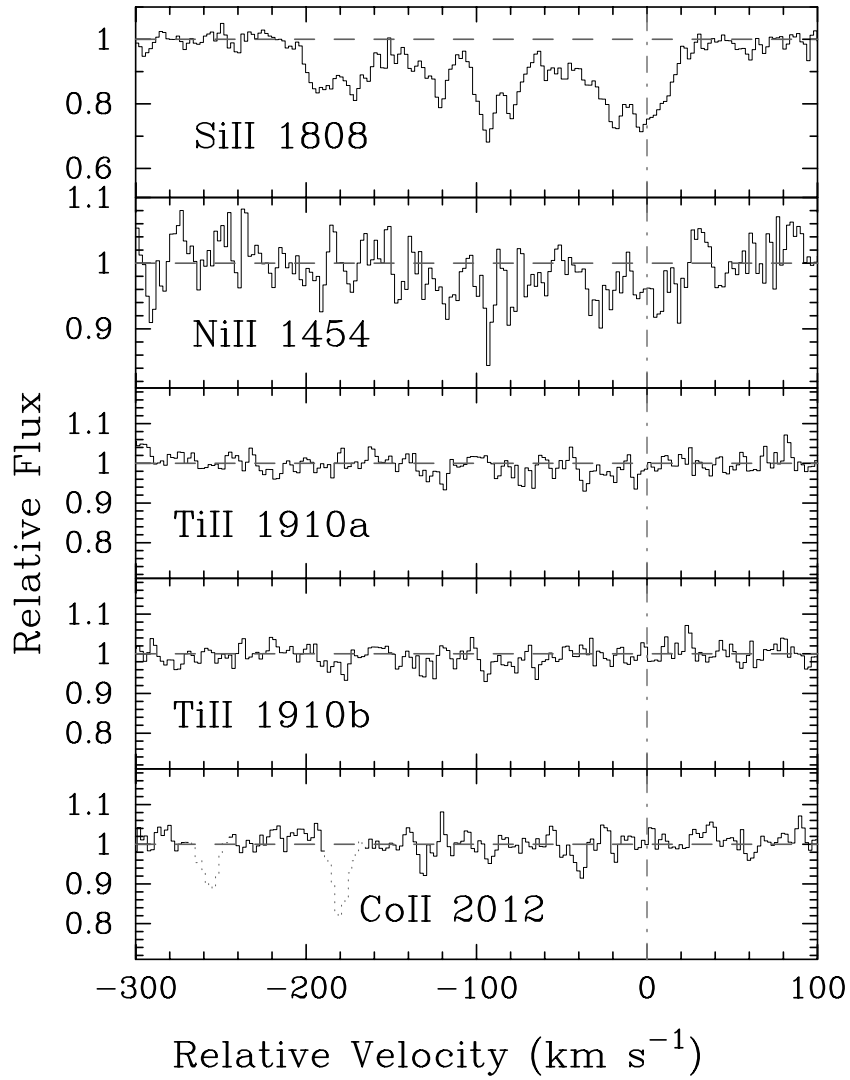


FIG. 6.—Velocity plot of several new metal line transitions for the DLA system at  $z = 2.463$  toward Q0201+36. For comparison, we also plot the Si II  $\lambda 1808$  profile. The vertical line at  $v = 0$  corresponds to  $z = 2.4628$ . [See the electronic edition of the *Journal* for a color version of this figure.]

TABLE 7  
IONIC COLUMN DENSITIES: Q0201+36,  $z = 2.463$

Ion	$\lambda$	AODM	$N_{\text{adopt}}$	[X/H]
H I.....	1215	$20.380 \pm 0.045$	...	...
C IV.....	1550	$14.612 \pm 0.005$	...	...
Al II.....	1670	$> 14.133$	$> 14.133$	$> -0.737$
Al III.....	1862	$13.601 \pm 0.007$	...	...
Si II.....	1808	$15.534 \pm 0.010$	$15.534 \pm 0.010$	$-0.406 \pm 0.046$
Si IV.....	1393	$> 14.071$	...	...
Ti II.....	1910	$< 12.196$	$< 12.196$	$< -1.124$
Cr II.....	2056	$13.266 \pm 0.030$	$13.248 \pm 0.029$	$-0.802 \pm 0.054$
Cr II.....	2066	$13.132 \pm 0.094$	...	...
Fe II.....	1608	$15.010 \pm 0.004$	$15.010 \pm 0.004$	$-0.870 \pm 0.045$
Co II.....	2012	$< 12.957$	$< 12.957$	$< -0.333$
Ni II.....	1454	$13.669 \pm 0.073$	$14.022 \pm 0.010$	$-0.608 \pm 0.046$
Ni II.....	1709	$14.080 \pm 0.021$	...	...
Ni II.....	1741	$14.021 \pm 0.013$	...	...
Ni II.....	1751	$13.984 \pm 0.021$	...	...

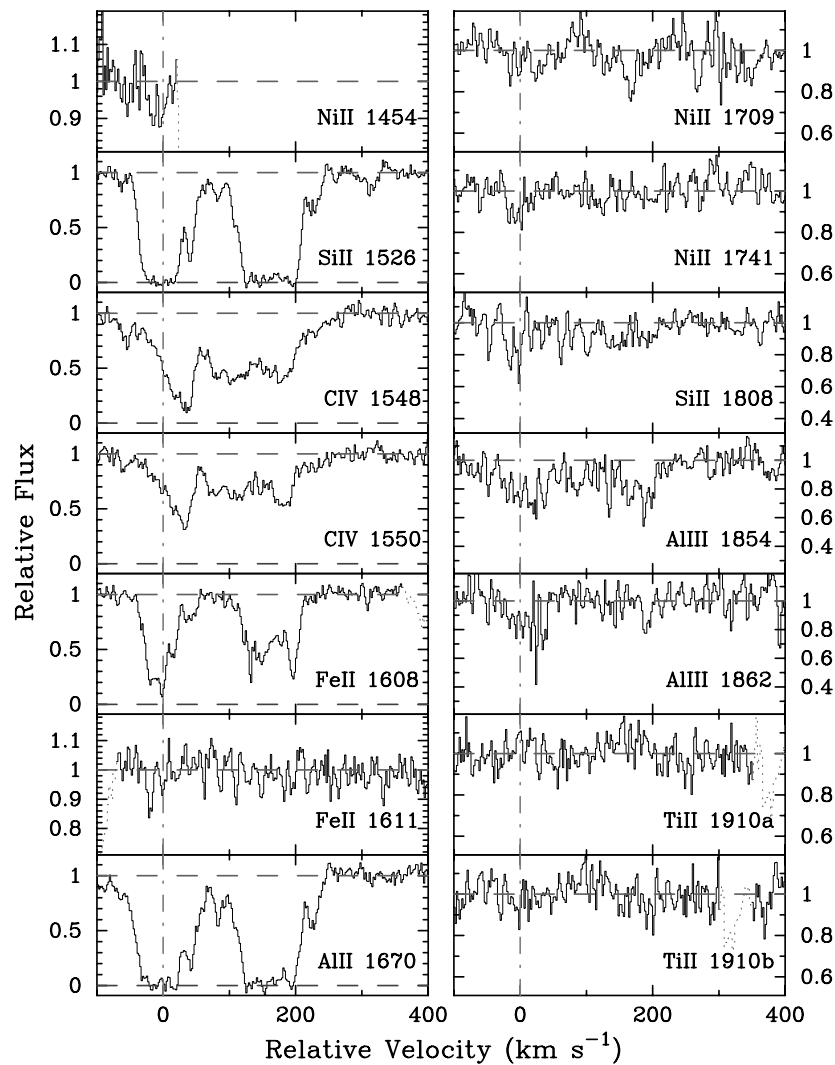


FIG. 7.—Velocity plot of the metal line transitions for the DLA system at  $z = 3.253$  toward J0255+00. The vertical line at  $v = 0$  corresponds to  $z = 3.252931$ . [See the electronic edition of the *Journal* for a color version of this figure.]

Although most of the transitions that we examine lie within the Ly $\alpha$  forest, we have carefully avoided lines that are clearly blended with forest clouds. Unfortunately, we only place a lower limit on  $N(\text{Si}^+)$  although we do report a

reasonably secure value for  $N(\text{S}^+)$ . The system also provides an accurate measurement of Ar I and a reasonable estimate of P II. Finally, we note a very large  $N(\text{O}^0)$  lower limit derived from the saturated O I  $\lambda 988$  transition. This limit

TABLE 8  
IONIC COLUMN DENSITIES: J0255+00,  $z = 3.253$

Ion	$\lambda$	AODM	$N_{\text{adopt}}$	[X/H]
H I .....	1215	$20.700 \pm 0.100$	...	...
C IV .....	1548	$14.437 \pm 0.007$	...	...
C IV .....	1550	$14.463 \pm 0.009$	...	...
Al II .....	1670	$> 13.879$	$> 13.879$	$> -1.311$
Al III .....	1854	$13.277 \pm 0.025$	...	...
Al III .....	1862	$12.977 \pm 0.102$	...	...
Si II .....	1526	$> 15.119$	$15.323 \pm 0.038$	$-0.937 \pm 0.107$
Si II .....	1808	$15.323 \pm 0.038$	...	...
Ti II .....	1910	$< 12.805$	$< 12.805$	$< -0.835$
Fe II .....	1608	$14.764 \pm 0.010$	$14.764 \pm 0.010$	$-1.436 \pm 0.100$
Fe II .....	1611	$< 14.832$	...	...
Ni II .....	1709	$13.771 \pm 0.075$	$13.608 \pm 0.066$	$-1.342 \pm 0.120$
Ni II .....	1741	$13.473 \pm 0.114$	...	...

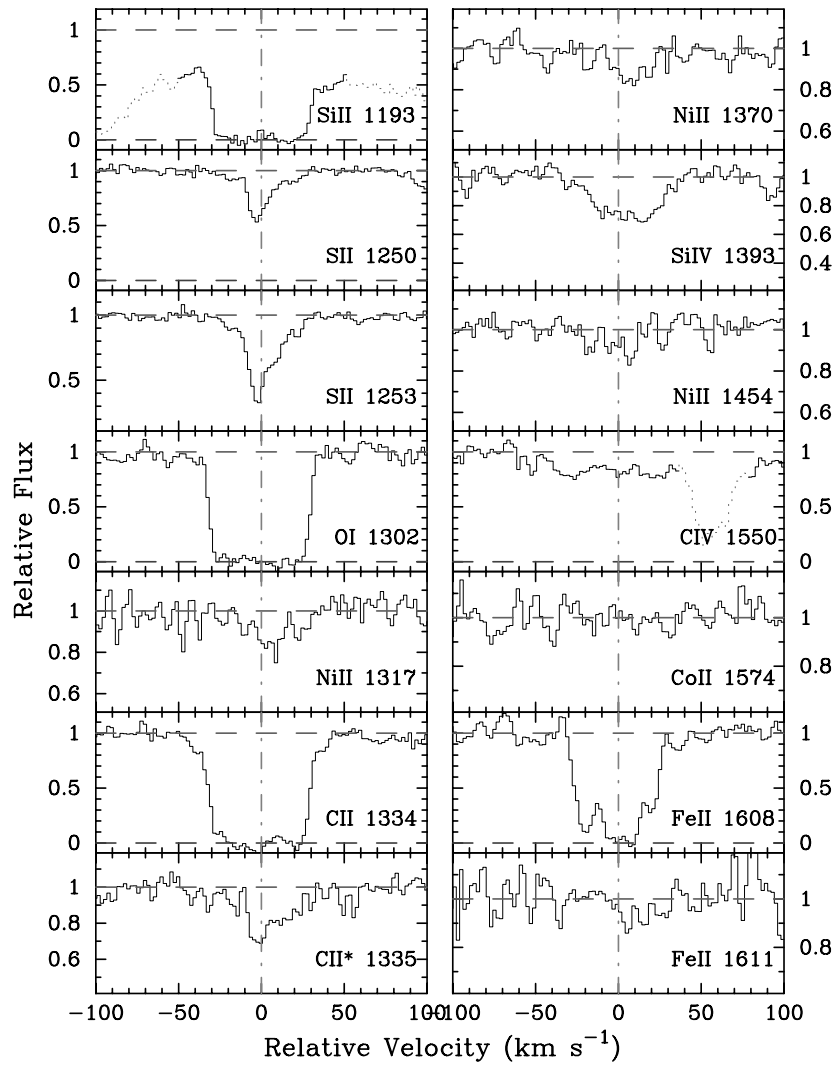


FIG. 8.—Velocity plot of the metal line transitions for the DLA system at  $z = 3.915$  toward J0255+00. The vertical line at  $v = 0$  corresponds to  $z = 3.914617$ . [See the electronic edition of the *Journal* for a color version of this figure.]

may be influenced by blending in the Ly $\alpha$  forest, but we have no reason to believe that this is the case at present (see Fig. 9 and Table 10).

### 3.8. Q0347–38, $z = 3.025$

Although this system was analyzed in PW99, we report a

number of measurements and limits based on the original data and new observations taken with a second, blue setup. Table 11 presents the ionic column densities, and Figure 10 plots the new profiles. We also reclassify the sulfur abundance as an upper limit because this transition is blended with an Ly $\alpha$  forest cloud.

TABLE 9  
IONIC COLUMN DENSITIES: J0255+00,  $z = 3.915$

Ion	$\lambda$	AODM	$N_{\text{adopt}}$	[X/H]
H I.....	1215	$21.300 \pm 0.050$	...	...
C II.....	1334	$> 14.732$	$> 14.732$	$> -3.118$
C II.....	1335	$13.442 \pm 0.040$	...	...
O I.....	1302	$> 15.167$	$> 15.167$	$> -3.003$
Si II.....	1193	$> 14.193$	$> 14.193$	$> -2.667$
Si IV.....	1393	$12.856 \pm 0.028$	...	...
S II.....	1250	$14.763 \pm 0.021$	$14.721 \pm 0.011$	$-1.779 \pm 0.051$
S II.....	1253	$14.707 \pm 0.013$	...	...
Fe II.....	1608	$> 14.707$	$14.750 \pm 0.088$	$-2.050 \pm 0.101$
Fe II.....	1611	$< 14.809$	...	...
Co II.....	1574	$< 13.212$	$< 13.212$	$< -0.998$
Ni II.....	1317	$13.315 \pm 0.052$	$13.271 \pm 0.037$	$-2.279 \pm 0.062$
Ni II.....	1370	$13.213 \pm 0.058$	...	...
Ni II.....	1454	$13.387 \pm 0.104$	...	...

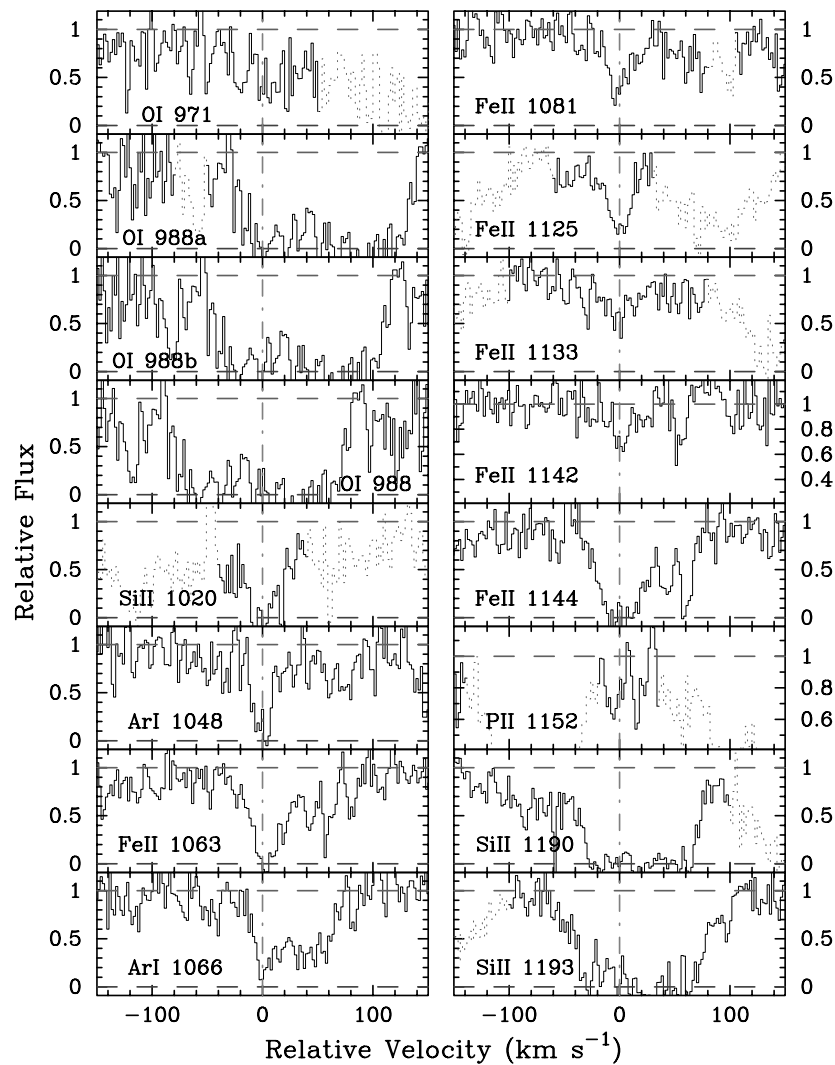


FIG. 9.—Velocity plot of the metal line transitions for the DLA system at  $z = 3.062$  toward Q0336 – 01. The vertical line at  $v = 0$  corresponds to  $z = 3.062078$ . [See the electronic edition of the *Journal* for a color version of this figure.]

### 3.9. Q0458–02, $z = 2.040$

In reviewing this system, we identified a number of transitions missed in PW99. Figure 11 presents the metal line profiles, and Table 12 shows the column densities. Most of these only yield upper limits on ionic column densities, but given the very large H I column density of this system, these

limits are valuable. For example, the limit on Ti II  $\lambda 1910$  implies  $[\text{Ti}/\text{Fe}] < -0.45$  dex, which is highly suggestive of dust depletion. As discussed in Paper II, § 2.1.6, we have revised the measurement of  $N(\text{Zn}^+)$  downward by 0.02 dex because of mild blending between the Zn II  $\lambda 2026$  and Mg I  $\lambda 2026$  profiles.

TABLE 10  
IONIC COLUMN DENSITIES: Q0336–01,  $z = 3.062$

Ion	$\lambda$	AODM	$N_{\text{adopt}}$	$[\text{X}/\text{H}]$
H I .....	1215	$21.200 \pm 0.100$	...	...
C II .....	1334	$> 14.958$	$> 14.958$	$> -2.792$
C II .....	1335	$14.041 \pm 0.025$	...	...
C IV .....	1548	$14.138 \pm 0.016$	...	...
C IV .....	1550	$14.180 \pm 0.023$	...	...
O I .....	988	$> 16.940$	$> 16.940$	$> -1.130$
O I .....	1302	$> 15.389$	...	...
Si II .....	1020	$> 15.141$	$> 15.141$	$> -1.619$
Si II .....	1193	$> 14.322$	...	...
Si II .....	1304	$> 14.926$	...	...
Si IV .....	1393	$13.767 \pm 0.015$	...	...
Si IV .....	1402	$13.656 \pm 0.032$	...	...

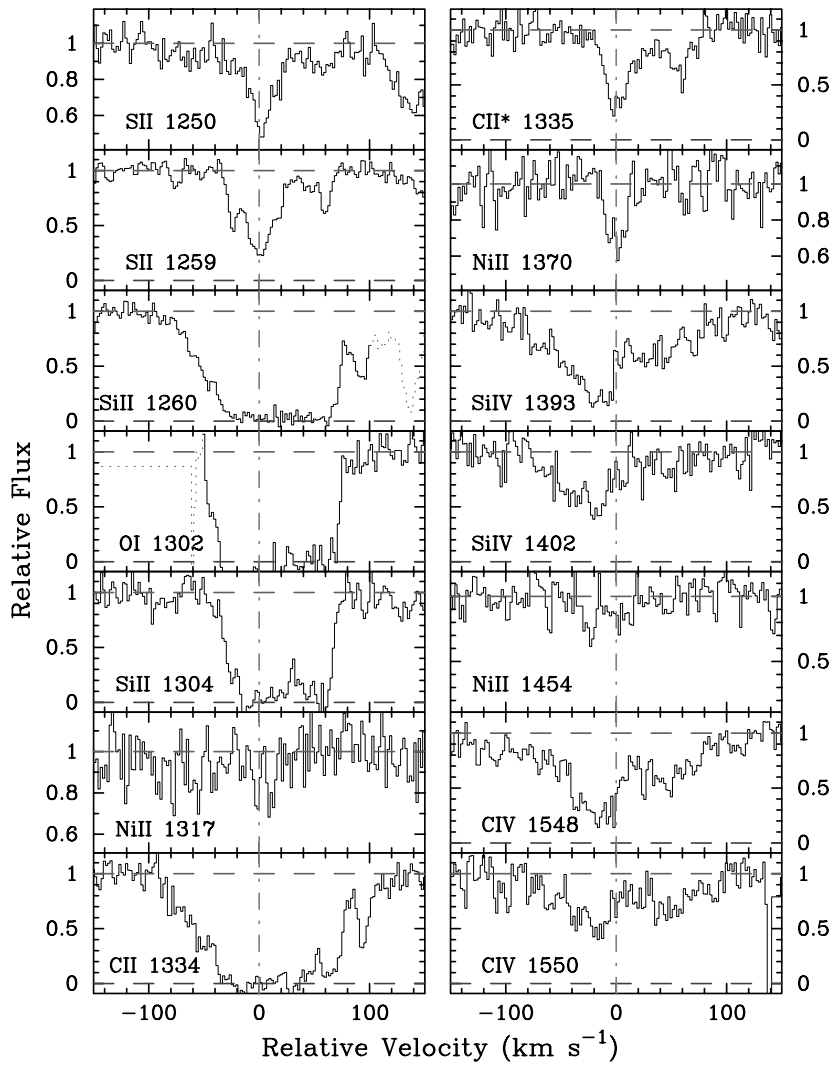


FIG. 9.—Continued

3.10. *HS 0741 + 47*,  $z = 3.017$ 

The very bright QSO *HS 0741 + 47* is taken from the Hamburg ESO QSO survey (Hagen, Engels, & Reimers 1999). Our wavelength coverage of the DLA system spans from 3600 to 7500 Å, and we have identified over 20 metal

line profiles. Figure 12 plots the velocity profiles, and Table 13 presents all of the measurements. Unfortunately, our observations do not include the Zn II and Cr II transitions, although the  $N(\text{Si}^+)$  value indicates that it would require very high S/N to obtain a measurement.

TABLE 10—Continued

Ion	$\lambda$	AODM	$N_{\text{adopt}}$	[X/H]
P II .....	1152	$13.133 \pm 0.075$	$13.133 \pm 0.075$	$-1.597 \pm 0.125$
S II .....	1250	$15.118 \pm 0.022$	$14.994 \pm 0.011$	$-1.406 \pm 0.101$
S II .....	1259	$14.970 \pm 0.012$	...	...
Ar I .....	1048	$> 13.860$	$14.346 \pm 0.065$	$-1.374 \pm 0.119$
Ar I .....	1066	$14.346 \pm 0.065$	...	...
Fe II .....	1081	$14.879 \pm 0.055$	$14.905 \pm 0.033$	$-1.795 \pm 0.105$
Fe II .....	1125	$14.920 \pm 0.046$	...	...
Fe II .....	1142	$14.936 \pm 0.099$	...	...
Fe II .....	1144	$> 14.719$	...	...
Ni II .....	1317	$< 13.389$	$13.469 \pm 0.057$	$-1.981 \pm 0.115$
Ni II .....	1370	$13.424 \pm 0.065$	...	...
Ni II .....	1454	$13.880 \pm 0.091$	...	...

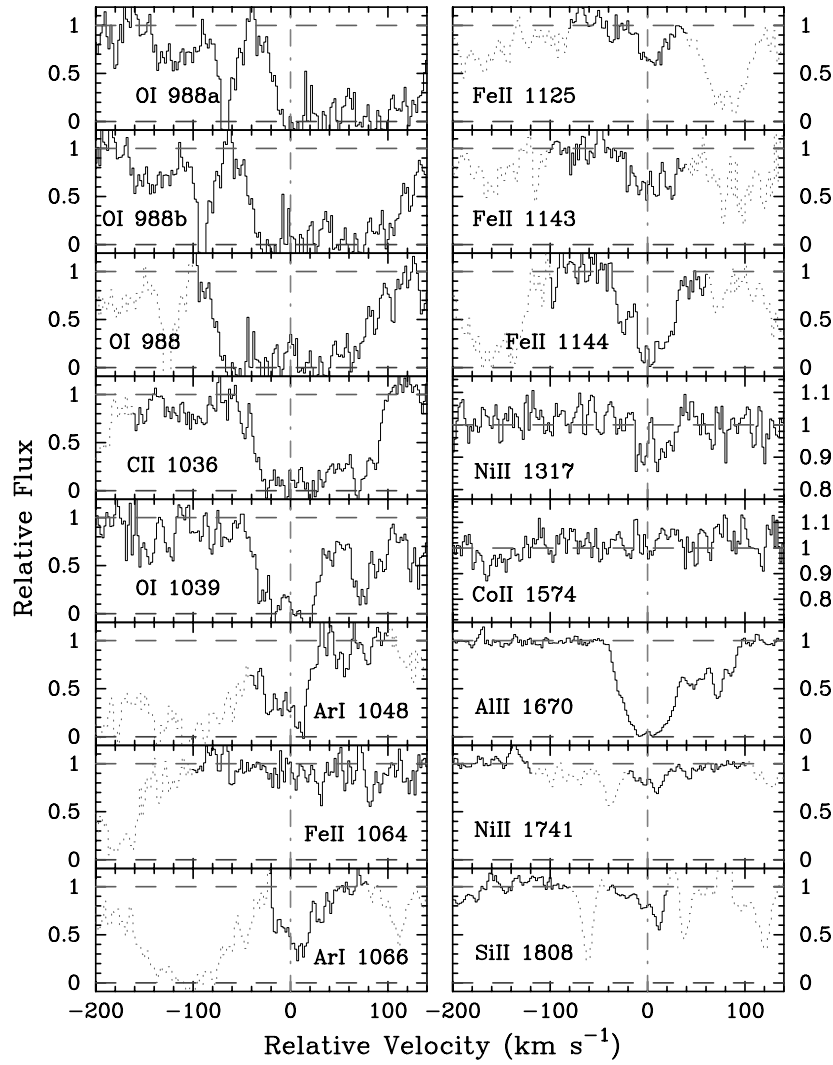


FIG. 10.—Velocity plot of several new metal line transitions for the DLA system at  $z = 3.025$  toward Q0347–38. The vertical line at  $v = 0$  corresponds to  $z = 3.0247$ . [See the electronic edition of the Journal for a color version of this figure.]

TABLE 11  
IONIC COLUMN DENSITIES: Q0347–38,  $z = 3.025$

Ion	$\lambda$	AODM	$N_{\text{adopt}}$	[X/H]
H I.....	1215	$20.800 \pm 0.100$	...	...
C II.....	1036	$> 14.930$	$> 15.065$	$> -2.285$
C II.....	1334	$> 15.066$	...	...
O I.....	1039	$> 15.953$	$> 15.953$	$> -1.717$
O I.....	1302	$> 15.449$	...	...
Al II.....	1670	$> 13.408$	$> 13.408$	$> -1.882$
Si II.....	1260	$> 14.329$	$15.017 \pm 0.026$	$-1.343 \pm 0.103$
Si II.....	1304	$> 14.889$	...	...
Si II.....	1808	$15.017 \pm 0.026$	...	...
S II.....	1259	$< 14.760$	$< 14.760$	$< -1.240$
Ar I.....	1048	$> 14.063$	$14.282 \pm 0.035$	$-1.038 \pm 0.106$
Ar I.....	1066	$14.282 \pm 0.035$	...	...
Fe II.....	1063	$14.763 \pm 0.143$	$14.503 \pm 0.007$	$-1.797 \pm 0.100$
Fe II.....	1125	$14.453 \pm 0.056$	...	...
Fe II.....	1143	$14.712 \pm 0.040$	...	...
Fe II.....	1608	$14.501 \pm 0.007$	...	...
Fe II.....	1611	$< 14.447$	...	...
Co II.....	1574	$< 13.196$	$< 13.196$	$< -0.514$
Ni II.....	1317	$13.034 \pm 0.093$	$13.383 \pm 0.031$	$-1.667 \pm 0.105$
Ni II.....	1370	$13.115 \pm 0.099$	...	...
Ni II.....	1741	$14.056 \pm 0.019$	...	...

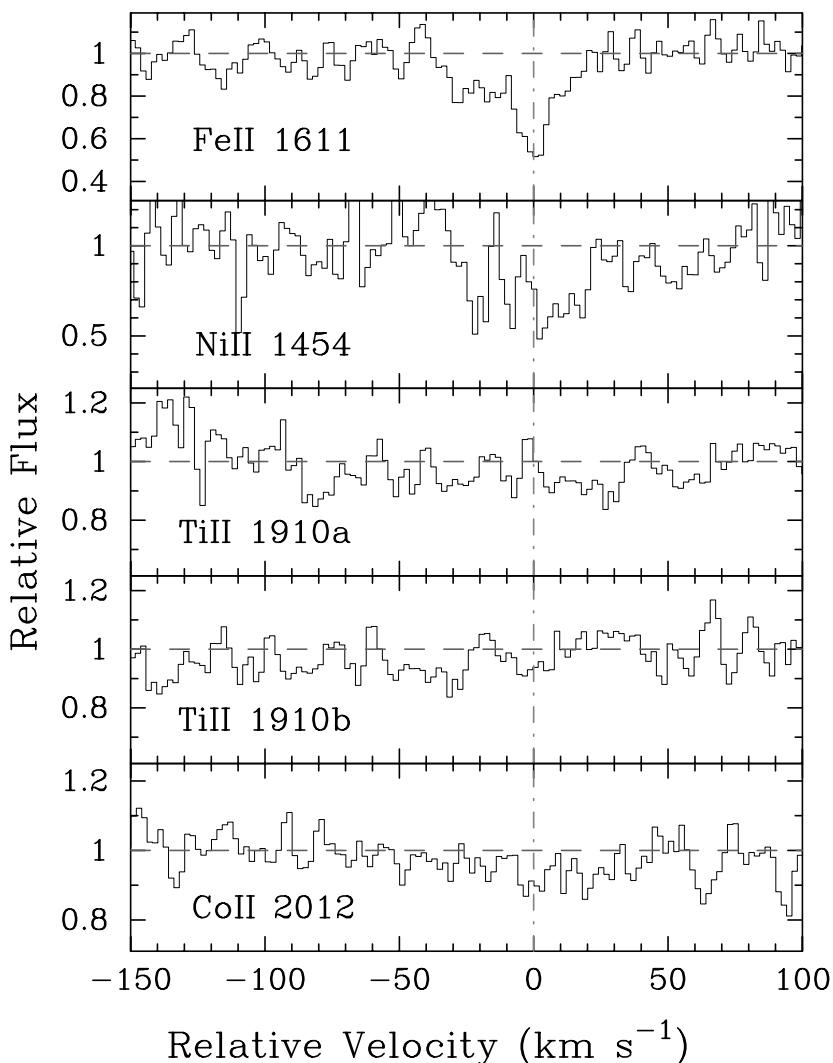


FIG. 11.—Velocity plot of several new metal line transitions for the DLA system at  $z = 2.040$  toward Q0458–02. The vertical line at  $v = 0$  corresponds to  $z = 2.03955$ . [See the electronic edition of the *Journal* for a color version of this figure.]

### 3.11. Q0836+11, $z = 2.465$

This DLA system is drawn from the LBQS survey (Wolfe et al. 1995), and we adopt the  $N(\text{H I})$  value obtained from their analysis. Our observations cover a large number of

transitions, many of which only provide upper limits owing to the relatively poor S/N (Fig. 13 and Table 14). In passing, we note that some of the Ni II upper limits are in contradiction with our adopted  $N(\text{Ni}^+)$  value. This might reflect an

TABLE 12  
IONIC COLUMN DENSITIES: Q0458–02,  $z = 2.040$

Ion	$\lambda$	AODM	$N_{\text{adopt}}$	[X/H]
H I.....	1215	$21.650 \pm 0.090$	...	...
C I.....	1656	$< 12.453$	...	...
Mg I.....	2026	$13.117 \pm 0.031$	...	...
Ti II.....	1910	$< 12.495$	$< 12.495$	$< -2.095$
Co II.....	2012	$< 13.092$	$< 13.093$	$< -1.467$
Ni II.....	1317	$14.257 \pm 0.024$	$14.181 \pm 0.018$	$-1.719 \pm 0.092$
Ni II.....	1370	$14.315 \pm 0.071$	...	...
Ni II.....	1454	$14.187 \pm 0.114$	...	...
Ni II.....	1703	$13.987 \pm 0.090$	...	...
Ni II.....	1709	$14.158 \pm 0.034$	...	...
Ni II.....	1741	$14.195 \pm 0.032$	...	...
Ni II.....	1751	$14.170 \pm 0.033$	...	...
Zn II.....	2026	$13.134 \pm 0.020$	$13.134 \pm 0.020$	$-1.186 \pm 0.092$
Zn II.....	2062	$> 13.031$	...	...

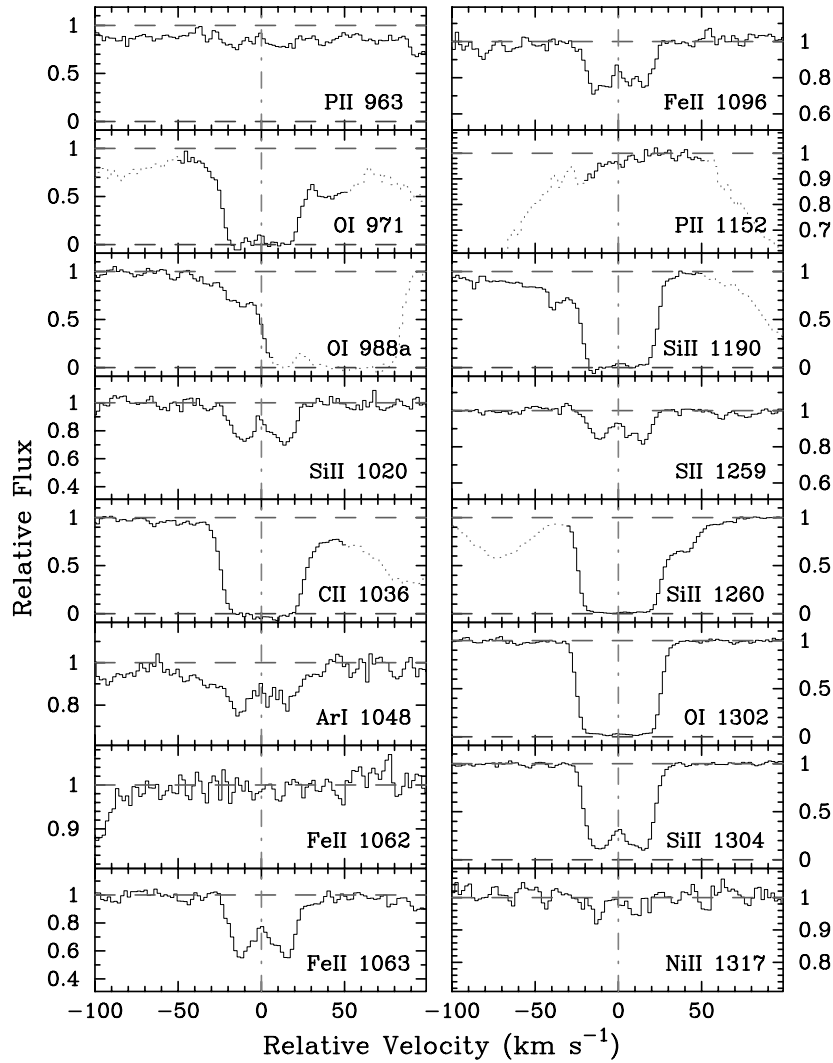
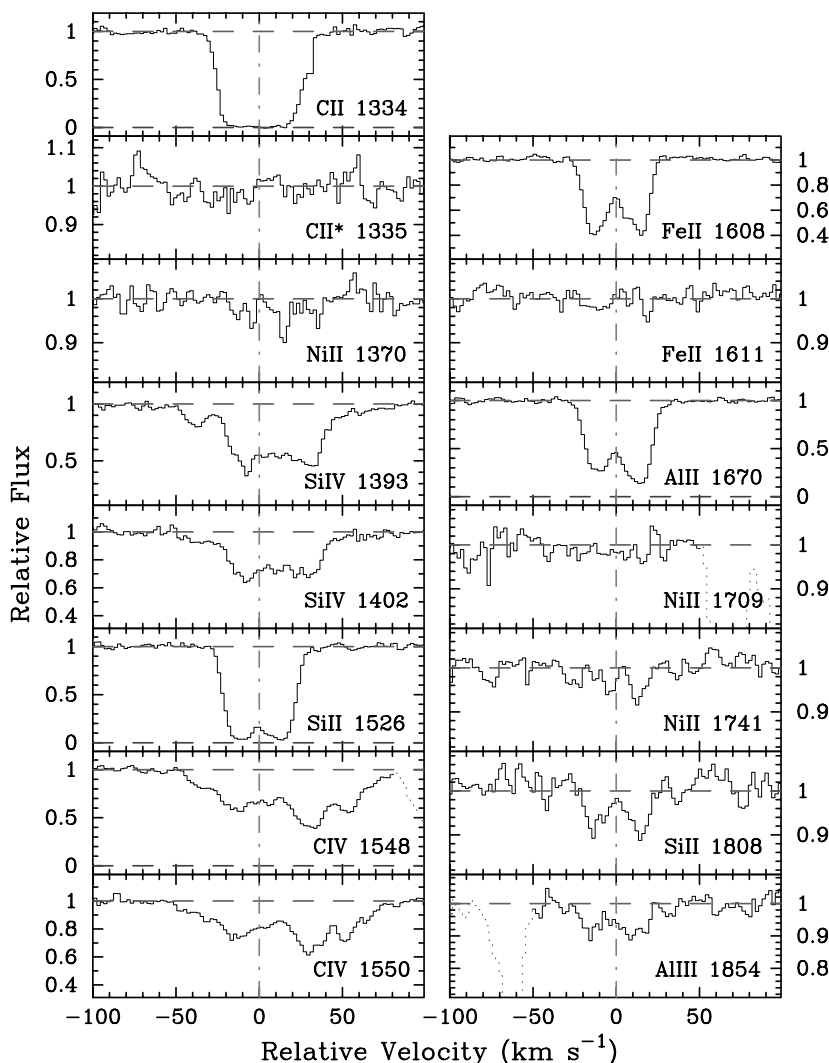


FIG. 12.—Velocity plot of the metal line transitions for the DLA system at  $z = 3.017$  toward HS 0741 + 4741. The vertical line at  $v = 0$  corresponds to  $z = 3.017399$ . [See the electronic edition of the Journal for a color version of this figure.]

TABLE 13  
IONIC COLUMN DENSITIES: HS 0741 + 4741,  $z = 3.017$

Ion	$\lambda$	AODM	$N_{\text{adopt}}$	[X/H]
H I .....	1215	$20.480 \pm 0.100$	...	...
C II .....	1036	$> 14.864$	$> 14.864$	$> -2.166$
C II .....	1334	$> 14.737$	...	...
C II .....	1335	$< 12.554$	...	...
C IV .....	1548	$13.827 \pm 0.005$	...	...
C IV .....	1550	$13.847 \pm 0.009$	...	...
O I .....	971	$> 15.711$	$> 15.711$	$> -1.639$
O I .....	1302	$> 15.229$	...	...
Al II .....	1670	$12.823 \pm 0.005$	$12.824 \pm 0.005$	$-2.146 \pm 0.100$
Al III .....	1854	$12.161 \pm 0.043$	...	...
Si II .....	1020	$14.162 \pm 0.019$	$14.354 \pm 0.003$	$-1.686 \pm 0.100$
Si II .....	1260	$> 13.937$	...	...
Si II .....	1304	$14.368 \pm 0.003$	...	...
Si II .....	1526	$> 14.469$	...	...
Si II .....	1808	$14.395 \pm 0.051$	...	...
Si IV .....	1393	$13.382 \pm 0.006$	...	...
Si IV .....	1402	$13.376 \pm 0.011$	...	...
P II .....	1152	$< 12.080$	$< 12.080$	$< -1.930$



FIG. 12.—*Continued*

error in the relative  $f$ -values but more likely reflects the large error in the adopted value.

### 3.12. $Q0841+12$ , $z = 2.375$ and $2.476$

We augment the measurements presented in PW99 with a few additional Ni II transitions and several Co II and Ti II upper limits. These transitions are plotted in Figures 14 and

15 and tabulated in Tables 15 and 16. As discussed in PW99, we based the Fe abundance for the  $z = 2.476$  system on the saturated Fe II  $\lambda 1608$  profile. We now choose to report the Fe II  $\lambda 1608$  column density as a lower limit on  $N(\text{Fe}^+)$  and adopt an Fe abundance based on averaging the lower and upper limits from Fe II  $\lambda 1608$  and Fe II  $\lambda 1611$ , respectively:  $\log N(\text{Fe}^+) = 14.53 \pm 0.05$ .

TABLE 13—*Continued*

Ion	$\lambda$	AODM	$N_{\text{adopt}}$	[X/H]
S II.....	1259	$14.000 \pm 0.016$	$14.000 \pm 0.016$	$-1.680 \pm 0.101$
Ar I.....	1048	$13.166 \pm 0.020$	$13.166 \pm 0.020$	$-1.834 \pm 0.102$
Fe II.....	1063	$14.075 \pm 0.010$	$14.052 \pm 0.005$	$-1.928 \pm 0.100$
Fe II.....	1096	$14.068 \pm 0.015$	...	...
Fe II.....	1608	$14.041 \pm 0.006$	...	...
Fe II.....	1611	$< 14.082$	...	...
Co II.....	1574	$< 12.958$	$< 12.958$	$< -0.432$
Ni II.....	1317	$12.658 \pm 0.110$	$12.758 \pm 0.049$	$-1.972 \pm 0.111$
Ni II.....	1370	$12.736 \pm 0.081$	...	...
Ni II.....	1454	$< 12.833$	...	...
Ni II.....	1709	$12.745 \pm 0.144$	...	...
Ni II.....	1741	$12.943 \pm 0.078$	...	...

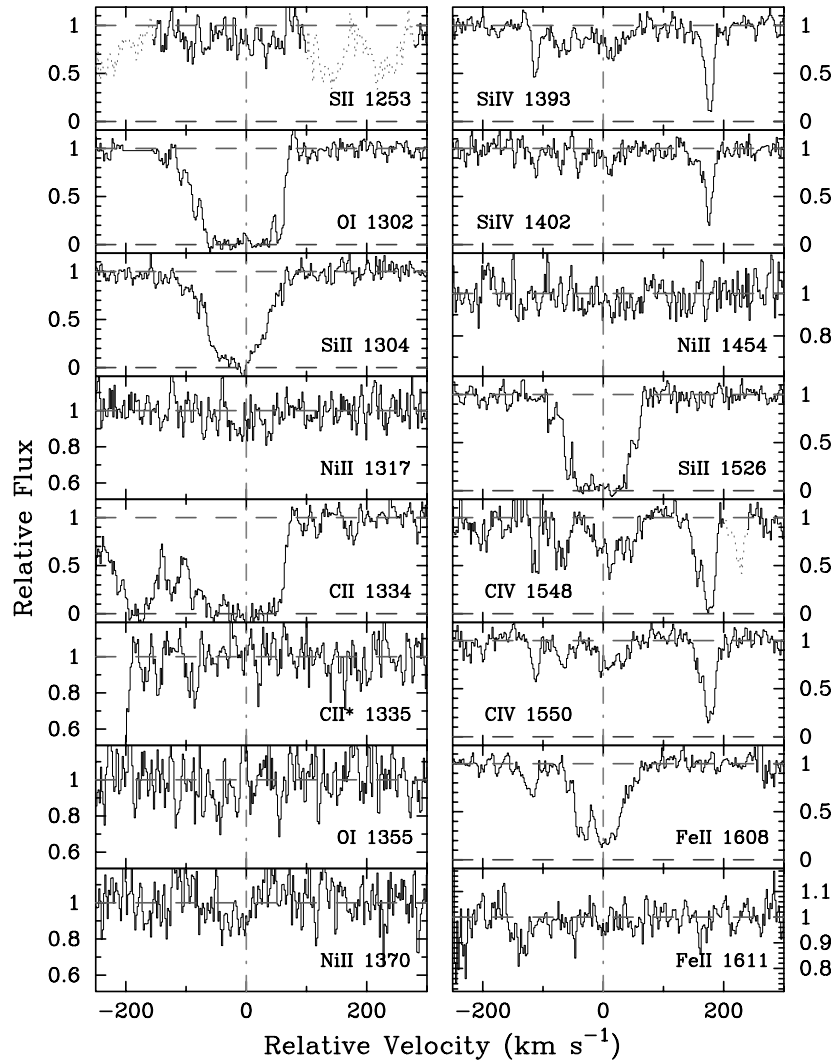
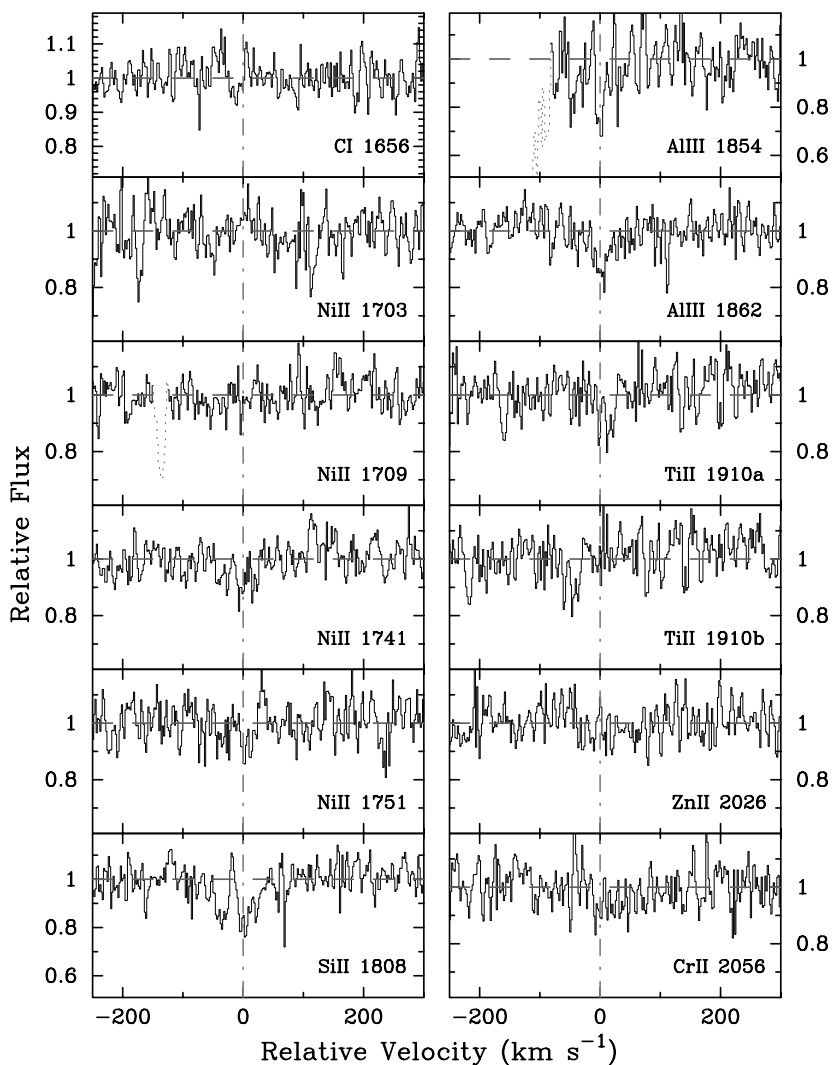


FIG. 13.—Velocity plot of the metal line transitions for the DLA system at  $z = 2.465$  toward Q0836 + 11. The vertical line at  $v = 0$  corresponds to  $z = 2.46527$ . [See the electronic edition of the Journal for a color version of this figure.]

TABLE 14  
IONIC COLUMN DENSITIES: Q0836 + 11,  $z = 2.465$

Ion	$\lambda$	AODM	$N_{\text{adopt}}$	[X/H]
H I .....	1215	$20.580 \pm 0.100$	...	...
C II .....	1334	$> 15.026$	$> 15.026$	$> -2.104$
C II .....	1335	$< 13.121$	...	...
C IV .....	1548	$> 14.218$	...	...
O I .....	1302	$> 15.485$	$> 15.485$	$> -1.965$
O I .....	1355	$< 18.186$	...	...
Al III .....	1854	$12.459 \pm 0.093$	...	...
Al III .....	1862	$12.634 \pm 0.076$	...	...
Si II .....	1304	$> 14.918$	$14.987 \pm 0.045$	$-1.153 \pm 0.110$
Si II .....	1526	$> 14.850$	...	...
Si II .....	1808	$14.987 \pm 0.045$	...	...
Si IV .....	1393	$13.557 \pm 0.024$	...	...
Si IV .....	1402	$13.592 \pm 0.043$	...	...
S II .....	1253	$< 14.660$	$< 14.660$	$< -1.120$
Ti II .....	1910	$< 12.537$	$< 12.538$	$< -0.982$
Cr II .....	2056	$< 12.898$	$< 12.898$	$< -1.352$
Cr II .....	2066	$< 13.230$	...	...

FIG. 13.—*Continued*3.13. *BRI 0951–04*,  $z = 3.857$  and  $4.203$ 

Our combined spectrum now includes a second setup with significant coverage blueward of the Ly $\alpha$  peak. Unfortunately, the new data add only a few unblended transitions to the analysis (Figs. 16 and 17 and Tables 17 and 18). With respect to PW99, we now suspect that the feature at 177 km

$s^{-1}$  in the  $z = 3.857$  Ni II  $\lambda 1370$  profile is unrelated to that transition and obtain an upper limit on  $N(\text{Ni}^+)$ . This value is in much better agreement with the Fe and Al abundances. In terms of the system at  $z = 4.203$ , we still have no reliable estimate of the Fe peak abundance. The combination of poor S/N and low H I column density has resulted in the

TABLE 14—*Continued*

Ion	$\lambda$	AODM	$N_{\text{adopt}}$	[X/H]
Fe II .....	1608	$14.677 \pm 0.011$	$14.677 \pm 0.011$	$-1.403 \pm 0.101$
Fe II .....	1611	$< 14.784$	...	...
Co II .....	1466	$< 13.383$	$< 13.383$	$< -0.107$
Co II .....	1574	$< 13.442$	...	...
Ni II .....	1317	$13.364 \pm 0.105$	$13.388 \pm 0.065$	$-1.442 \pm 0.119$
Ni II .....	1370	$< 13.339$	...	...
Ni II .....	1454	$< 13.365$	...	...
Ni II .....	1703	$< 14.058$	...	...
Ni II .....	1709	$< 13.275$	...	...
Ni II .....	1741	$13.406 \pm 0.083$	...	...
Ni II .....	1751	$< 13.393$	...	...
Zn II .....	2026	$< 12.119$	$< 12.119$	$< -1.131$

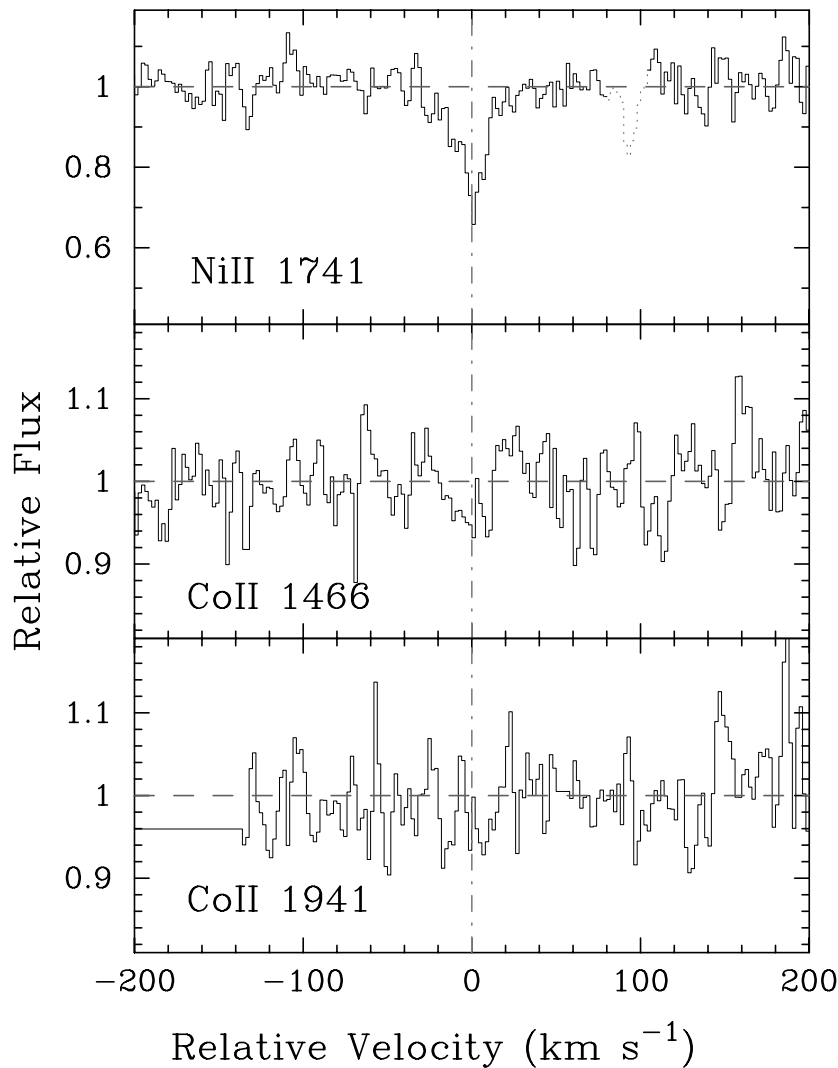


FIG. 14.—Velocity plot of two Co II profiles for the DLA system at  $z = 2.375$  toward Q0841 + 12. For comparison, we also plot the Ni II  $\lambda 1741$  profile. The vertical line at  $v = 0$  corresponds to  $z = 2.374518$ . [See the electronic edition of the *Journal* for a color version of this figure.]

nondetection of Fe II  $\lambda 1608$ , and our observations did not cover C II  $\lambda 1334$  or Al II  $\lambda 1670$ . Finally, we revise the oxygen abundance to account for the saturated O I  $\lambda 1302$  profile.

#### 3.14. BRI 0952–01, $z = 4.024$

This DLA system was identified by Storrie-Lombardi et al. (1996) and confirmed with a follow-up LRIS spectrum by Storrie-Lombardi & Wolfe (2000). We adopt the  $N(\text{H I})$

value from the latter analysis. Figure 18 presents the velocity profiles covered by our single setup. Unfortunately, a misestimate of the absorption redshift coupled with several line blends has limited our ionic column density measurements of this system (Table 19). As reported in Prochaska & Wolfe (2000), we estimate the  $\text{Fe}^+$  column density by combining the unblended features observed for the Fe II  $\lambda\lambda 1144$  and 1608 profiles. With the updated oscillator strengths, we find  $N(\text{Fe}^+) = 14.187 \pm 0.07$ .

TABLE 15  
IONIC COLUMN DENSITIES: Q0841 + 12,  $z = 2.375$

Ion	$\lambda$	AODM	$N_{\text{adopt}}$	[X/H]
H I.....	1215	$20.950 \pm 0.087$	...	...
Co II.....	1466	$< 13.047$	$< 12.990$	$< -0.870$
Co II.....	1941	$< 12.990$	...	...
Ni II.....	1454	$13.415 \pm 0.075$	$13.523 \pm 0.030$	$-1.677 \pm 0.092$
Ni II.....	1741	$13.560 \pm 0.040$	...	...
Ni II.....	1751	$13.547 \pm 0.055$	...	...

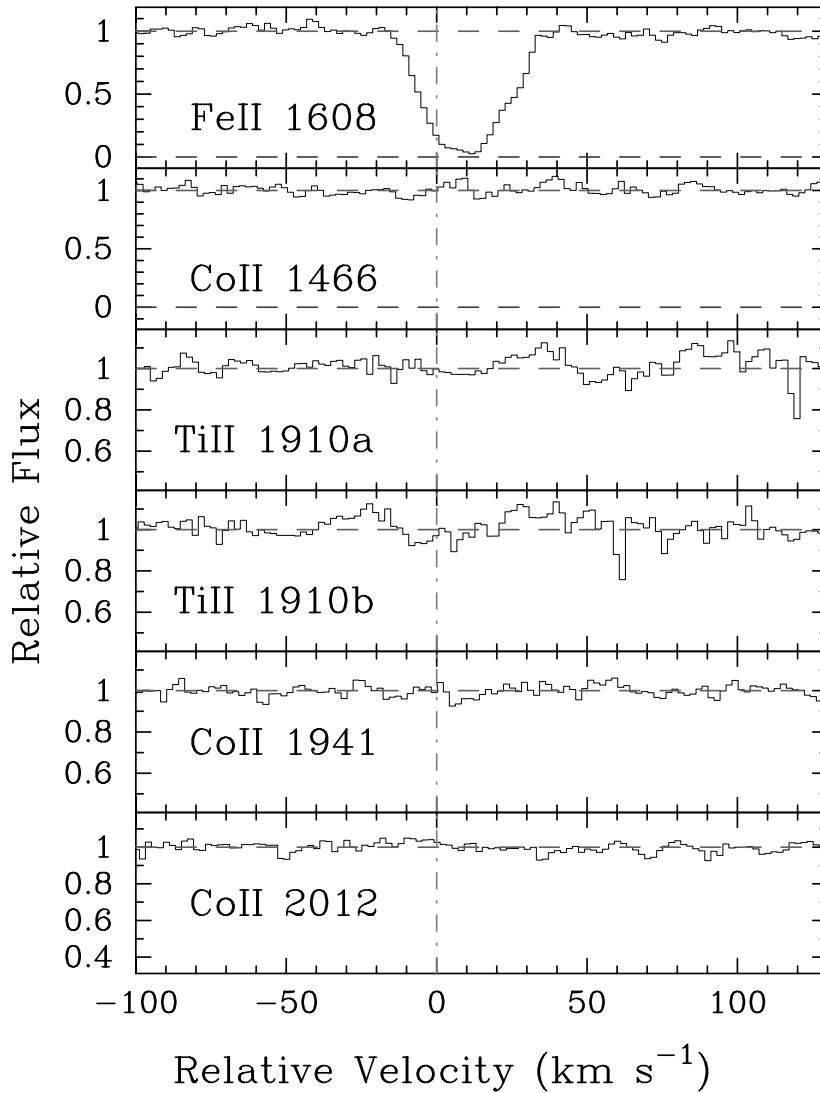


FIG. 15.—Velocity plot of the new metal line transitions for the DLA system at  $z = 2.476$  toward Q0841 + 12. For comparison, we also plot the Fe II  $\lambda 1608$  profile. The vertical line at  $v = 0$  corresponds to  $z = 2.476219$ . [See the electronic edition of the Journal for a color version of this figure.]

### 3.15. PSS 0957 + 33, $z = 3.279$ and 4.178

The two DLA systems toward this PSS quasar (Djorgovski et al. 1998) were discovered during the first night of our ongoing Echelle Spectrograph and Imager (ESI) project designed to discover and measure the metallicity of  $z > 3$  damped systems (PGW01). Given the appar-

ent brightness of this quasar we chose to obtain a HIRES spectrum. Figures 19 and 20 present the metal line transition identified in our HIRES spectrum, and Tables 20 and 21 give the ionic column densities.

To test the metallicities obtained with the ESI spectrum, we can compare the HIRES values with the Fe<sup>+</sup> column densities adopted in PGW01 after correcting for the new

TABLE 16  
IONIC COLUMN DENSITIES: Q0841 + 12,  $z = 2.476$

Ion	$\lambda$	AODM	$N_{\text{adopt}}$	[X/H]
H I.....	1215	$20.780 \pm 0.097$	...	...
Ti II.....	1910	$< 12.158$	$< 12.158$	$< -1.562$
Fe II.....	1608	$> 14.517$	...	...
Fe II.....	1611	$< 14.543$	...	...
Co II.....	1466	$< 13.206$	$< 12.726$	$< -0.964$
Co II.....	1941	$< 12.783$	...	...
Co II.....	2012	$< 12.726$	...	...
Ni II.....	1709	$13.415 \pm 0.060$	$13.355 \pm 0.040$	$-1.675 \pm 0.105$
Ni II.....	1741	$13.321 \pm 0.054$	...	...
Ni II.....	1751	$< 13.348$	...	...

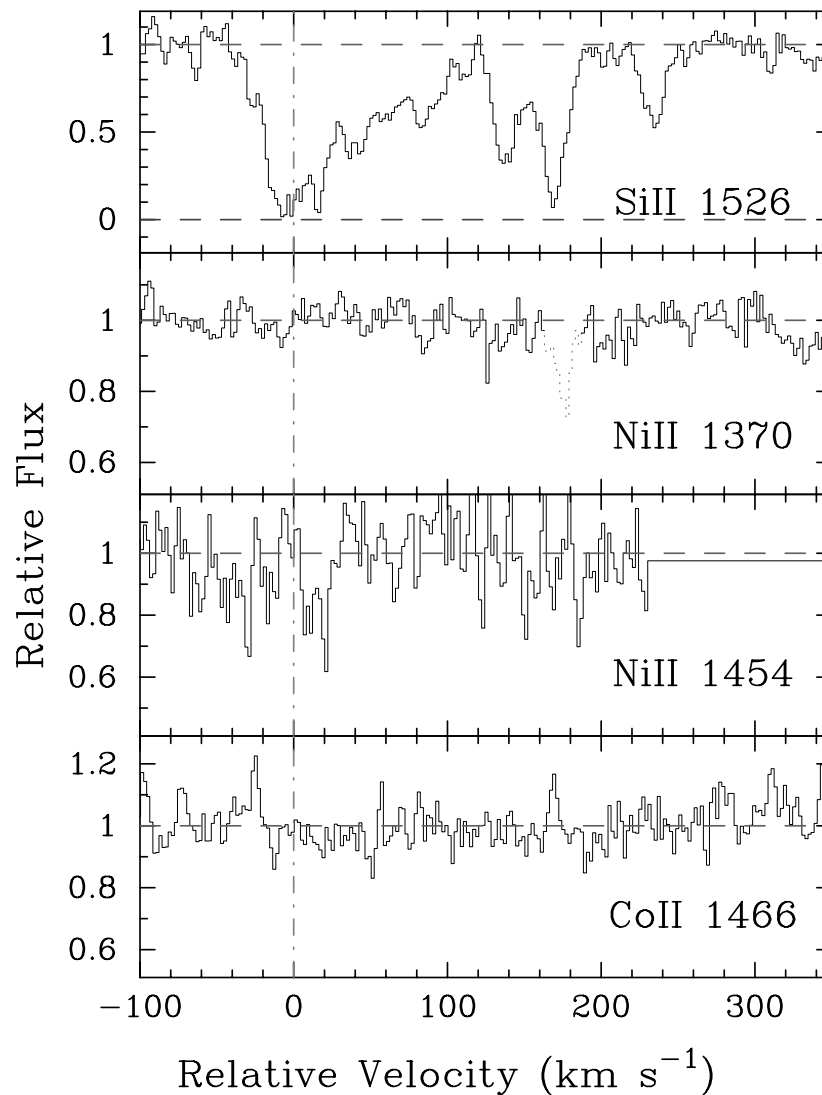


FIG. 16.—Velocity plot of the new metal line transitions for the DLA system at  $z = 3.857$  toward BRI 0951–04. For comparison, we also plot the Si II  $\lambda 1526$  profile. The vertical line at  $v = 0$  corresponds to  $z = 3.856689$ . [See the electronic edition of the *Journal* for a color version of this figure.]

oscillator strengths. For the system at  $z = 3.279$ , the Fe II  $\lambda 1608$  column densities are in excellent agreement, but because this transition is blended with telluric absorption, it might only provide an upper limit on  $N(\text{Fe}^+)$ . In PGW01, we derived the  $\text{Fe}^+$  column density from Fe II  $\lambda 2344$ , which is redward of our HIRES coverage. We now suspect that this value was an underestimate of  $N(\text{Fe}^+)$  as it implies  $[\text{Ni}/\text{Fe}] > 0.3$  dex. For now, we adopt an  $\text{Fe}^+$  column density based on the Fe II  $\lambda 1608$  profile.

The system at  $z = 4.178$  presents a more worrisome picture regarding column densities derived from ESI echel-

lette observations. Comparing the column densities for Fe II  $\lambda 1608$ , we find that we underestimated  $N(\text{Fe}^+)$  by  $\approx 0.3$  dex with the ESI spectrum. It is somewhat puzzling given that the profile is not very strong (unlike the Si II profiles, for example) and the quality of the ESI data is high. The strongest features are relatively narrow, so the difference is probably an effect of the lower resolution. Another puzzling aspect of the  $z = 4.178$  systems is the  $\text{S}^+$  column density derived from S II  $\lambda\lambda 1250$  and  $1253$ . Although the S II  $\lambda 1250$  profile is partially blended with an unrelated C IV system ( $z_{\text{abs}} = 3.181$ ), we are confident that the absorption at

TABLE 17  
IONIC COLUMN DENSITIES: BRI 0951–04,  $z = 3.857$

Ion	$\lambda$	AODM	$N_{\text{adopt}}$	$[\text{X}/\text{H}]$
H I.....	1215	$20.600 \pm 0.100$		
Co II.....	1466	$< 13.597$	$< 13.597$	$< 0.087$
Ni II.....	1370	$< 12.977$	$< 12.977$	$< -1.873$
Ni II.....	1454	$< 13.927$		

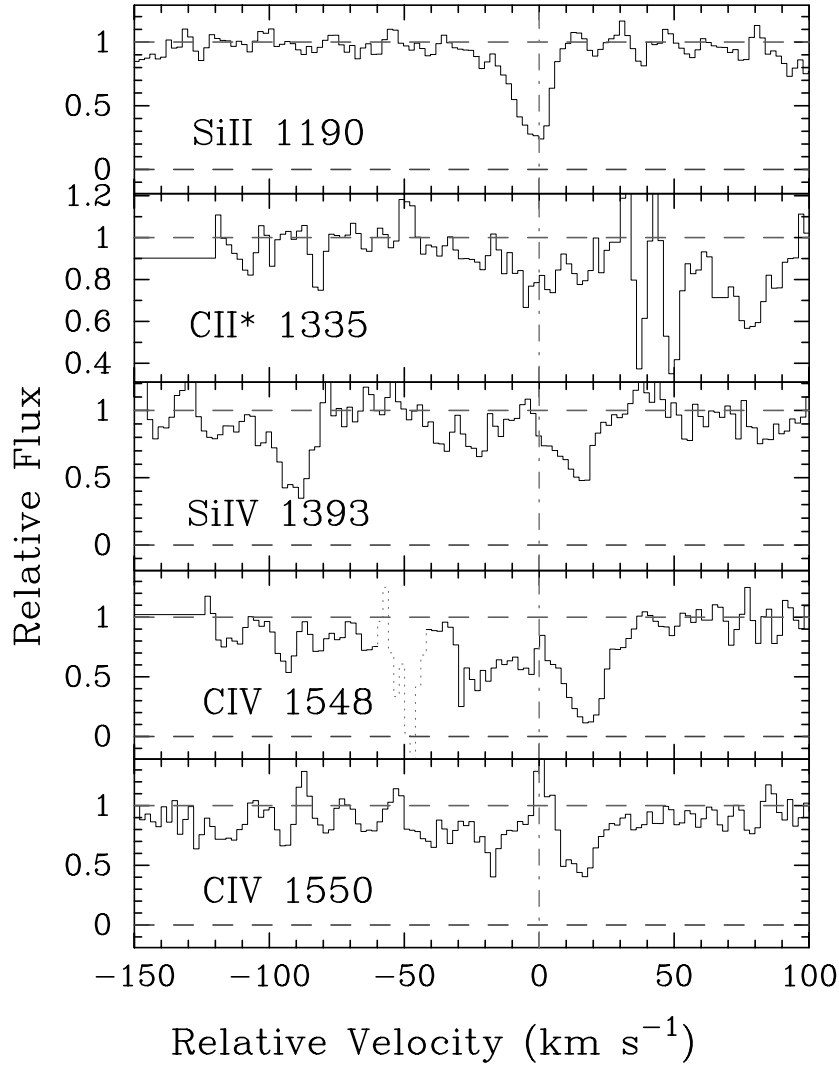


FIG. 17.—Velocity plot of the new metal line transitions for the DLA system at  $z = 4.203$  toward BRI 0951–04. The vertical line at  $v = 0$  corresponds to  $z = 4.202896$ . [See the electronic edition of the *Journal* for a color version of this figure.]

$-100 < v < 20 \text{ km s}^{-1}$  is free of contamination from the C IV system. In this case,  $N(\text{S II } \lambda 1250)$  provides a lower limit on  $\log N(\text{S}^+) > 14.65$ . This lower limit, however, is well in excess of the  $N(\text{S}^+)$  value derived from the unblended S II  $\lambda 1253$  transition. The component at  $v = 0 \text{ km s}^{-1}$  in the S II  $\lambda 1250$  profile is wider than its counterpart in the S II  $\lambda 1253$  profile, but there is no identifiable blend. Perhaps the difference suggests an extreme case of hidden saturation (Savage & Sembach 1991). If it is line saturation, this helps explain

why the ESI data significantly underestimate the column densities in this case, and it also raises the possibility that the abundances derived from the HIRES observations are underestimates. This would be particularly surprising given that the spectra have a resolution of  $R = 47,000$ . Unfortunately, our HIRES spectrum did not cover any other pair of unsaturated transitions from the same ion to test this issue further. Furthermore, the difference even exists in a comparison of S II  $\lambda\lambda 1250$  and  $1253$  with respect to the

TABLE 18  
IONIC COLUMN DENSITIES: BRI 0951–04,  $z = 4.203$

Ion	$\lambda$	AODM	$N_{\text{adopt}}$	[X/H]
H I .....	1215	$20.400 \pm 0.100$	...	...
C IV .....	1548	...	...	...
C IV .....	1550	$13.945 \pm 0.052$	...	...
O I .....	1302	$> 14.596$	$> 14.596$	$> -2.674$
Si II .....	1190	$13.417 \pm 0.042$	$13.342 \pm 0.030$	$-2.618 \pm 0.104$
Si II .....	1526	$13.302 \pm 0.056$	...	...
Si IV .....	1393	$12.918 \pm 0.063$	...	...

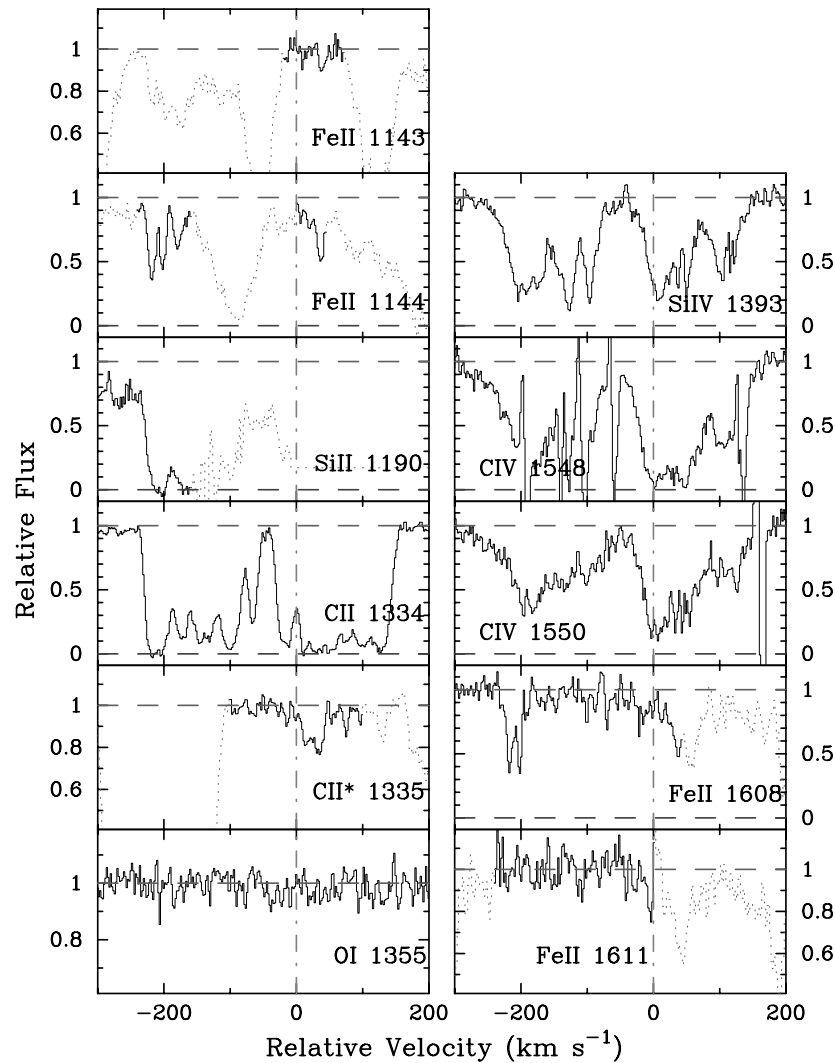


FIG. 18.—Velocity plot of the metal line transitions for the DLA system at  $z = 4.024$  toward BRI 0952–01. The vertical line at  $v = 0$  corresponds to  $z = 4.024433$ . [See the electronic edition of the *Journal* for a color version of this figure.]

feature at  $v \approx -75 \text{ km s}^{-1}$ . Perhaps this is all the result of errors in the S II oscillator strengths, but it would have likely been identified by researchers who study the interstellar medium (ISM) (e.g., Howk, Savage, & Fabian 1999).

### 3.16. BRI 1108–07, $z = 3.608$

This DLA system was discovered and confirmed by

Storrie-Lombardi et al. (1996). The quasar is relatively bright, and we obtained a reasonably high S/N HIRES spectrum. Figure 21 presents the velocity profiles, and Table 22 lists the ionic column densities. The  $\text{Fe}^+$  and  $\text{Si}^+$  column densities are well measured and indicate a very large Si/Fe ratio, perhaps indicative of substantial Type II supernova (SN) enrichment.

TABLE 19  
IONIC COLUMN DENSITIES: BRI 0952–01,  $z = 4.024$

Ion	$\lambda$	AODM	$N_{\text{adopt}}$	[X/H]
H I.....	1215	$20.550 \pm 0.100$	...	...
C II.....	1334	$> 15.312$	$> 15.312$	$> -1.788$
C II.....	1335	$13.549 \pm 0.024$	...	...
C IV.....	1550	$14.796 \pm 0.009$	...	...
Si IV.....	1393	$14.134 \pm 0.006$	...	...
Fe II.....	1144	$> 13.864$	$14.187 \pm 0.076$	$-1.863 \pm 0.126$
Fe II.....	1608	$> 13.746$	...	...
Co II.....	1574	$< 13.750$	$< 13.750$	$< 0.290$
Ni II.....	1454	$< 13.439$	$< 13.439$	$< -1.361$



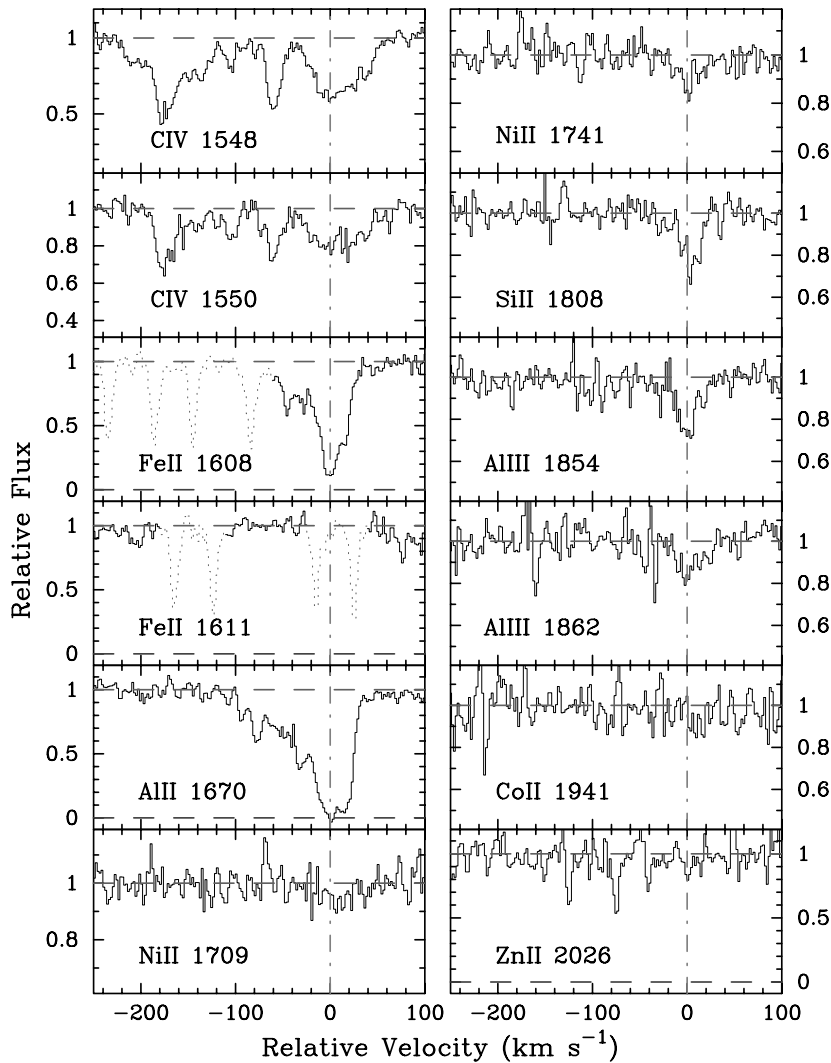


FIG. 19.—Velocity plot of the metal line transitions for the DLA system at  $z = 3.279$  toward PSS 0957+33. The vertical line at  $v = 0$  corresponds to  $z = 3.279576$ . [See the electronic edition of the *Journal* for a color version of this figure.]

### 3.17. *Q1210+17*, $z = 1.892$

This system is a member of the LBQS sample, and we have adopted the  $N(\text{H I})$  value from their analysis. We plot all of the transitions covered by our observations in Figure

22 and list the column densities in Table 23. This damped system exhibits a relatively low  $\text{Zn}/\text{Fe}$  ratio, which suggests that it is largely free of dust depletion. In passing, we note a remarkable similarity between the relative abundances of

TABLE 20  
IONIC COLUMN DENSITIES: PSS 0957+33,  $z = 3.279$

Ion	$\lambda$	AODM	$N_{\text{adopt}}$	$[\text{X}/\text{H}]$
H I.....	1215	$20.320 \pm 0.080$	...	...
C IV .....	1548	$13.979 \pm 0.009$	...	...
C IV .....	1550	$13.956 \pm 0.019$	...	...
Al II .....	1670	$> 13.322$	$> 13.322$	$> -1.488$
Al III.....	1854	$12.514 \pm 0.048$	...	...
Al III.....	1862	$12.578 \pm 0.087$	...	...
Si II .....	1808	$14.880 \pm 0.053$	$14.880 \pm 0.053$	$-1.000 \pm 0.096$
Fe II .....	1608	$14.367 \pm 0.016$	$14.367 \pm 0.016$	$-1.453 \pm 0.082$
Co II .....	1941	$< 13.285$	$< 13.285$	$< 0.055$
Ni II .....	1709	$13.283 \pm 0.122$	$13.318 \pm 0.070$	$-1.252 \pm 0.106$
Ni II .....	1741	$13.339 \pm 0.085$	...	...
Zn II .....	2026	$< 12.127$	$< 12.127$	$< -0.863$

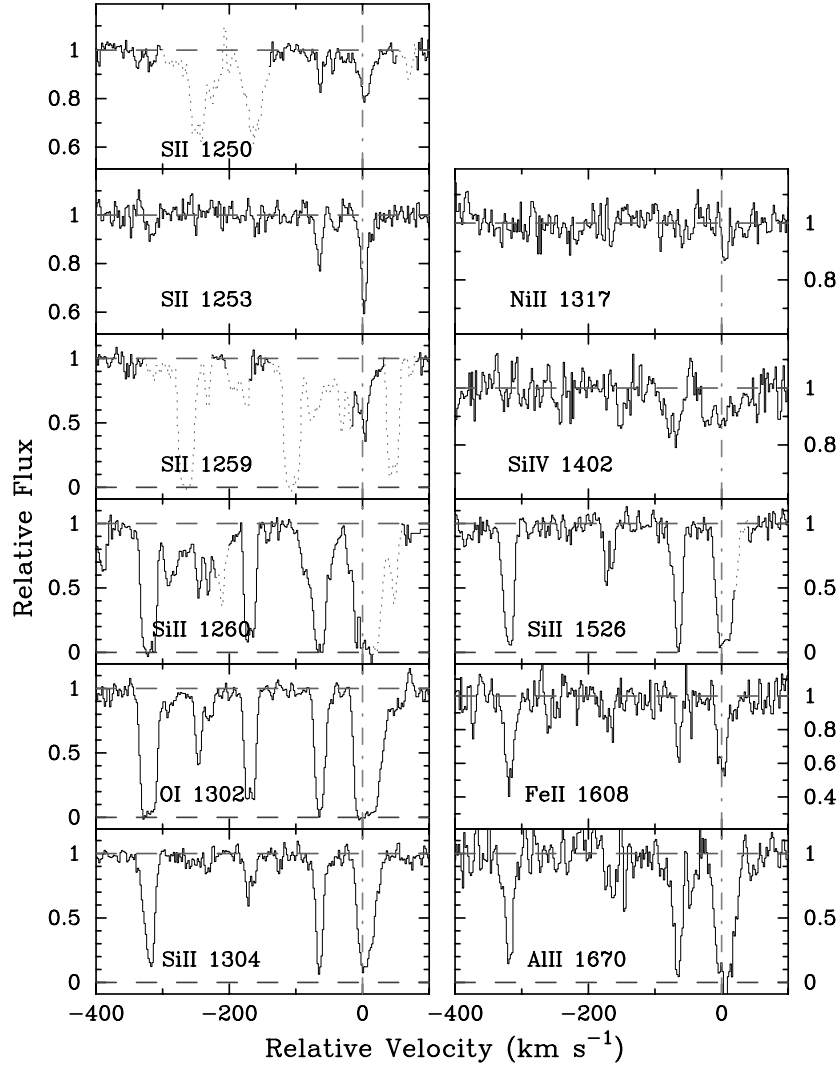


FIG. 20.—Velocity plot of the metal line transitions for the DLA system at  $z = 4.178$  toward PSS 0957+33. The vertical line at  $v = 0$  corresponds to  $z = 4.179825$ . [See the electronic edition of the *Journal* for a color version of this figure.]

TABLE 21  
IONIC COLUMN DENSITIES: PSS 0957+33,  $z = 4.178$

Ion	$\lambda$	AODM	$N_{\text{adopt}}$	[X/H]
H I.....	1215	$20.500 \pm 0.100$	...	...
O I.....	1302	$> 15.344$	$> 15.344$	$> -2.026$
Al II.....	1670	$> 13.256$	$> 13.256$	$> -1.734$
Si II.....	1304	$14.556 \pm 0.012$	$14.556 \pm 0.012$	$-1.504 \pm 0.101$
Si II.....	1526	$> 14.488$	...	...
Si IV.....	1402	$13.155 \pm 0.049$	...	...
S II.....	1250	$> 14.647$	$14.392 \pm 0.060$	$-1.308 \pm 0.117$
S II.....	1253	$14.392 \pm 0.060$	...	...
Fe II.....	1608	$14.129 \pm 0.045$	$14.129 \pm 0.045$	$-1.871 \pm 0.110$
Co II.....	1466	$< 13.648$	$< 13.648$	$< 0.238$
Co II.....	1574	$< 13.907$	...	...
Ni II.....	1317	$< 12.910$	$< 12.910$	$< -1.840$

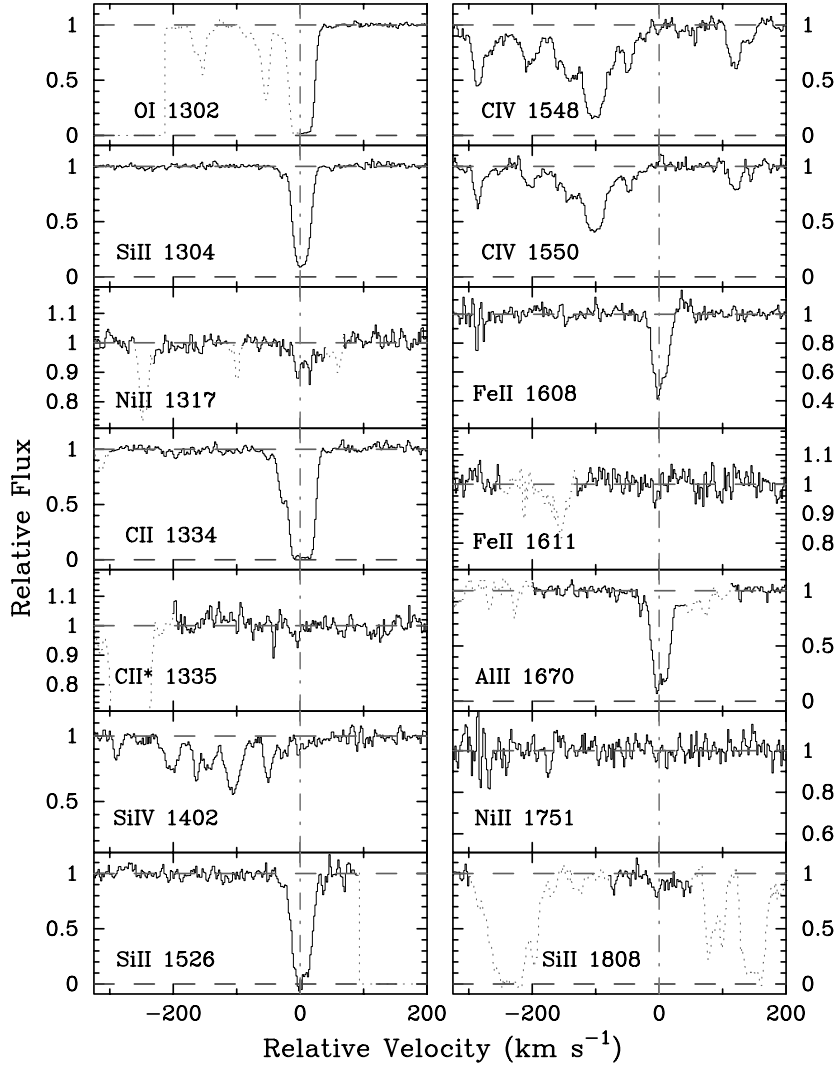


FIG. 21.—Velocity plot of the metal line transitions for the DLA system at  $z = 3.608$  toward BRI 1108–07. The vertical line at  $v = 0$  corresponds to  $z = 3.607619$ . [See the electronic edition of the *Journal* for a color version of this figure.]

TABLE 22  
IONIC COLUMN DENSITIES: BRI 1108–07,  $z = 3.608$

Ion	$\lambda$	AODM	$N_{\text{adopt}}$	[X/H]
H I .....	1215	$20.500 \pm 0.100$	...	...
C II .....	1334	$> 14.675$	$> 14.675$	$> -2.375$
C II .....	1335	$< 12.341$	...	...
C IV .....	1548	$14.293 \pm 0.006$	...	...
C IV .....	1550	$14.219 \pm 0.011$	...	...
O I .....	1302	$> 14.873$	$> 14.873$	$> -2.497$
Al II .....	1670	$12.822 \pm 0.015$	$12.822 \pm 0.015$	$-2.168 \pm 0.101$
Si II .....	1304	$14.262 \pm 0.004$	$14.262 \pm 0.004$	$-1.798 \pm 0.100$
Si II .....	1526	$> 14.260$	...	...
Si II .....	1808	$< 14.665$	...	...
Si IV .....	1402	$13.685 \pm 0.010$	...	...
Fe II .....	1608	$13.884 \pm 0.014$	$13.884 \pm 0.014$	$-2.116 \pm 0.101$
Fe II .....	1611	$< 14.269$	...	...
Ni II .....	1317	$< 13.136$	$< 13.136$	$< -1.614$
Ni II .....	1751	$< 13.180$	...	...

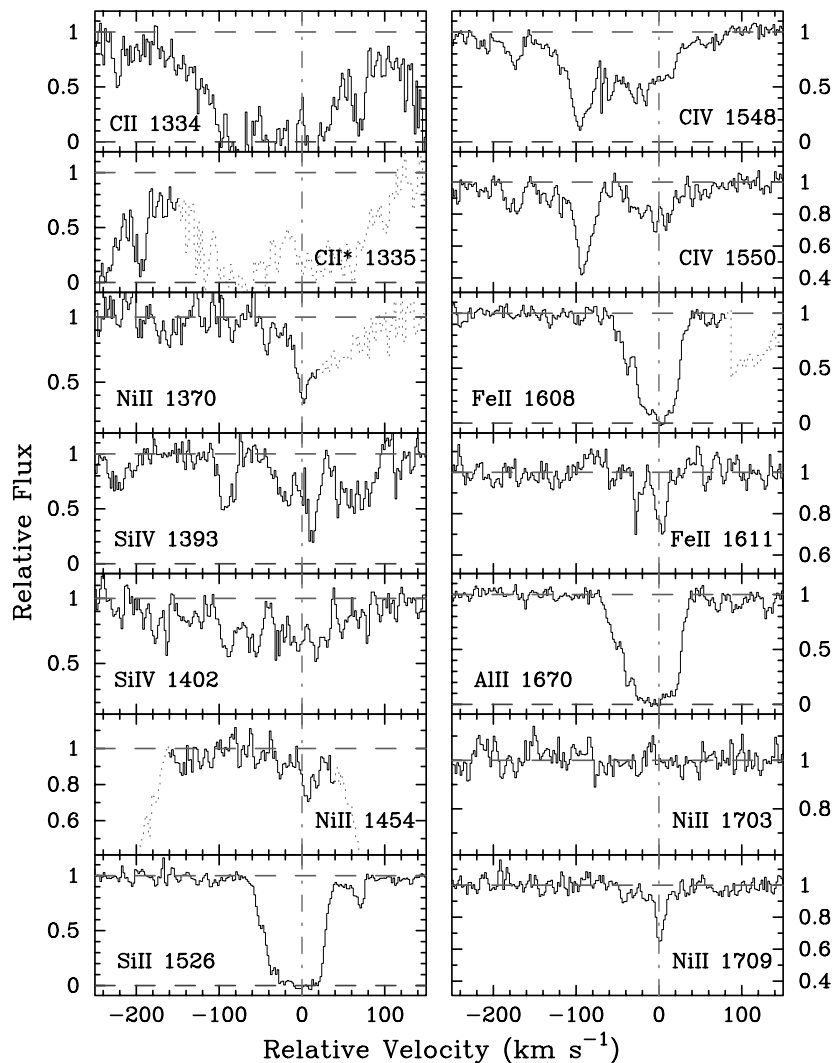


FIG. 22.—Velocity plot of the metal line transitions for the DLA system at  $z = 1.892$  toward Q1210 + 17. The vertical line at  $v = 0$  corresponds to  $z = 1.891755$ . [See the electronic edition of the *Journal* for a color version of this figure.]

Si, Ni, Cr, Fe, and Zn with the same pattern observed by Molaro et al. (2000) for the damped system toward Q0000–26, albeit at a much higher metallicity.

### 3.18. Q1215 + 33, $z = 1.999$

Although we presented a full analysis of this damped system in PW99, a number of transitions were overlooked,

and we have revised the Fe abundance. Figure 23 plots the new transitions, and Table 24 lists the ionic column densities. We now report only a limit on  $N(\text{Fe}^+)$  because the Fe  $\pi$   $\lambda 1608$  profile is saturated and the Fe  $\pi$   $\lambda 1611$  transition is too weak to provide a reasonable measurement. In the subsequent analysis, we assume a value based on an average of the two limits:  $N(\text{Fe}^+) = 10^{14.748 \pm 0.05} \text{ cm}^{-2}$ . Finally, we

TABLE 23  
IONIC COLUMN DENSITIES: Q1210 + 17,  $z = 1.892$

Ion	$\lambda$	AODM	$N_{\text{adopt}}$	[X/H]
H I .....	1215	$20.600 \pm 0.100$	...	...
C IV .....	1548	$< 14.230$	...	...
C IV .....	1550	$14.053 \pm 0.017$	...	...
Al II .....	1670	$> 13.440$	$> 13.440$	$> -1.650$
Al III .....	1854	$12.999 \pm 0.017$	...	...
Al III .....	1862	$13.005 \pm 0.021$	...	...
Si II .....	1526	$> 14.780$	$15.285 \pm 0.018$	$-0.875 \pm 0.102$
Si II .....	1808	$15.285 \pm 0.018$	...	...
Si IV .....	1393	$13.594 \pm 0.025$	...	...
Cr II .....	2056	$13.291 \pm 0.019$	$13.243 \pm 0.016$	$-1.027 \pm 0.101$

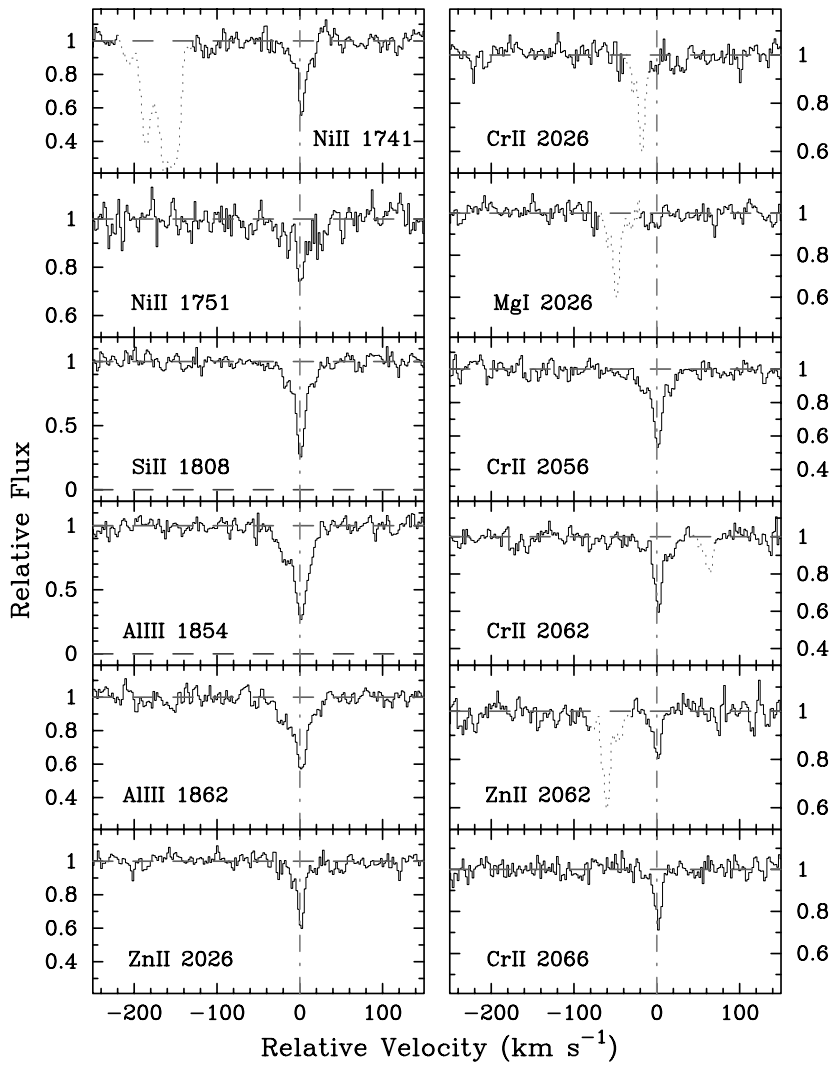


FIG. 22.—Continued

also report an upper limit on  $N(\text{Zn}^+)$  based on the  $\text{Zn II } \lambda 2062$  profile. It is 0.2 dex lower than the value derived from  $\text{Zn II } \lambda 2026$ , which is difficult to understand aside from the fact that the  $\text{Zn II } \lambda 2026$  profile is noisy and the continuum is poorly constrained in that region. For now, we continue to adopt the value from  $\text{Zn II } \lambda 2026$ .

3.19.  $Q1223+17$ ,  $z = 2.466$ 

The combination of a very large  $N(\text{H I})$  value and extensive wavelength coverage allows for the analysis of a terrific number of transitions. Figure 24 and Table 25 present over 20 transitions including a large number of limits. One of the most interesting ratios is  $\text{Ti}/\text{Fe}$ , whose upper limit is less

TABLE 23—Continued

Ion	$\lambda$	AODM	$N_{\text{adopt}}$	$[\text{X}/\text{H}]$
Cr II	2062	$13.219 \pm 0.030$	...	...
Cr II	2066	$13.091 \pm 0.058$	...	...
Fe II	1608	$> 14.780$	$14.951 \pm 0.063$	$-1.149 \pm 0.118$
Fe II	1611	$14.951 \pm 0.063$	...	...
Co II	1574	$< 13.513$	$< 12.728$	$< -0.782$
Co II	2012	$< 12.728$	...	...
Ni II	1370	$< 13.964$	$13.632 \pm 0.020$	$-1.218 \pm 0.102$
Ni II	1454	$< 13.832$	...	...
Ni II	1709	$13.657 \pm 0.031$	...	...
Ni II	1741	$13.628 \pm 0.029$	...	...
Ni II	1751	$13.590 \pm 0.049$	...	...
Zn II	2026	$12.409 \pm 0.032$	$12.370 \pm 0.029$	$-0.900 \pm 0.104$
Zn II	2062	$12.263 \pm 0.069$	...	...

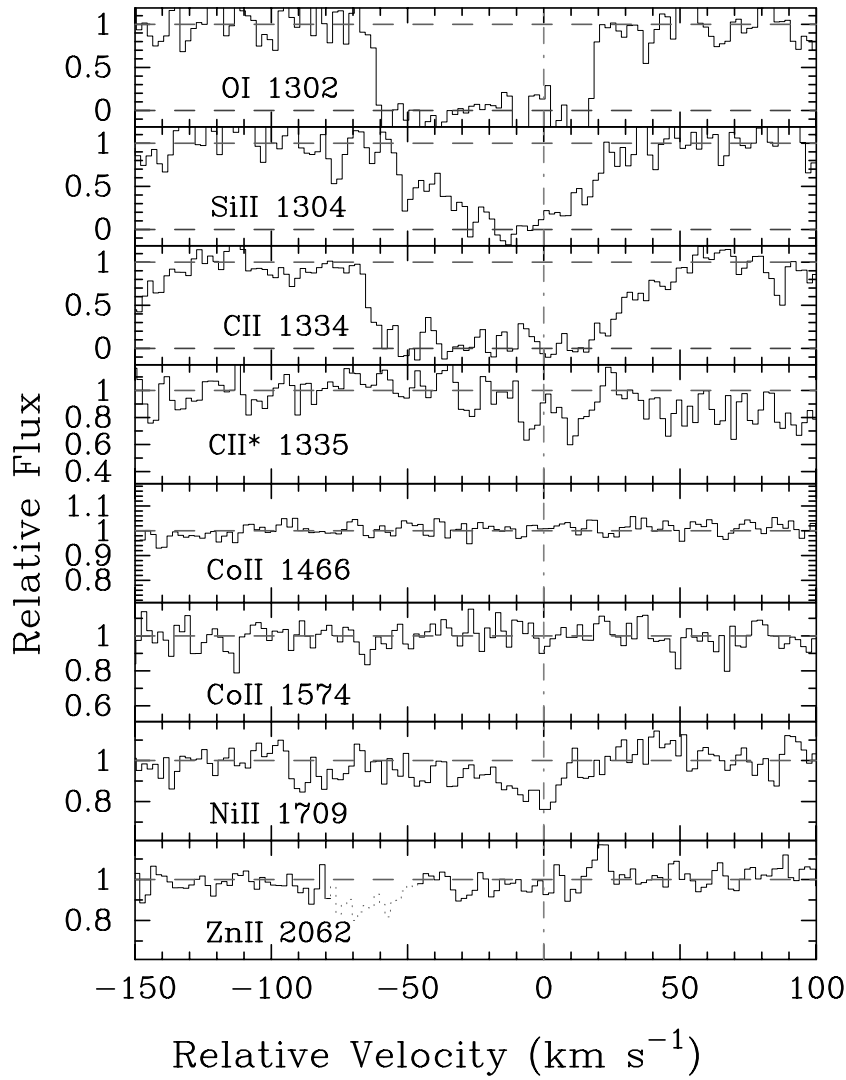


FIG. 23.—Velocity plot of the new metal line transitions for the DLA system at  $z = 1.999$  toward Q1215+33. The vertical line at  $v = 0$  corresponds to  $z = 1.9991$ . [See the electronic edition of the Journal for a color version of this figure.]

TABLE 24  
IONIC COLUMN DENSITIES: Q1215+33,  $z = 1.999$

Ion	$\lambda$	AODM	$N_{\text{adopt}}$	[X/H]
H I.....	1215	$20.950 \pm 0.067$	...	...
C II.....	1334	$> 14.630$	$> 14.630$	$> -2.870$
C II.....	1335	$< 13.173$	...	...
O I.....	1302	$> 15.127$	$> 15.127$	$> -2.693$
O I.....	1355	$< 18.065$	...	...
Si II.....	1304	$> 14.617$	$15.030 \pm 0.025$	$-1.480 \pm 0.072$
Si II.....	1526	$> 14.660$	...	...
Si II.....	1808	$15.030 \pm 0.025$	...	...
Fe II.....	1608	$> 14.696$	$14.748 \pm 0.053$	$-1.702 \pm 0.085$
Fe II.....	1611	$< 14.800$	...	...
Co II.....	1466	$< 12.860$	$< 12.860$	$< -1.000$
Co II.....	1574	$< 13.358$	...	...
Ni II.....	1709	$13.579 \pm 0.061$	$13.594 \pm 0.027$	$-1.606 \pm 0.072$
Ni II.....	1741	$13.602 \pm 0.039$	...	...
Ni II.....	1751	$13.592 \pm 0.048$	...	...
Zn II.....	2026	$12.330 \pm 0.049$	$12.330 \pm 0.049$	$-1.290 \pm 0.083$
Zn II.....	2062	$< 12.138$	...	...

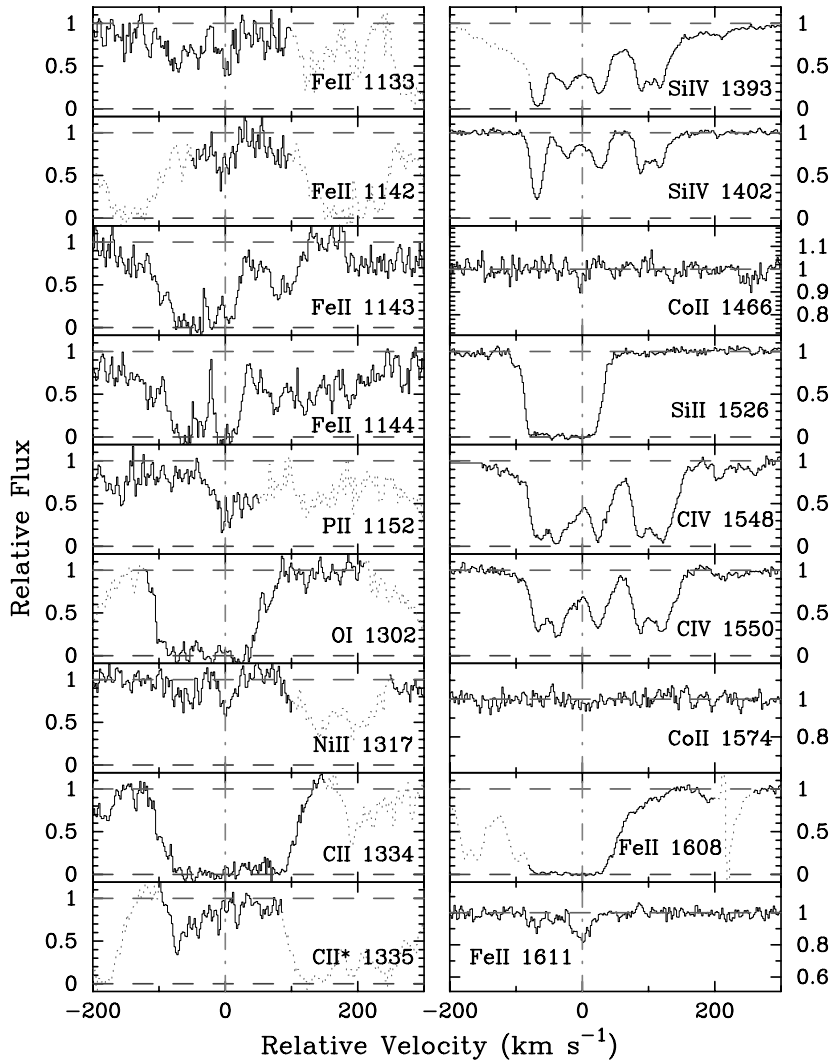


FIG. 24.—Velocity plot of the metal line transitions for the DLA system at  $z = 2.466$  toward Q1223 + 17. The vertical line at  $v = 0$  corresponds to  $z = 2.466083$ . [See the electronic edition of the Journal for a color version of this figure.]

TABLE 25  
IONIC COLUMN DENSITIES: Q1223 + 17,  $z = 2.466$

Ion	$\lambda$	AODM	$N_{\text{adopt}}$	[X/H]
H I .....	1215	$21.500 \pm 0.100$	...	...
C I .....	1656	$< 12.426$	...	...
C II .....	1334	$> 15.155$	$> 15.155$	$> -2.895$
C II .....	1335	$< 14.007$	...	...
C IV .....	1548	$> 14.696$	...	...
C IV .....	1550	$14.658 \pm 0.004$	...	...
O I .....	1302	$> 15.477$	$> 15.477$	$> -2.893$
Al III .....	1862	$12.909 \pm 0.023$	...	...
Si II .....	1526	$> 15.037$	$15.468 \pm 0.008$	$-1.592 \pm 0.100$
Si II .....	1808	$15.468 \pm 0.008$	...	...
Si IV .....	1402	$13.891 \pm 0.004$	...	...
P II .....	1152	$< 13.883$	$< 13.883$	$< -1.147$
Ti II .....	1910	$< 12.252$	$< 12.252$	$< -2.188$
Cr II .....	2056	$13.521 \pm 0.013$	$13.493 \pm 0.010$	$-1.677 \pm 0.100$
Cr II .....	2062	$13.480 \pm 0.018$	...	...
Cr II .....	2066	$13.411 \pm 0.032$	...	...
Fe II .....	1133	$15.098 \pm 0.059$	$15.157 \pm 0.022$	$-1.843 \pm 0.102$
Fe II .....	1142	$15.258 \pm 0.051$	...	...
Fe II .....	1611	$15.152 \pm 0.027$	...	...

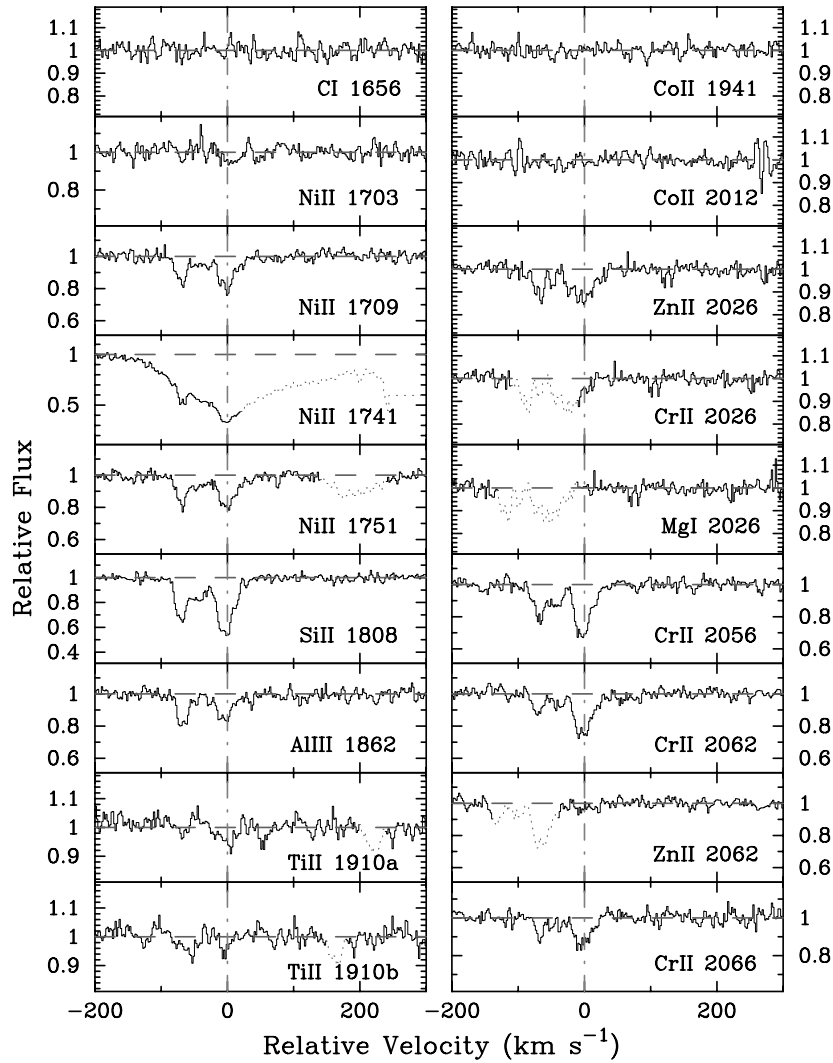


FIG. 24.—Continued

than  $\frac{1}{2}$  the solar value ( $[\text{Ti}/\text{Fe}] < -0.4$ ). In general, a sub-solar Ti/Fe ratio implies significant dust depletion because Ti is more readily locked up into dust grains, but the Zn/Fe ratio is not particularly large as one would expect in a significantly dust depleted region ( $[\text{Zn}/\text{Fe}] = 0.22$ ). Our observations also place a tight constraint on Co/Fe, which is described in greater detail in Ellison, Ryan, & Prochaska (2001).

### 3.20. Q1331+17, $z = 1.776$

An analysis of the damped system toward the very bright quasar Q1331+17 was given by PW99, but a number of transitions were missed (notably Ti II  $\lambda 1910$  and Co II  $\lambda 2012$ ). The new transitions are plotted in Figure 25, and the ionic column densities are given in Table 26.

With respect to the  $N(\text{Zn}^+)$  value presented by PW99, this system exhibits one of the largest Zn/Fe ratios of any

TABLE 25—Continued

Ion	$\lambda$	AODM	$N_{\text{adopt}}$	[X/H]
Co II.....	1466	<13.174	<12.631	<-1.779
Co II.....	1574	<13.122	...	...
Co II.....	1941	<12.917	...	...
Co II.....	2012	<12.631	...	...
Ni II.....	1317	$13.853 \pm 0.051$	$13.949 \pm 0.011$	$-1.801 \pm 0.101$
Ni II.....	1703	<13.817	...	...
Ni II.....	1709	$13.901 \pm 0.020$	...	...
Ni II.....	1751	$14.000 \pm 0.014$	...	...
Zn II.....	2026	$12.550 \pm 0.026$	$12.550 \pm 0.026$	$-1.620 \pm 0.103$
Zn II.....	2062	>11.785	...	...



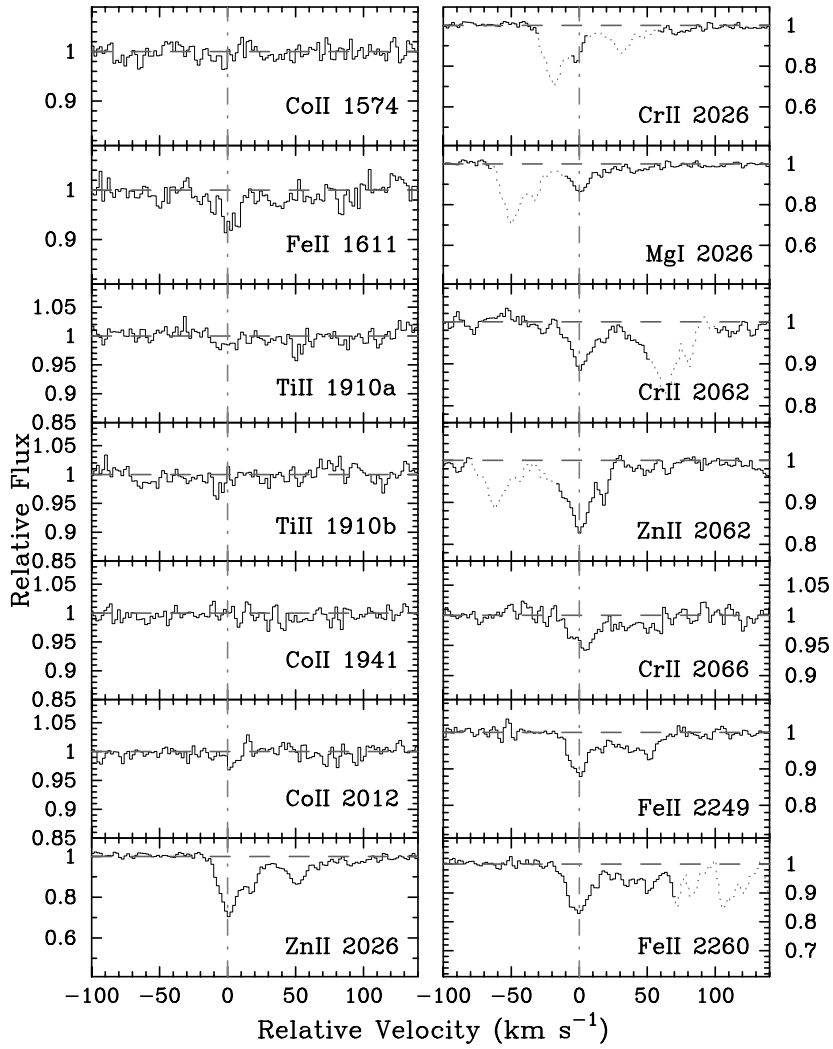


FIG. 25.—Velocity plot of the new metal line transitions for the DLA system at  $z = 1.776$  toward Q1331 + 17. The vertical line at  $v = 0$  corresponds to  $z = 1.77636$ . [See the electronic edition of the *Journal* for a color version of this figure.]

TABLE 26  
IONIC COLUMN DENSITIES: Q1331 + 17,  $z = 1.776$

Ion	$\lambda$	AODM	$N_{\text{adopt}}$	[X/H]
H I.....	1215	$21.176 \pm 0.041$	...	...
C I.....	1560	$13.573 \pm 0.013$	...	...
C I.....	1656	$13.312 \pm 0.012$	...	...
Mg I.....	2026	$12.419 \pm 0.048$	...	...
Ti II.....	1910	$11.836 \pm 0.118$	$11.836 \pm 0.118$	$-2.280 \pm 0.125$
Cr II.....	2056	$12.957 \pm 0.017$	$12.874 \pm 0.012$	$-1.972 \pm 0.043$
Cr II.....	2066	$12.834 \pm 0.034$	...	...
Fe II.....	1608	$14.630 \pm 0.003$	$14.618 \pm 0.001$	$-2.058 \pm 0.041$
Fe II.....	1611	$14.709 \pm 0.046$	...	...
Fe II.....	2249	$14.595 \pm 0.015$	...	...
Fe II.....	2260	$14.647 \pm 0.010$	...	...
Fe II.....	2344	$> 14.723$	...	...
Fe II.....	2374	$14.616 \pm 0.002$	...	...
Fe II.....	2382	$> 14.461$	...	...
Co II.....	1574	$< 12.659$	$< 12.306$	$< -1.780$
Co II.....	1941	$< 12.367$	...	...
Co II.....	2012	$< 12.306$	...	...
Zn II.....	2026 <sup>a</sup>	$12.542 \pm 0.029$	$12.542 \pm 0.029$	$-1.304 \pm 0.050$

<sup>a</sup> The Zn column density is based on a line profile analysis performed with the VPFIT software package.

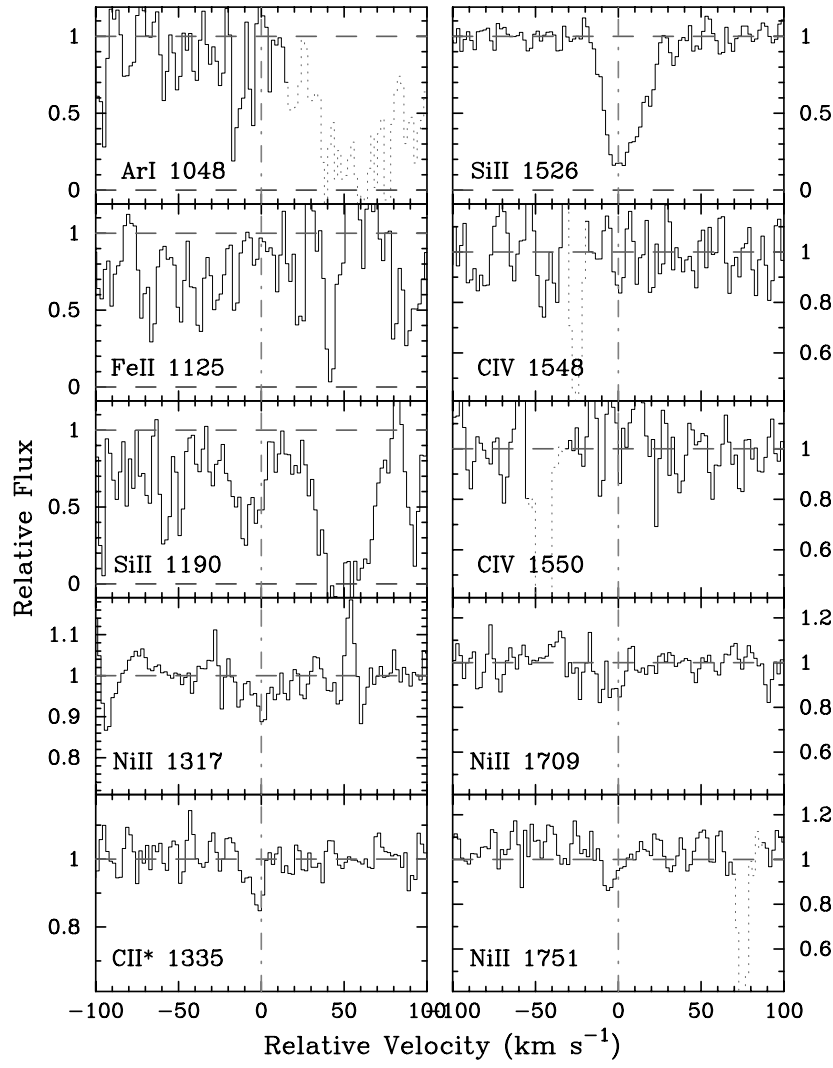


FIG. 26.—Velocity plot of the new metal line transitions for the DLA system at  $z = 3.736$  toward BRI 1346–03. The vertical line at  $v = 0$  corresponds to  $z = 3.73583$ . [See the electronic edition of the *Journal* for a color version of this figure.]

TABLE 27  
IONIC COLUMN DENSITIES: BRI 1346–03,  $z = 3.736$

Ion	$\lambda$	AODM	$N_{\text{adopt}}$	[X/H]
H I.....	1215	$20.720 \pm 0.100$	...	...
C II.....	1335	$12.550 \pm 0.113$	$> 14.486$	$> -2.784$
C IV.....	1548	$< 12.717$	...	...
C IV.....	1550	$< 13.146$	...	...
O I.....	1302	$> 15.018$	$> 15.019$	$> -2.571$
Si II.....	1190	$13.430 \pm 0.122$	$13.948 \pm 0.009$	$-2.332 \pm 0.100$
Si II.....	1304	$13.983 \pm 0.009$	...	...
Si II.....	1526	$13.880 \pm 0.026$	...	...
Ar I.....	1048	$< 13.114$	$< 13.113$	$< -2.127$
Fe II.....	1125	$< 14.126$	$< 14.126$	$< -2.094$
Co II.....	1574	$< 13.260$	$< 13.260$	$< -0.370$
Ni II.....	1317	$< 12.759$	$< 12.760$	$< -2.210$
Ni II.....	1370	$< 12.876$	...	...
Ni II.....	1709	$< 13.345$	...	...
Ni II.....	1741	$< 13.284$	...	...
Ni II.....	1751	$< 13.428$	...	...

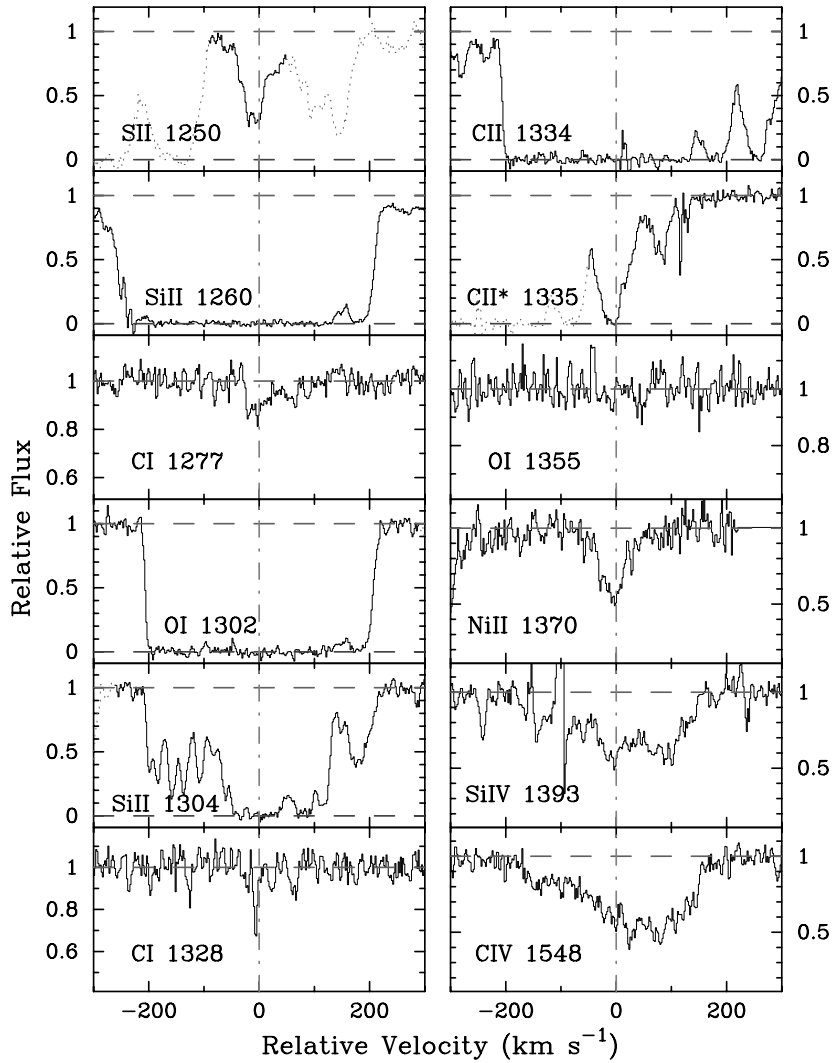


FIG. 27.—Velocity plot of the metal line transitions for the DLA system at  $z = 4.224$  toward PSS 1443 + 27. The vertical line at  $v = 0$  corresponds to  $z = 4.224099$ . [See the electronic edition of the Journal for a color version of this figure.]

TABLE 28  
IONIC COLUMN DENSITIES: PSS 1443 + 27,  $z = 4.224$

Ion	$\lambda$	AODM	$N_{\text{adopt}}$	[X/H]
H I.....	1215	$20.800 \pm 0.100$	...	...
C I.....	1277	$13.446 \pm 0.037$	...	...
C I.....	1328	$13.367 \pm 0.090$	...	...
C I.....	1656	$13.041 \pm 0.133$	...	...
C II.....	1334	$> 15.613$	$> 15.612$	$> -1.738$
C II.....	1335	$> 14.709$	...	...
C IV.....	1548	$14.245 \pm 0.009$	...	...
C IV.....	1550	$14.213 \pm 0.017$	...	...
O I.....	1302	$> 16.048$	$> 16.048$	$> -1.622$
O I.....	1355	$< 17.734$	...	...
Al II.....	1670	$> 13.959$	$> 13.958$	$> -1.332$
Si II.....	1304	$> 15.434$	$> 15.434$	$> -0.926$
Si IV.....	1393	$13.706 \pm 0.011$	...	...
S II.....	1253	...	...	...
Fe II.....	1608	$> 15.101$	$15.204 \pm 0.056$	$-1.096 \pm 0.115$
Fe II.....	1611	$15.204 \pm 0.056$	...	...
Co II.....	1574	$< 13.508$	$< 13.509$	$< -0.201$
Ni II.....	1370	$14.079 \pm 0.025$	$14.091 \pm 0.024$	$-0.959 \pm 0.103$
Ni II.....	1709	$14.229 \pm 0.069$	...	...
Ni II.....	1741	$13.877 \pm 0.074$	...	...

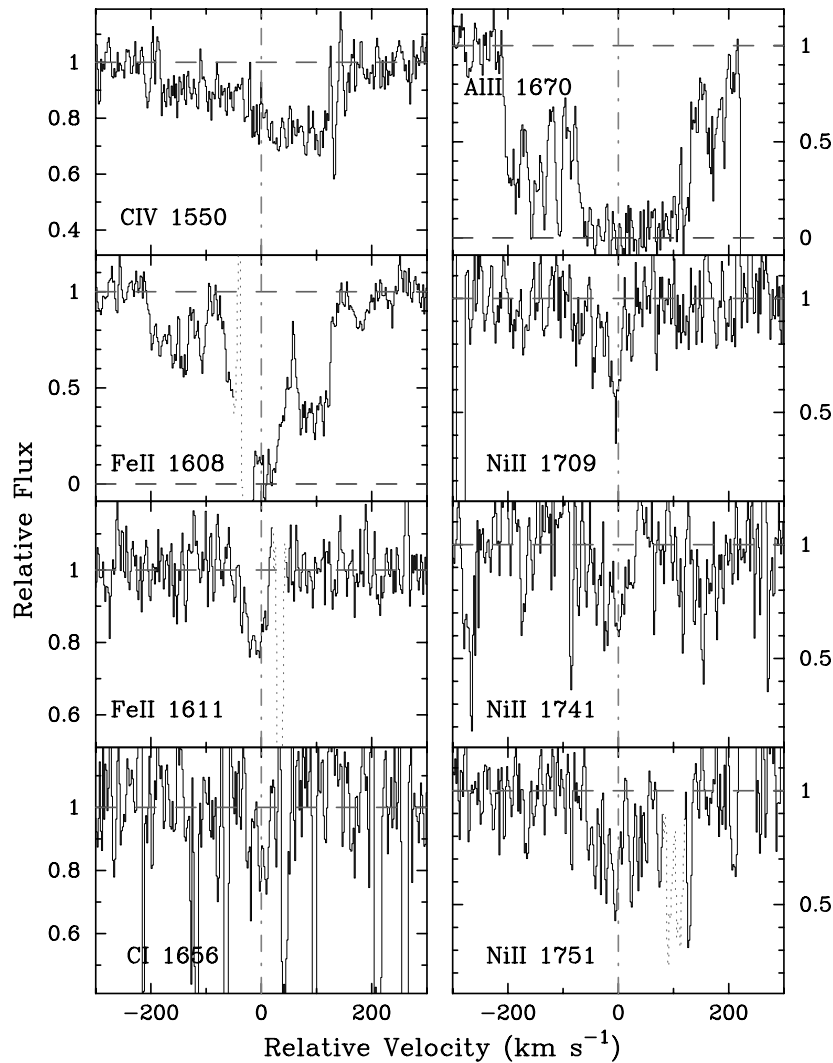


FIG. 27.—Continued

damped system. This  $N(\text{Zn}^+)$  value is nearly 0.3 dex higher than the value reported in Pettini et al. (1994), however, because we did not correct for possible contamination from the Mg I  $\lambda 2026$  transition. Although a significant feature is apparent at  $v = 0 \text{ km s}^{-1}$  of the Mg I  $\lambda 2026$  profile, this feature is perfectly aligned with an absorption feature at  $v = 52 \text{ km s}^{-1}$  in the unsaturated Fe II profiles. Furthermore, the  $N(\text{Zn}^+)$  value from Zn II  $\lambda 2062$  is identical to the value derived from Zn II  $\lambda 2026$  using the AODM method. We suspect, however, that this is a coincidence resulting from blending between the Zn II  $\lambda 2062$  and Cr II  $\lambda 2062$  profiles. Performing a detailed line profile analysis of the Zn and Cr lines and including Mg I  $\lambda 2026$ , we find  $\log N(\text{Zn}^+) = 12.542 \pm 0.029$  and  $\log N(\text{Mg}^0) = 12.419 \pm 0.048$ . We discuss this issue further and its impact on studies of Zn in Paper II, § 2.1.6.

In addition to the large Zn/Fe ratio, this system shows rarely observed C I absorption and a significant subsolar Ti/Fe ratio. Altogether the chemical abundances of this system represent the most compelling evidence for dust depletion in any DLA system. It is particularly important to note, therefore, that it is one of the brightest (apparent magnitude) quasars observed in our sample. In Paper II, § 5

we consider the obscuration of this quasar due to this damped system and the implications for dust obscuration in general.

This DLA system is one of the few cases in which one can derive  $N(\text{Fe}^+)$  values from both Fe II  $\lambda\lambda 1608$  and  $1611$ . Furthermore, our observations also cover several of the Fe II transitions longward of  $2000 \text{ \AA}$ , including Fe II  $\lambda\lambda 2249$  and  $2260$ , which are the principal diagnostics of  $\text{Fe}^+$  in the Galactic ISM. Examining Table 26, one notes that nearly all of the  $N(\text{Fe}^+)$  values are consistent at the  $2\sigma$  level and all are in accordance at  $3\sigma$ . One also notes that  $N(\text{Fe II } \lambda 1611)$  exceeds all of the other measurements, suggesting that it is unlikely that the Raassen & Uylings (1998) analysis overestimated the Fe II  $\lambda 1611$  oscillator strength, at least relative to the other Fe II transitions.

### 3.21. BRI 1346–03, $z = 3.736$

Our additional observations blueward of the data presented in PW99 provide coverage of a few new transitions (Fig. 26 and Table 27). Unfortunately, we still do not have coverage of a single unsaturated Fe II profile or any other Fe peak metal transition. Therefore, we have adopted Al as a proxy for Fe (i.e., assume  $[\text{Fe}/\text{H}] = [\text{Al}/\text{H}]$ ) and in this

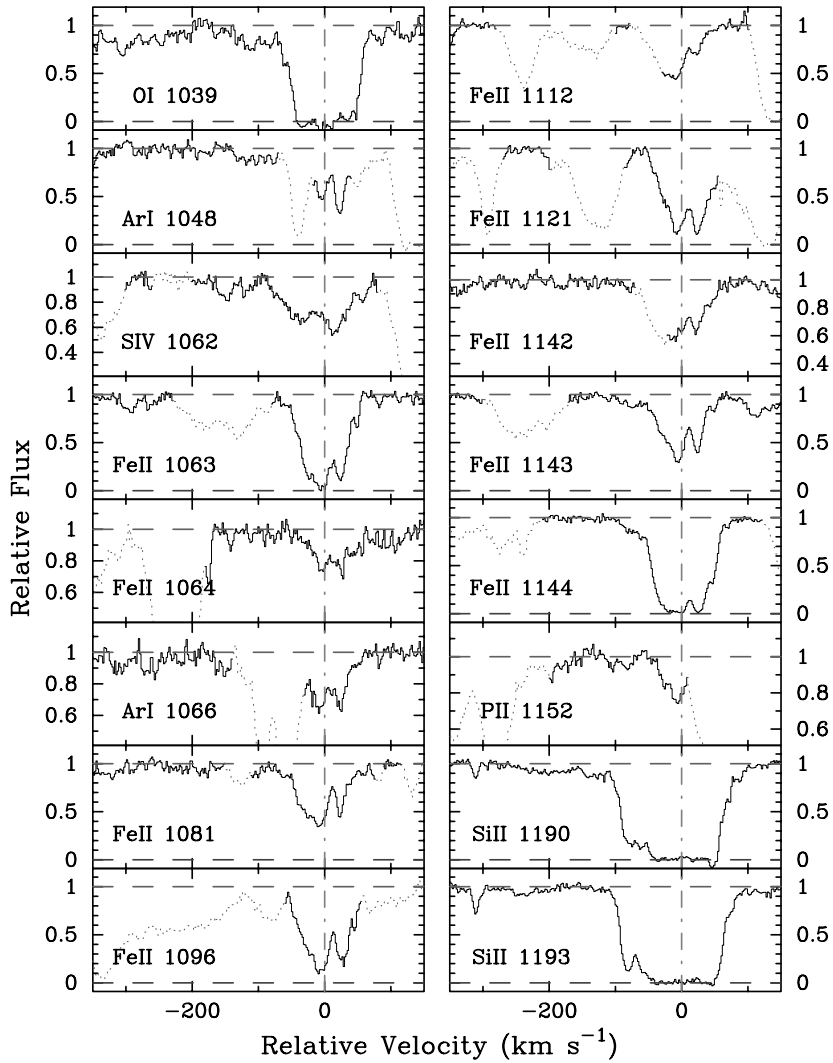


FIG. 28.—Velocity plot of the new metal line transitions for the DLA system at  $z = 2.625$  toward Q1759 + 75. The vertical line at  $v = 0$  corresponds to  $z = 2.62530$ . [See the electronic edition of the *Journal* for a color version of this figure.]

TABLE 29  
IONIC COLUMN DENSITIES: Q1759 + 75,  $z = 2.625$

Ion	$\lambda$	AODM	$N_{\text{adopt}}$	[X/H]
H I .....	1215	$20.800 \pm 0.100$	...	...
C I .....	1656	$< 12.336$	...	...
C II .....	1334	$> 15.300$	$> 15.300$	$> -2.050$
C II .....	1335	$13.138 \pm 0.032$	...	...
O I .....	1039	$> 16.261$	$> 16.261$	$> -1.409$
O I .....	1302	$> 15.759$	...	...
Si II .....	1190	$> 14.928$	$15.536 \pm 0.008$	$-0.824 \pm 0.100$
Si II .....	1193	$> 14.614$	...	...
Si II .....	1260	$> 14.396$	...	...
Si II .....	1304	$> 15.198$	...	...
Si II .....	1808	$15.536 \pm 0.008$	...	...
P II .....	1152	$> 13.046$	$> 13.047$	$> -1.283$
S II .....	1250	$15.243 \pm 0.009$	$15.243 \pm 0.010$	$-0.757 \pm 0.100$
S II .....	1253	$< 15.486$	...	...
S II .....	1259	$< 15.335$	...	...
Ar I .....	1048	$< 13.714$	$< 13.714$	$< -1.606$
Ar I .....	1066	$< 14.053$	...	...
Fe II .....	1062	$14.860 \pm 0.037$	$15.091 \pm 0.004$	$-1.209 \pm 0.100$

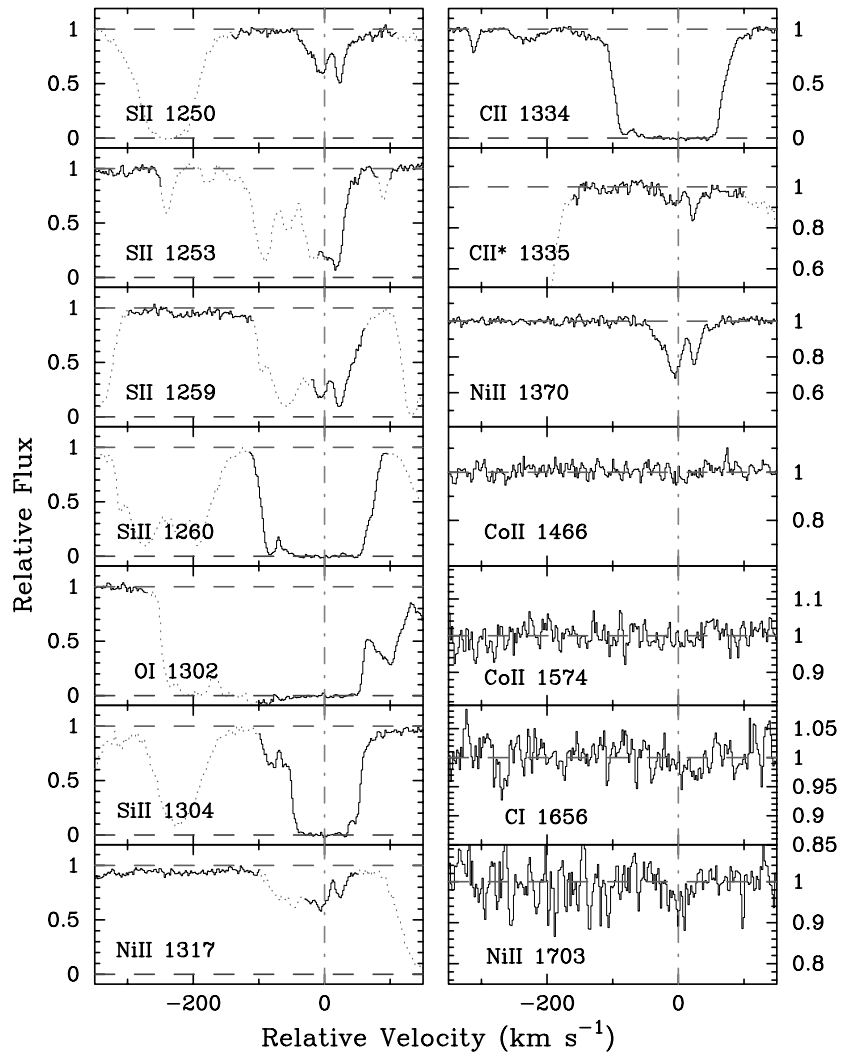


FIG. 28.—Continued

TABLE 29—Continued

Ion	$\lambda$	AODM	$N_{\text{adopt}}$	[X/H]
Fe II	1063	> 15.002	...	...
Fe II	1063	$15.287 \pm 0.020$	...	...
Fe II	1081	$15.182 \pm 0.007$	...	...
Fe II	1096	$15.059 \pm 0.007$	...	...
Fe II	1112	< 15.389	...	...
Fe II	1121	< 15.260	...	...
Fe II	1142	< 15.565	...	...
Fe II	1143	$15.079 \pm 0.005$	...	...
Fe II	1144	> 15.051	...	...
Fe II	1608	> 15.077	...	...
Fe II	1611	$14.923 \pm 0.034$	...	...
Co II	1466	< 13.066	< 13.019	< -0.691
Co II	1466	< 13.019	...	...
Co II	1574	< 13.108	...	...
Ni II	1317	< 14.248	$13.802 \pm 0.007$	$-1.248 \pm 0.100$
Ni II	1370	$13.766 \pm 0.010$	...	...
Ni II	1454	$13.791 \pm 0.039$	...	...
Ni II	1703	< 13.908	...	...
Ni II	1709	$13.929 \pm 0.020$	...	...
Ni II	1741	$13.841 \pm 0.017$	...	...
Ni II	1751	$13.868 \pm 0.021$	...	...

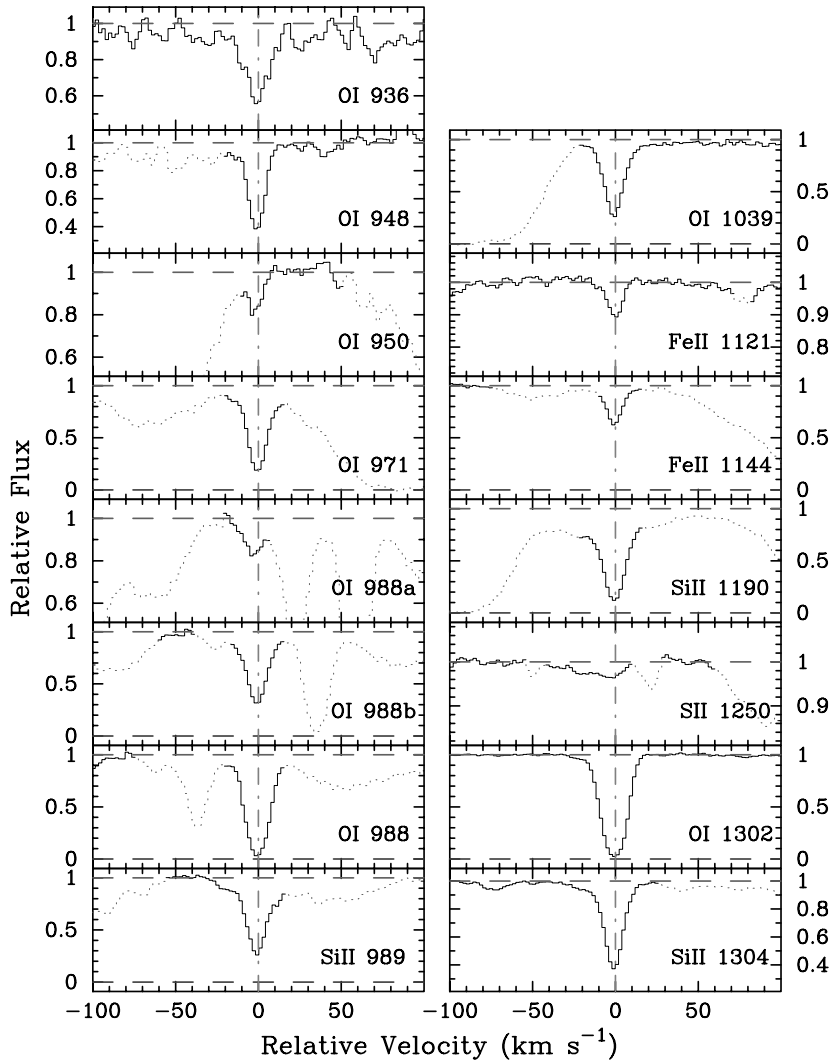


FIG. 29.—Velocity plot of the metal line transitions for the DLA system at  $z = 2.844$  toward Q1946+76. The vertical line at  $v = 0$  corresponds to  $z = 2.8443$ . [See the electronic edition of the Journal for a color version of this figure.]

manner include the system in the metallicity and relative abundance analyses of Paper II. The implied Si/Fe ratios match typical values. If the feature at  $v = 0$  km s<sup>-1</sup> in the Ni II  $\lambda$ 1317 profile is not noise or a coincident metal line, it

implies a very large Ni/Al ratio indicating that we might be underestimating  $N(\text{Fe}^+)$ . For the moment, we consider it as an upper limit.

Our new observations also cover the C IV doublet at 1550

TABLE 30  
IONIC COLUMN DENSITIES: Q1946+7658,  $z = 2.844$

Ion	$\lambda$	AODM	$N_{\text{adopt}}$	[X/H]
H I.....	1215	$20.270 \pm 0.060$	...	...
O I.....	936	$15.036 \pm 0.030$	$14.819 \pm 0.007$	$-2.321 \pm 0.060$
O I.....	948	$14.835 \pm 0.025$	...	...
O I.....	971	$< 14.725$	...	...
O I.....	988	$< 15.244$	...	...
O I.....	988	$< 14.862$	...	...
O I.....	988	$> 14.627$	...	...
O I.....	1039	$14.811 \pm 0.008$	...	...
O I.....	1302	$> 14.587$	...	...
Si II.....	1190	$< 13.579$	$13.602 \pm 0.005$	$-2.228 \pm 0.060$
Si II.....	1304	$13.602 \pm 0.005$	...	...
S II.....	1250	$< 13.491$	$< 13.491$	$< -1.979$
Fe II.....	1121	$13.241 \pm 0.057$	$13.238 \pm 0.009$	$-2.532 \pm 0.061$
Fe II.....	1144	$13.238 \pm 0.009$	...	...

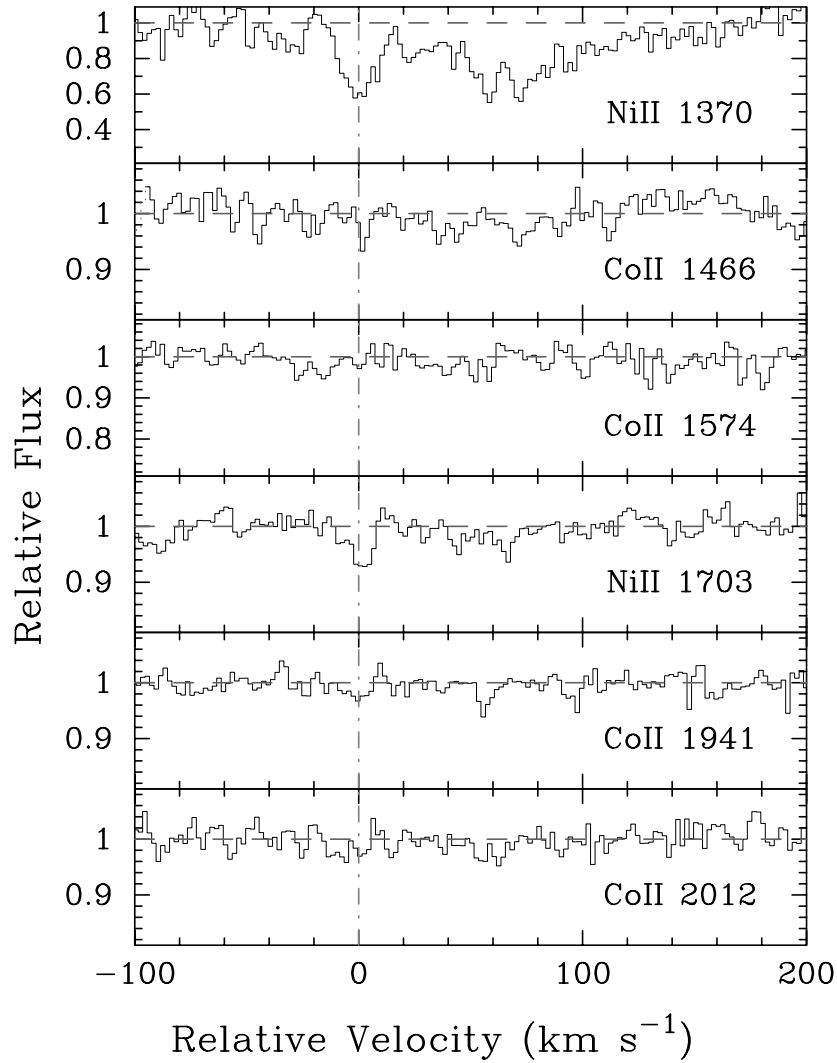


FIG. 30.—Velocity plot of the new metal line transitions for the DLA system at  $z = 1.920$  toward Q2206–19. The vertical line at  $v = 0$  corresponds to  $z = 1.920$ . [See the electronic edition of the *Journal* for a color version of this figure.]

TABLE 31  
IONIC COLUMN DENSITIES: Q2206–19,  $z = 1.920$

Ion	$\lambda$	AODM	$N_{\text{adopt}}$	[X/H]
H I.....	1215	$20.653 \pm 0.071$	...	...
Al II.....	1670	$> 14.070$	$> 14.070$	$> -1.073$
Si II.....	1526	$> 15.275$	$15.796 \pm 0.005$	$-0.417 \pm 0.071$
Si II.....	1808	$15.796 \pm 0.005$	...	...
Ti II.....	1910	$12.768 \pm 0.040$	$12.768 \pm 0.040$	$-0.825 \pm 0.081$
Cr II.....	2056	$13.627 \pm 0.009$	$13.638 \pm 0.007$	$-0.685 \pm 0.071$
Cr II.....	2066	$13.665 \pm 0.013$	...	...
Fe II.....	1608	$> 15.376$	$15.296 \pm 0.018$	$-0.857 \pm 0.073$
Fe II.....	1611	$15.296 \pm 0.018$	...	...
Co II.....	1574	$12.960 \pm 0.139$	$12.960 \pm 0.140$	$-0.603 \pm 0.157$
Co II.....	1941	$< 12.814$	...	...
Co II.....	2012	$< 12.832$	...	...
Ni II.....	1370	$14.154 \pm 0.022$	$14.232 \pm 0.005$	$-0.671 \pm 0.071$
Ni II.....	1703	$13.807 \pm 0.116$	...	...
Ni II.....	1709	$14.221 \pm 0.009$	...	...
Ni II.....	1741	$14.239 \pm 0.006$	...	...
Ni II.....	1751	$14.266 \pm 0.010$	...	...
Zn II.....	2026	$12.914 \pm 0.009$	$12.914 \pm 0.009$	$-0.409 \pm 0.072$



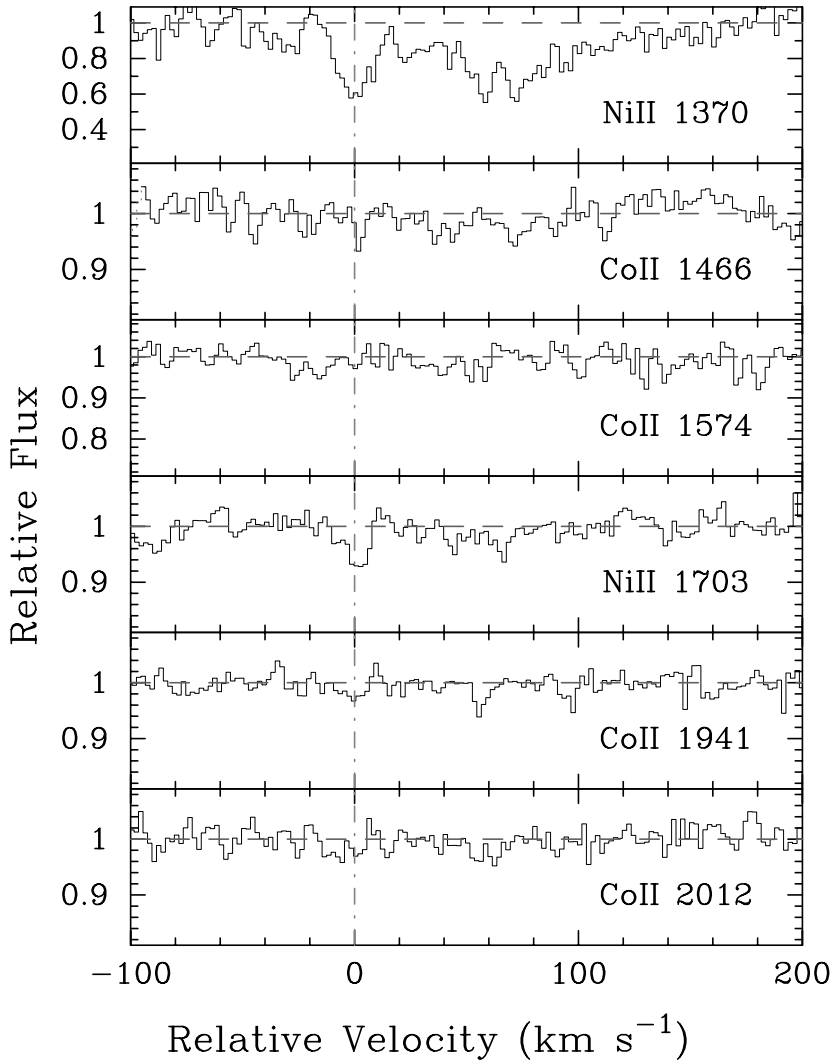


FIG. 31.—Velocity plot of the new metal line transitions for the DLA system at  $z = 2.076$  toward Q2206–19. The vertical line at  $v = 0$  corresponds to  $z = 2.07623$ . [See the electronic edition of the *Journal* for a color version of this figure.]

TABLE 32  
IONIC COLUMN DENSITIES: Q2206–19,  $z = 2.076$

Ion	$\lambda$	AODM	$N_{\text{adopt}}$	[X/H]
H I .....	1215	$20.431 \pm 0.060$	...	...
C II .....	1334	$> 14.207$	$> 14.207$	$> -2.774$
C II .....	1335	$< 13.157$	...	...
C IV .....	1548	$13.707 \pm 0.005$	...	...
C IV .....	1550	$13.739 \pm 0.008$	...	...
O I .....	1302	$> 14.540$	$> 14.540$	$> -2.761$
Al II .....	1670	$12.158 \pm 0.012$	$12.158 \pm 0.012$	$-2.763 \pm 0.061$
Al III .....	1854	$11.515 \pm 0.098$	...	...
Al III .....	1862	$11.719 \pm 0.103$	...	...
Si II .....	1304	$13.682 \pm 0.035$	$13.682 \pm 0.035$	$-2.309 \pm 0.069$
Si IV .....	1402	$12.845 \pm 0.016$	...	...
Cr II .....	2056	$< 11.911$	$< 11.911$	$< -2.190$
Cr II .....	2062	$< 12.158$	...	...
Fe II .....	1608	$13.325 \pm 0.017$	$13.325 \pm 0.017$	$-2.606 \pm 0.062$
Fe II .....	1611	$< 13.948$	...	...
Ni II .....	1709	$< 12.585$	$< 12.585$	$< -2.096$
Ni II .....	1751	$< 12.591$	...	...
Zn II .....	2026	$< 11.199$	$< 11.199$	$< -1.902$

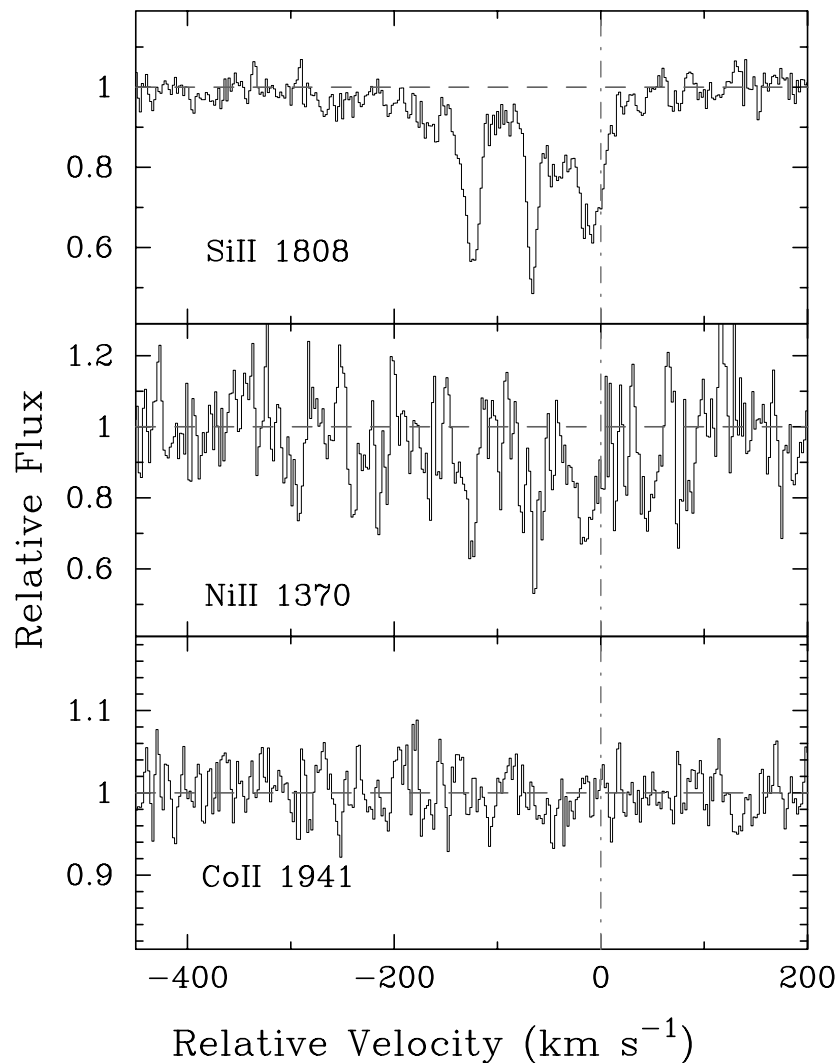


FIG. 32.—Velocity plot of C II\*  $\lambda$ 1335 transition for the DLA system at  $z = 1.864$  toward Q2230+02. For comparison, we plot the Si II  $\lambda$ 1304 and C II  $\lambda$ 1334 profiles. The vertical line at  $v = 0$  corresponds to  $z = 1.864388$ . [See the electronic edition of the *Journal* for a color version of this figure.]

Å. Although the spectra are particularly noisy over this region, there is no obvious C IV absorption. This marks the first DLA system with no detectable C IV absorption, and we note in passing a possible trend of weaker C IV absorption at  $z > 3$ .

### 3.22. PSS 1443+27, $z = 4.224$

This  $z > 4$  DLA system was discovered by Storrie-Lombardi & Wolfe (2000), who determined the  $N(\text{H I})$  value from a spectrum obtained using LRIS at Keck observatories. Its very high metallicity was first reported in Pro-

TABLE 33  
IONIC COLUMN DENSITIES: Q2230+02,  $z = 1.864$

Ion	$\lambda$	AODM	$N_{\text{adopt}}$	[X/H]
H I.....	1215	$20.850 \pm 0.084$	...	...
Fe II.....	1608	$> 15.160$	$15.184 \pm 0.016$	$-1.166 \pm 0.086$
Fe II.....	1611	$15.148 \pm 0.084$	...	...
Fe II.....	2249	$15.119 \pm 0.036$	...	...
Fe II.....	2260	$15.210 \pm 0.019$	...	...
Fe II.....	2344	$> 15.039$	...	...
Fe II.....	2374	$> 15.213$	...	...
Fe II.....	2382	$> 14.744$	...	...
Co II.....	1941	$< 13.118$	$< 13.118$	$< -0.642$
Ni II.....	1370	$14.161 \pm 0.052$	$14.128 \pm 0.011$	$-0.972 \pm 0.085$
Ni II.....	1709	$14.171 \pm 0.014$	...	...
Ni II.....	1741	$14.097 \pm 0.023$	...	...
Ni II.....	1751	$14.049 \pm 0.028$	...	...

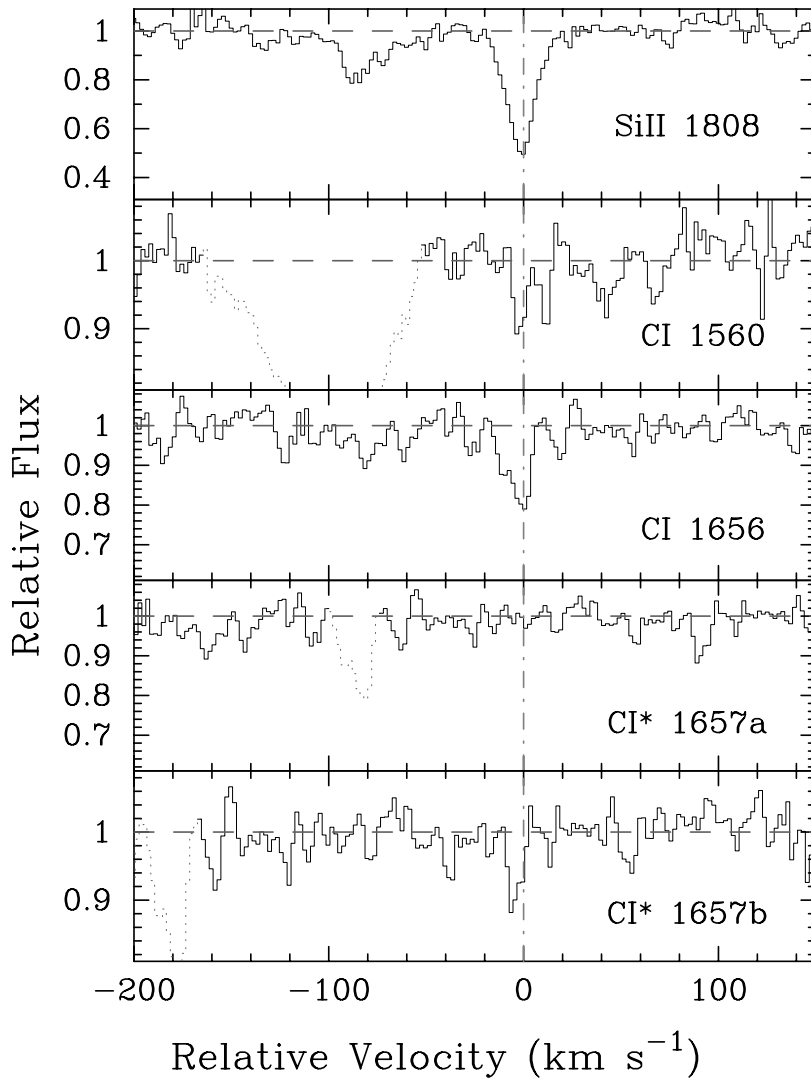


FIG. 33.—Velocity plot of the new metal line transitions for the DLA system at  $z = 2.066$  toward Q2231–00. For comparison, we also plot the Si II  $\lambda 1808$  profile. The vertical line at  $v = 0$  corresponds to  $z = 2.066150$ . [See the electronic edition of the *Journal* for a color version of this figure.]

chaska & Wolfe (2000). We have since acquired further observations of this system that confirm the  $[\text{Fe}/\text{H}]$  metallicity. In particular, we observed the Ni II  $\lambda\lambda 1370, 1709$ , and 1741 transitions at reasonably high S/N and found  $[\text{Ni}/\text{H}] \approx [\text{Fe}/\text{H}]$ . Figure 27 presents the transitions observed for this system, and the ionic column densities are presented in Table 28.

In passing, we note the remarkable C II\*  $\lambda 1335$  profile, which is heavily saturated and suggests a large star formation rate for this system (Wolfe et al. 2001). In addition, we identify possible absorption from two C I profiles, which we

expect is not due to coincident metal line systems. Unfortunately, our observations did not cover the stronger C II  $\lambda 1556$  profile, and the strongest C I  $\lambda 1656$  profile is located within a forest of sky lines.

### 3.23. Q1759+75, $z = 2.625$

This system was presented in PW99 and has been subsequently analyzed by Outram, Chaffee, & Carswell (1999). Here we present an analysis of our spectrum blueward of Ly $\alpha$  emission. Figure 28 presents the transitions and Table 29 the column densities.

TABLE 34  
IONIC COLUMN DENSITIES: Q2231–002,  $z = 2.066$

Ion	$\lambda$	AODM	$N_{\text{adopt}}$	$[\text{X}/\text{H}]$
H I.....	1215	$20.560 \pm 0.100$	...	...
C I.....	1656	$12.701 \pm 0.035$	...	...
C I.....	1657	$12.662 \pm 0.108$	...	...
Co II.....	1941	$< 12.816$	$< 12.816$	$< -0.654$

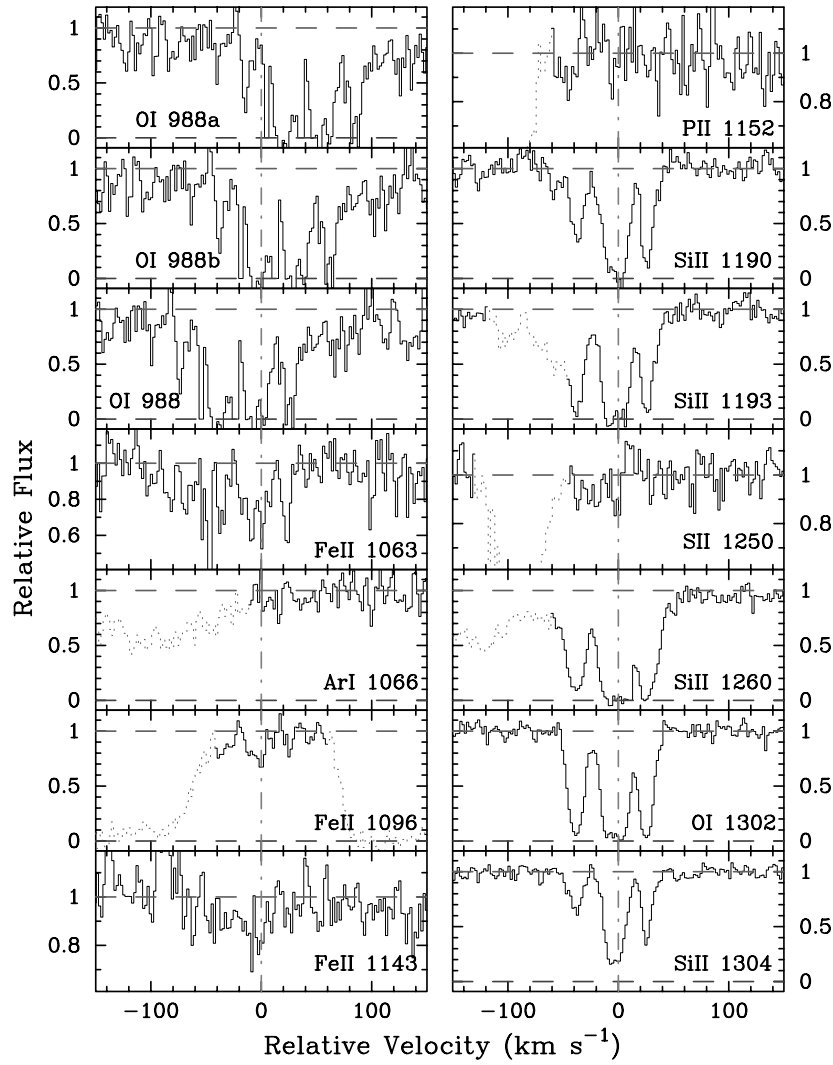


FIG. 34.—Velocity plot of the metal line transitions for the DLA system at  $z = 2.538$  toward Q2344 + 12. The vertical line at  $v = 0$  corresponds to  $z = 2.53790$ . [See the electronic edition of the Journal for a color version of this figure.]

TABLE 35  
IONIC COLUMN DENSITIES: Q2344 + 12,  $z = 2.538$

Ion	$\lambda$	AODM	$N_{\text{adopt}}$	[X/H]
H I .....	1215	$20.360 \pm 0.100$	...	...
C II .....	1334	$> 14.646$	$> 14.645$	$> -2.265$
C II .....	1335	$< 12.831$	...	...
O I .....	988	$> 15.031$	$> 15.031$	$> -2.199$
O I .....	1302	$> 15.020$	...	...
O I .....	1355	$< 17.814$	...	...
Si II .....	1190	$> 14.131$	$14.179 \pm 0.012$	$-1.741 \pm 0.101$
Si II .....	1193	$> 14.007$	...	...
Si II .....	1260	$> 13.838$	...	...
Si II .....	1304	$14.179 \pm 0.012$	...	...
Si IV .....	1393	$12.569 \pm 0.087$	...	...
P II .....	1152	$< 12.744$	$< 12.744$	$< -1.146$
S II .....	1250	$< 14.201$	$< 14.201$	$< -1.359$
Ar I .....	1066	$< 13.262$	$< 13.262$	$< -1.618$
Fe II .....	1063	$14.021 \pm 0.046$	$14.030 \pm 0.032$	$-1.830 \pm 0.105$
Fe II .....	1096	$14.007 \pm 0.053$	...	...
Fe II .....	1143	$14.147 \pm 0.077$	...	...
Ni II .....	1317	$< 12.814$	$< 12.814$	$< -1.796$
Ni II .....	1370	$< 12.999$	...	...

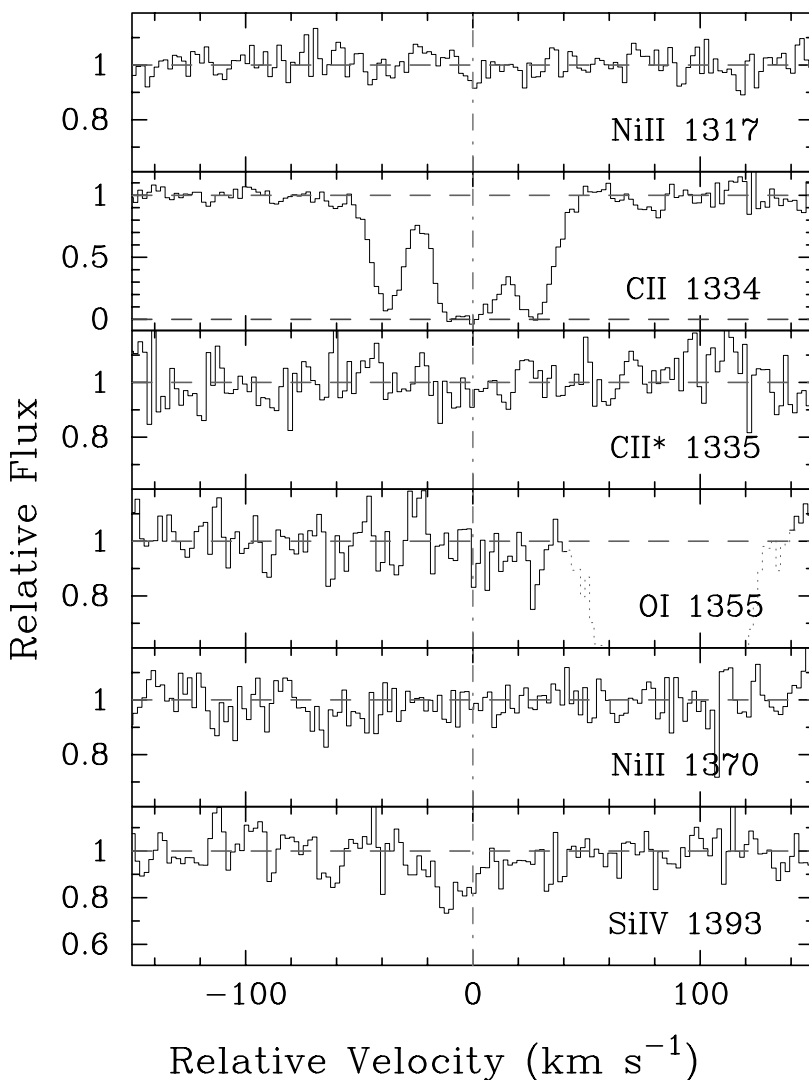


FIG. 34.—Continued

Our observations present measurements of a number of lines in the Ly $\alpha$  forest. In particular, we have excellent coverage of the far-ultraviolet (FUV) Fe II transitions, good measurements of the N I triplets at 1134 and 1200 Å, moderate limits on Ar I and O I, and an excellent measurement of  $N(\text{S}^+)$ . Regarding the Fe II lines, we find very good agreement between the many transitions, which confirms the  $f$ -values measured by Howk et al. (2000). The only exception is Fe II  $\lambda$ 1062 (not analyzed by Howk et al. 2000), whose  $f$ -value appears to be systematically high. We recommend using a value  $\approx 0.2$  dex below the value reported by Morton (1991). Finally, we point out significant absorption at  $v \approx -300$  km s $^{-1}$  in the Si II  $\lambda\lambda$ 1190 and 1193 transitions, which coincide with a strong feature in C IV and a weaker feature in Al II  $\lambda$ 1670 (PW99). We suspect that this metal line system corresponds to a nearby Lyman limit system although there is no significant evidence for asymmetry in the Ly $\alpha$  profile.

### 3.24. Q1946+76, $z = 2.844$

Kirkman & Tytler (1997) analyzed this very high S/N spectrum of Q1946+76 to describe the Ly $\alpha$  forest at

$z \sim 2.8$ . Here we analyze the metal line transitions for the system at  $z = 2.844$ , ignoring the probably DLA system at  $z = 1.73$  because we have no measure of its H I column density. Figure 29 presents the metal line profiles for the  $z = 2.844$  system, and Table 30 summarizes the column density measurements. For the H I column density we adopt the value presented in L96. This system is notable for providing one of the few cases in which one can accurately determine  $N(\text{O}^0)$ . The observed O/Fe ratio is enhanced relative to solar, but at a lower level than metal-poor halo stars with comparable metallicity. Interestingly, the implied O/Si ratio is subsolar, which is almost never observed in metal-poor stars. Nevertheless, we believe that the  $N(\text{O}^0)$  value is accurate. In a separate paper we examine the N/O ratio of this system.

### 3.25. Q2206–19, $z = 1.920$ and 2.076

In Figures 30 and 31 we show a number of transitions left unanalyzed by Prochaska & Wolfe (1997) and PW99 for the two DLA systems toward Q2206–19. Furthermore, we now consider only ionic column densities measured with the AODM in order to coincide with the rest of the data-

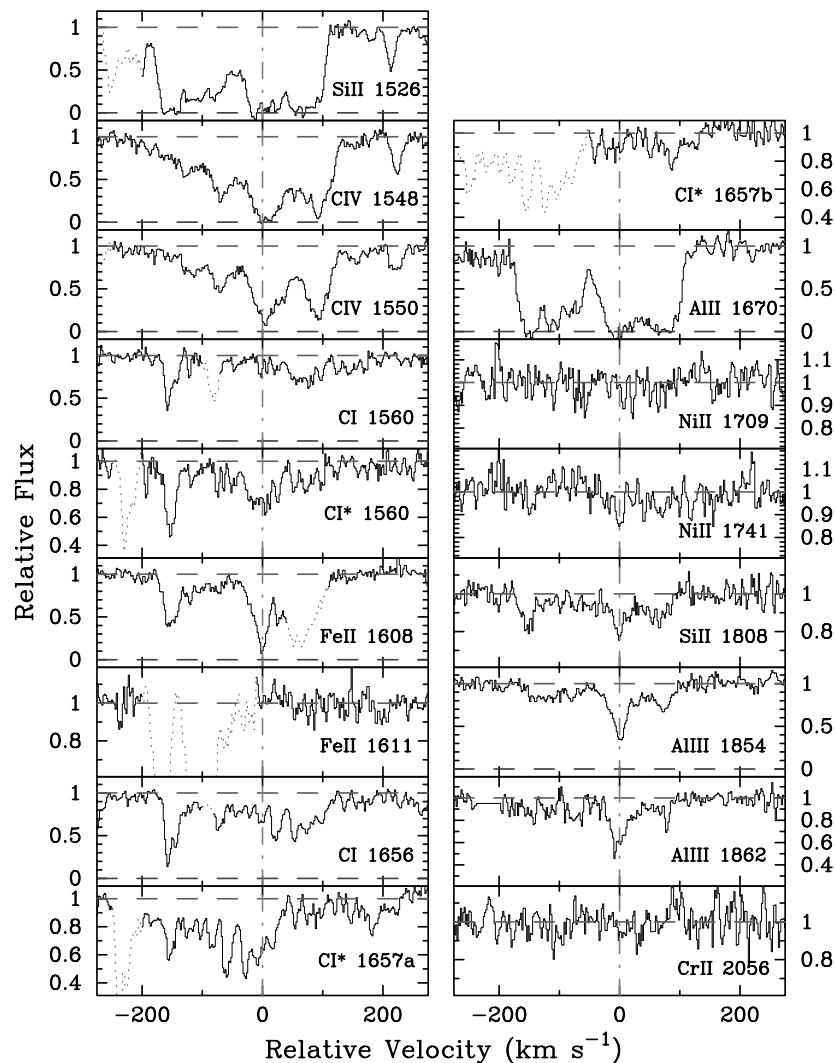


FIG. 35.—Velocity plot of the metal line transitions for the DLA system at  $z = 2.426$  toward Q2348–01. The vertical line at  $v = 0$  corresponds to  $z = 2.426301$ . [See the electronic edition of the *Journal* for a color version of this figure.]

base. As we showed in Prochaska & Wolfe (1997), there is very little difference between the abundances derived from a Voigt profile analysis and those from the AODM. All of the values are listed in Tables 31 and 32.

### 3.26. Q2230+02, $z = 1.864$

This system was extensively analyzed in PW99. We simply add a limit on  $N(\text{Co}^+)$  from the  $\text{Co II } \lambda 1941$  transition and a measurement for  $\text{Ni II } \lambda 1370$  (Fig. 32 and Table

TABLE 36  
IONIC COLUMN DENSITIES: Q2348–01,  $z = 2.426$

Ion	$\lambda$	AODM	$N_{\text{adopt}}$	[X/H]
H I .....	1215	$20.500 \pm 0.100$	...	...
C IV .....	1548	$> 14.705$	...	...
C IV .....	1550	$14.767 \pm 0.008$	...	...
Al II .....	1670	$> 13.939$	$> 13.939$	$> -1.051$
Al III .....	1854	$13.379 \pm 0.011$	...	...
Al III .....	1862	$13.515 \pm 0.021$	...	...
Si II .....	1526	$> 15.160$	$15.365 \pm 0.022$	$-0.695 \pm 0.102$
Si II .....	1808	$15.365 \pm 0.022$	...	...
Cr II .....	2056	$< 12.713$	$< 12.713$	$< -1.457$
Fe II .....	1608	$14.614 \pm 0.012$	$14.614 \pm 0.012$	$-1.386 \pm 0.101$
Ni II .....	1709	$13.434 \pm 0.109$	$13.350 \pm 0.104$	$-1.400 \pm 0.144$
Ni II .....	1741	$13.350 \pm 0.104$	...	...

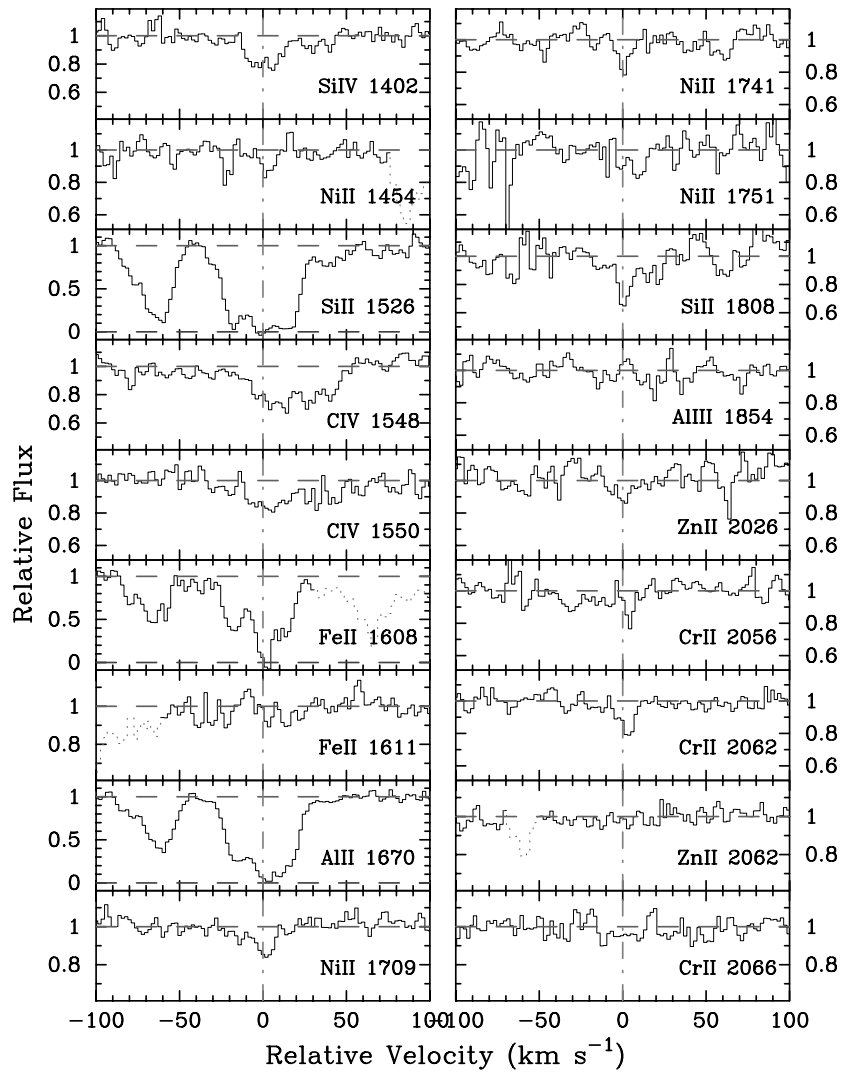


FIG. 36.—Velocity plot of the metal line transitions for the DLA system at  $z = 2.615$  toward Q2348–01. The vertical line at  $v = 0$  corresponds to  $z = 2.614714$ . [See the electronic edition of the Journal for a color version of this figure.]

TABLE 37  
IONIC COLUMN DENSITIES: Q2348–01,  $z = 2.615$

Ion	$\lambda$	AODM	$N_{\text{adopt}}$	[X/H]
H I .....	1215	$21.300 \pm 0.100$	...	...
C IV .....	1548	$13.291 \pm 0.024$	...	...
C IV .....	1550	$13.336 \pm 0.046$	...	...
Al II .....	1670	$> 13.139$	$> 13.139$	$> -2.651$
Al III .....	1854	$< 12.203$	...	...
Si II .....	1526	$> 14.562$	$14.892 \pm 0.072$	$-1.968 \pm 0.123$
Si II .....	1808	$14.892 \pm 0.072$	...	...
Si IV .....	1402	$12.899 \pm 0.051$	...	...
Cr II .....	2056	$12.619 \pm 0.100$	$12.674 \pm 0.060$	$-2.296 \pm 0.117$
Cr II .....	2062	$12.718 \pm 0.075$	...	...
Fe II .....	1608	$> 14.483$	$14.573 \pm 0.088$	$-2.227 \pm 0.133$
Fe II .....	1611	$< 14.663$	...	...
Ni II .....	1454	$13.121 \pm 0.110$	$13.193 \pm 0.074$	$-2.357 \pm 0.124$
Ni II .....	1709	$13.296 \pm 0.097$	...	...
Ni II .....	1741	$< 13.100$	...	...
Zn II .....	2026	$< 11.871$	$< 11.871$	$< -2.099$

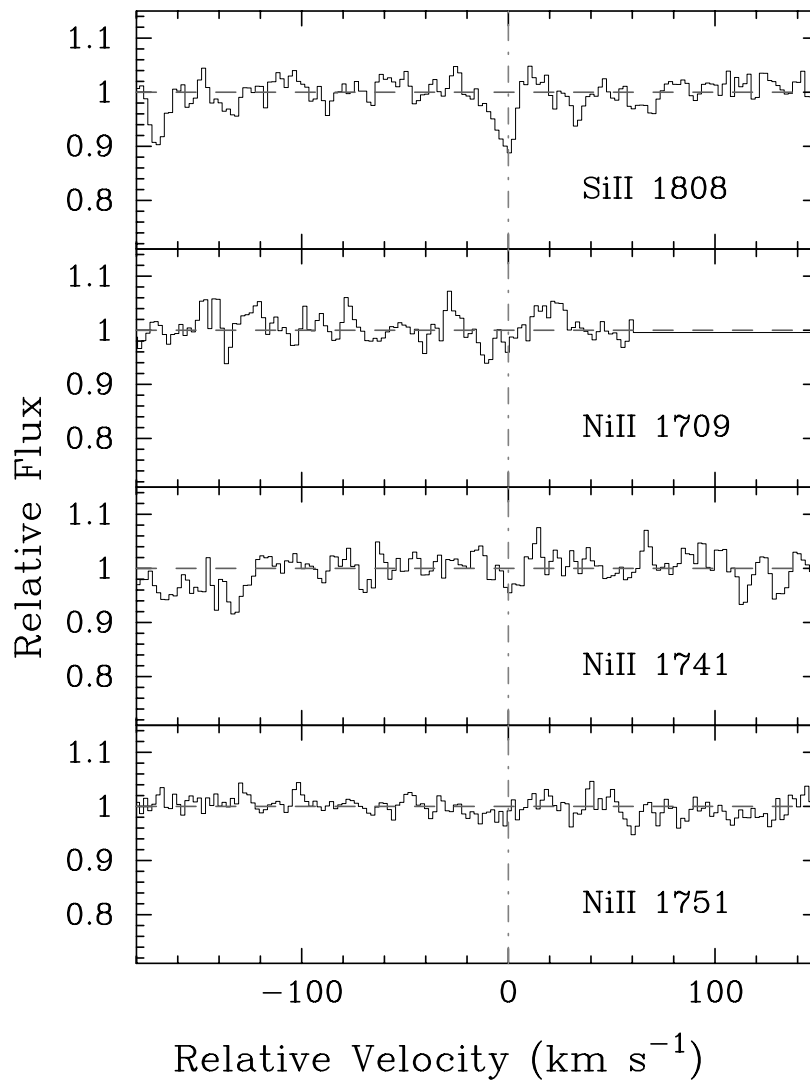


FIG. 37.—Velocity plot of the new metal line transitions for the DLA system at  $z = 2.066$  toward Q2348–14. For comparison, we also plot the Si II  $\lambda 1808$  profile. The vertical line at  $v = 0$  corresponds to  $z = 2.066150$ . [See the electronic edition of the *Journal* for a color version of this figure.]

33). We also include the new values for  $N(\text{Fe}^+)$  as the extensive wavelength coverage provides a comparison between the Fe II  $\lambda\lambda 1611, 2249,$  and  $2260$  transitions. All three values are in good agreement, which indicates that the relative  $f$ -values are reasonably accurate.

### 3.27. Q2231–00, $z = 2.066$

This damped system was analyzed in PW99. At the time we considered possible absorption from the C I  $\lambda 1656$  and C I\*  $\lambda 1657$  transitions but were unconvinced that the profiles were associated with the DLA system. Figure 33

presents the two transitions and the Si II  $\lambda 1808$  profile for comparison, and Table 34 presents the column densities. We are now reasonably confident that these profiles arise in the DLA system and their relative strengths place constraints on the temperature of the cosmic microwave background (CMB) at this redshift (J. X. Prochaska, J. M. O’Meara, & A. M. Wolfe 2001, in preparation).

### 3.28. Q2344+12, $z = 2.538$

This system has been observed previously by Lu, Sargent, & Barlow (1997), and they presented an  $[\text{Fe}/\text{H}]$  metallicity

TABLE 38  
IONIC COLUMN DENSITIES: Q2348–14,  $z = 2.279$

Ion	$\lambda$	AODM	$N_{\text{adopt}}$	$[\text{X}/\text{H}]$
H I .....	1215	$20.560 \pm 0.075$	...	...
Ni II .....	1709	$< 12.752$	$< 12.583$	$< -2.227$
Ni II .....	1741	$< 12.583$	...	...
Ni II .....	1751	$< 12.704$	...	...



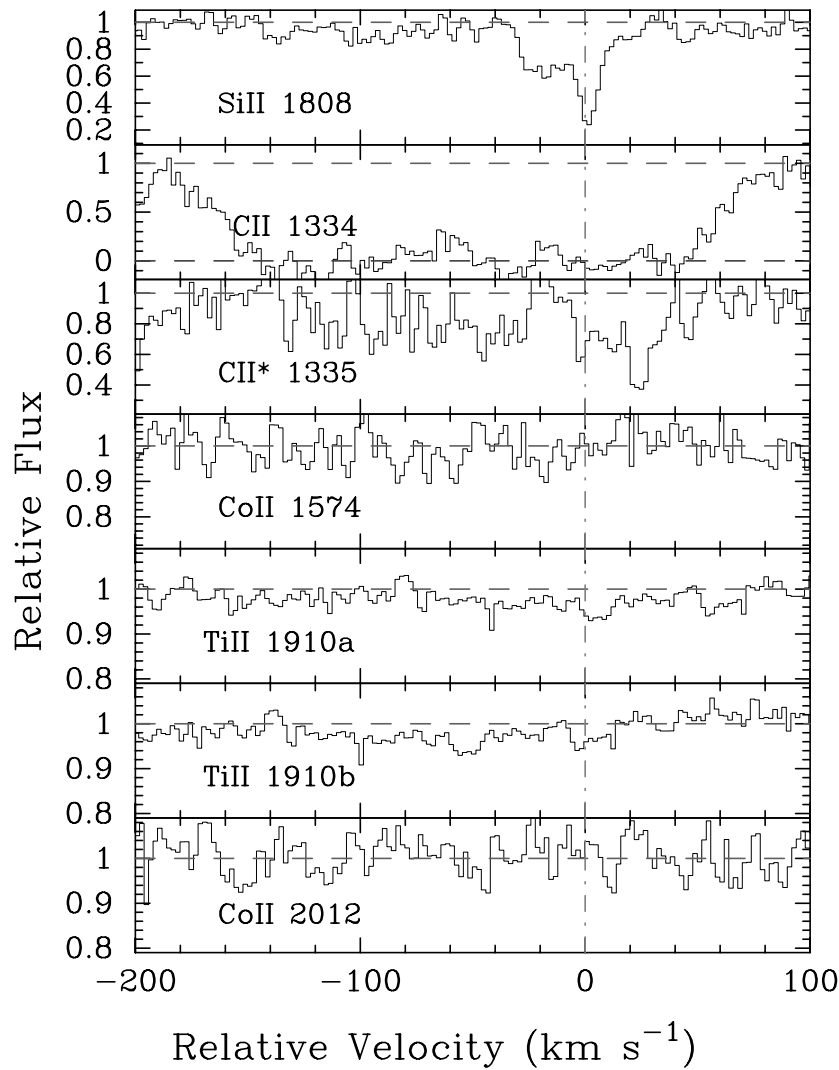


FIG. 38.—Velocity plot of the new metal line transitions for the DLA system at  $z = 2.095$  toward Q2359–02. For comparison, we also plot the Si II  $\lambda 1808$  profile. The vertical line at  $v = 0$  corresponds to  $z = 2.095067$ . [See the electronic edition of the *Journal* for a color version of this figure.]

and an  $N(\text{H I})$  value. We adopt their measurement of the H I column density and have an independent measurement of  $N(\text{Fe}^+)$  from several FUV Fe II transitions. In addition, our blue spectra cover a number of transitions in the Ly $\alpha$  forest (Fig. 34 and Table 35).

### 3.29. Q2348–01, $z = 2.426$ and 2.615

The two damped systems along this sight line were first identified by Turnshek et al. (1989) and are both part of the LBQS statistical sample. This quasar is very faint, and the

S/N of our 4.5 hr spectrum is relatively poor. Figures 35 and 36 and Tables 36 and 37 present the transitions and column densities for the two systems. With respect to the system at  $z = 2.426$ , the Fe II  $\lambda 1608$  profile is blended at  $v > 40$  km  $\text{s}^{-1}$  and we estimate the  $N(\text{Fe}^+)$  value by integrating this profile at  $v < 40$  km  $\text{s}^{-1}$ . Therefore, the value is strictly a lower limit, although the Fe II  $\lambda 1611$  indicates that the column density at  $v > 40$  km  $\text{s}^{-1}$  is less than  $10^{14.46}$   $\text{cm}^{-2}$ . The system at  $z = 2.426$  is special for showing absorption from C I and C I\*. In a companion paper we analyze these

TABLE 39  
IONIC COLUMN DENSITIES: Q2359–02,  $z = 2.095$

Ion	$\lambda$	AODM	$N_{\text{adopt}}$	[X/H]
H I.....	1215	$20.700 \pm 0.100$	...	...
C II.....	1334	$> 15.147$	$> 15.147$	$> -2.103$
C II.....	1335	$13.704 \pm 0.061$	...	...
Ti II.....	1910	$12.330 \pm 0.055$	$12.330 \pm 0.055$	$-1.310 \pm 0.114$
Co II.....	1574	$< 13.398$	$< 12.828$	$< -0.782$
Co II.....	2012	$< 12.828$	...	...

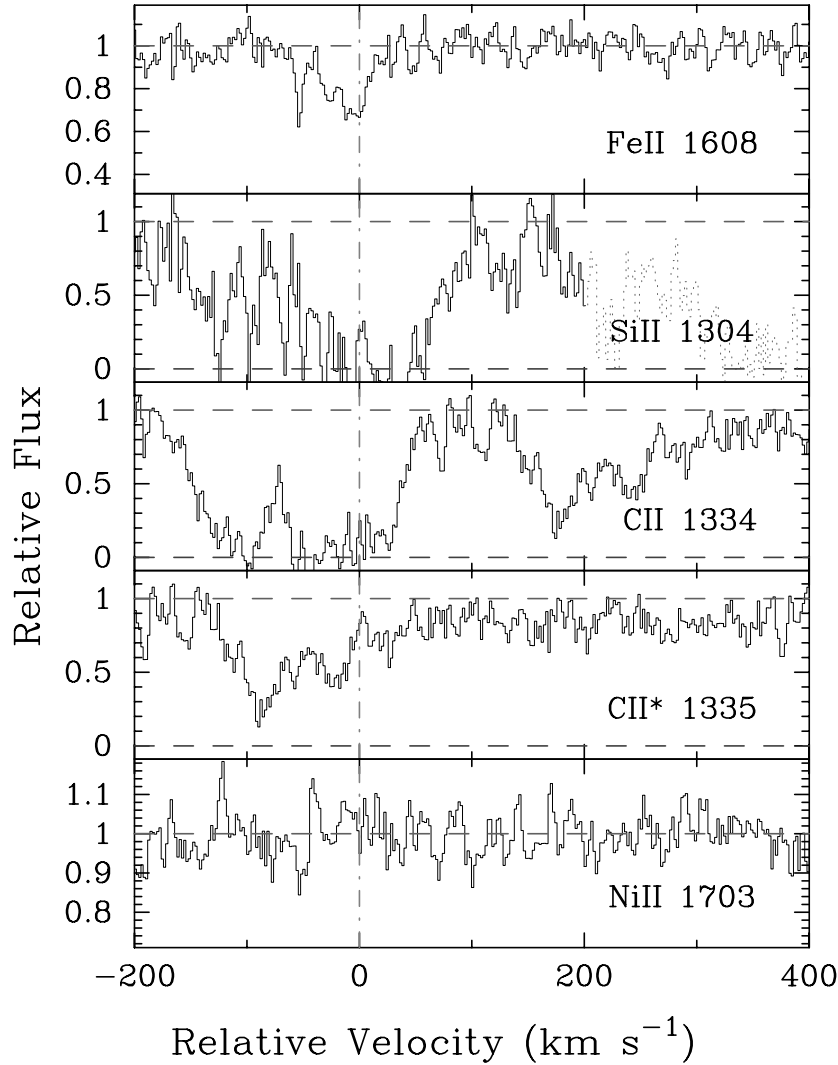


FIG. 39.—Velocity plot of the new metal line transitions for the DLA system at  $z = 2.154$  toward Q2359–02. For comparison, we also plot the Fe II  $\lambda 1608$  profile. The vertical line at  $v = 0$  corresponds to  $z = 2.153934$ . [See the electronic edition of the *Journal* for a color version of this figure.]

transitions to place a limit on the temperature of the CMB radiation at  $z = 2.4$  (J. X. Prochaska, J. M. O’Meara, & A. M. Wolfe 2001, in preparation). The system at  $z = 2.615$  is notable for exhibiting a very low metallicity ( $[\text{Fe}/\text{H}] \sim -2.2$ ,  $[\text{Ni}/\text{H}] \sim -2.5$ ). In fact, this is the only system with  $N(\text{H I}) > 10^{21} \text{ cm}^{-2}$ , which also has a metallicity less than 1/100 solar. For the  $\text{Fe}^+$  column density, we have averaged the lower and upper limits established by Fe II  $\lambda\lambda 1608$  and  $1611$ , respectively.

### 3.30. Q2348–14, $z = 2.279$

The abundances for this damped system were first mea-

sured by Pettini, Lipman, & Hunstead (1995) and subsequently by PW99. We now include a limit on  $N(\text{Ni}^+)$  from the nondetection of two Ni II transitions (Fig. 37 and Table 38).

### 3.31. Q2359–02, $z = 2.095$ and $2.154$

Although these two systems were analyzed in PW99, we have now identified several new profiles including measurements for C II\*  $\lambda 1335$  for the two systems. The C II\* column density for the  $z = 2.154$  is very high and, as we discuss in Wolfe et al. (2001), may indicate a high star formation rate in this DLA system. The C II\* profile is within the Ly $\alpha$  forest, however, and may be significantly blended with an

TABLE 40  
IONIC COLUMN DENSITIES: Q2359–02,  $z = 2.154$

Ion	$\lambda$	AODM	$N_{\text{adopt}}$	[X/H]
H I .....	1215	$20.300 \pm 0.100$	...	...
C II .....	1334	$> 14.991$	$> 14.991$	$> -1.859$
C II .....	1335	$14.475 \pm 0.020$	...	...
Si II .....	1304	$> 15.098$	$14.277 \pm 0.015$	$-1.583 \pm 0.101$
Ni II .....	1703	$< 14.171$	$< 13.208$	$< -1.342$

TABLE 41  
ABUNDANCE SUMMARY

Name	$\tau_{\text{abs}}$	$N(H\text{ I})$	[C/H]	[O/H]	[Al/H]	[Si/H]	[P/H]	[S/H]	[Ar/H]	[Ti/H]	[Cr/H]	[Fe/H]	[Co/H]	[Ni/H]	[Zn/H]
Q0000-2619	3.390	21.41	...	...	...	-1.884	...	...	...	...	...	-2.160	...	-2.295	...
BR 0019-15	3.439	20.92	...	...	...	-1.057	...	...	...	...	...	>	...	-1.487	...
PH 957	2.309	21.40	...	<-0.596	...	>-2.241	...	...	...	<-2.133	...	-1.929	<-1.146	-1.778	-1.623
Q0149+33	2.141	20.50	>-2.406	<-0.428	>-2.017	>-1.488	...	...	...	<-1.271	-1.686	-1.770	...	-1.581	-1.674
Q0201+36	2.463	20.38	...	...	>-0.737	-0.406	...	...	...	<-1.124	-0.802	-0.870	<-0.333	-0.608	-0.286
J0255+00	3.253	20.70	...	...	>-1.311	-0.937	...	...	...	<-0.835	...	-1.436	<-0.352	-1.342	...
J0255+00	3.915	21.30	>-3.118	>-3.003	...	>-2.667	...	-1.779	...	...	...	-2.050	<-0.998	-2.279	...
Q0336-01	3.062	21.20	>-2.792	>-1.130	...	>-1.619	-1.597	-1.406	-1.374	...	...	-1.795	...	-1.981	...
Q0347-38	3.025	20.80	>-2.285	>-1.717	>-1.882	-1.343	...	<-1.240	-1.038	<-2.095	...	-1.767	<-0.514	-1.667	...
Q0458-02	2.040	21.65	...	>-3.110	>-2.377	>-1.167	...	...	...	<-0.982	-1.501	-1.928	<-0.432	-1.719	-1.186
HS 0741+4741	3.017	20.48	>-2.166	>-1.639	-2.146	-1.686	<-1.930	-1.680	-1.834	...	...	-1.403	<-0.107	-1.442	<-1.131
Q0836+11	2.465	20.58	>-2.104	>-1.965	...	-1.153	...	<-1.120	...	<-0.982	<-1.352	-1.403	<-0.870	-1.677	-1.507
Q0841+12	2.375	20.95	...	...	>-2.105	-1.271	...	...	...	...	-1.548	...	<-0.964	-1.675	-1.401
Q0841+12	2.476	20.78	...	...	>-2.054	>-1.845	...	...	...	<-1.562	-1.608	-1.977	<-0.087	-1.873	...
BRI 0951-04	3.857	20.60	...	>-2.674	-1.814	>-1.535	...	...	...	...	...	<-2.591	...	-1.730	...
BRI 0951-04	4.203	20.40	...	...	...	-2.618	...	...	...	...	...	<-2.591	...	-1.730	...
BRI 0952-01	4.024	20.55	>-1.788	...	...	...	...	...	...	...	...	<-2.591	...	-1.730	...
BRI 0952-01	4.024	20.55	>-1.788	...	...	...	...	...	...	...	...	<-2.591	...	-1.730	...
PSS 0957+33	3.279	20.32	...	...	>-1.488	-1.000	...	...	...	...	...	-1.863	<0.290	<-1.361	...
PSS 0957+33	4.178	20.50	...	>-2.026	>-1.734	-1.504	...	...	...	...	...	-1.453	<0.055	-1.252	<-0.863
PSS 0957+33	3.608	20.50	>-2.375	>-2.497	-2.168	-1.798	...	-1.308	...	...	...	-1.871	<0.238	<-1.840	...
BRI 1108-07	1.892	20.60	...	...	>-1.650	-0.875	...	...	...	...	...	-2.116	...	<-1.614	...
Q1210+17	1.999	20.95	>-2.870	>-2.693	>-2.039	-1.480	...	...	...	...	-1.027	-1.149	<-0.782	-1.218	-0.900
Q1215+33	1.892	20.95	>-2.870	>-2.693	>-2.039	-1.480	...	...	...	...	-1.516	-1.702	<-1.000	-1.606	-1.290
Q1223+17	2.466	21.50	>-2.895	>-2.893	...	-1.592	<-1.147	...	...	<-2.188	-1.677	-1.843	<-1.779	-1.801	-1.620
Q1331+17	1.776	21.18	...	...	>-1.927	-1.451	...	...	...	<-2.280	-1.972	-2.058	<-1.780	-1.890	-1.304
BRI 1346-03	3.736	20.72	>-2.784	>-2.571	-2.634	-2.332	...	...	<-2.127	...	...	<-2.094	<-0.370	<-2.210	...
PSS 1443+27	4.224	20.80	>-1.738	>-1.622	>-1.332	>-0.926	...	...	...	...	...	-1.096	<-0.201	-0.959	...
Q1759+75	2.625	20.80	>-2.050	>-1.409	...	-0.824	>-1.283	-0.757	-1.606	...	-1.259	-1.209	<-0.691	-1.248	>-1.782
Q1946+7658	2.844	20.27	...	-2.321	...	-2.228	...	<-1.979	...	...	...	-2.532	...	...	...
Q2206-19	1.920	20.65	...	...	>-1.073	-0.417	...	...	...	...	...	-0.857	<-0.603	-0.671	-0.409
Q2206-19	2.076	20.43	>-2.774	>-2.761	-2.763	-2.309	...	...	...	-0.825	-0.685	-2.606	...	<-2.096	<-1.902
Q2230+02	1.864	20.85	...	...	...	-0.754	...	...	...	-1.175	-1.117	-1.166	<-0.642	-0.972	-0.720
Q2234+12	2.066	20.56	...	>-1.877	...	-0.873	...	...	...	-1.022	-1.065	-1.402	<-0.654	-1.206	-0.882
Q2344+12	2.538	20.36	>-2.265	>-2.199	...	-1.741	<-1.146	<-1.359	-1.618	...	...	-1.830	...	<-1.796	...
Q2348-01	2.426	20.50	...	...	>-1.051	-0.695	...	...	...	...	<-1.457	-1.386	...	-1.400	...
Q2348-01	2.615	21.30	...	...	>-2.651	-1.968	...	...	...	...	-2.296	-2.227	...	-2.357	<-2.099
Q2348-14	2.279	20.56	>-2.459	>-2.581	-2.393	-1.917	...	-2.035	...	...	...	-2.238	...	<-2.227	...
Q2359-02	2.095	20.70	>-2.103	...	>-1.476	-0.777	...	...	...	-1.310	-1.550	-1.655	<-0.782	-1.526	-0.775
Q2359-02	2.154	20.30	>-1.859	...	-1.625	-1.583	...	...	...	...	-1.368	-1.877	...	<-1.342	<-1.069

TABLE 42

## RELATIVE ABUNDANCE SUMMARY

Name	$z_{\text{abs}}$	$N(\text{H I})$	[C/Fe]	[O/Fe]	[Al/Fe]	[Si/Fe]	[P/Fe]	[S/Fe]	[Ar/Fe]	[Ti/Fe]	[Cr/Fe]	[Co/Fe]	[Ni/Fe]	[Zn/Fe]
Q0000 - 2619 <sup>a</sup>	3.390	21.41	...	...	...	0.411	...	...	...	...	...	...	...	...
BR 0019 - 15 <sup>a</sup>	3.439	20.92	...	...	...	0.430	...	...	...	...	...	...	...	...
PH 957	2.309	21.40	...	<1.333	...	> -0.312	...	...	...	<-0.204	0.243	<0.783	0.151	0.306
Q0149 + 33	2.141	20.50	> -0.636	<2.198	> -0.247	0.282	...	...	...	<-0.499	0.320	...	0.189	0.096
Q0201 + 36	2.463	20.38	...	...	>0.133	0.464	...	...	...	<-0.254	0.068	<0.537	0.262	0.584
J0255 + 00	3.253	20.70	...	...	>0.125	0.499	...	...	...	<-0.601	...	<1.084	0.094	...
J0255 + 00	3.915	21.30	> -1.068	> -0.953	...	> -0.617	...	0.271	...	...	...	<1.052	-0.229	...
Q0336 - 01	3.062	21.20	> -0.997	>0.665	...	>0.176	0.198	0.389	0.421	...	...	...	-0.186	...
Q0347 - 38	3.025	20.80	> -0.488	>0.080	> -0.085	0.454	...	<0.557	0.759	...	...	<1.283	0.130	...
Q0458 - 02	2.040	21.65	...	> -1.343	> -0.610	>0.600	...	...	...	<-0.328	0.266	<0.300	0.048	0.581
HS 0741 + 4741	3.017	20.48	> -0.238	>0.289	> -0.218	0.242	< -0.002	0.248	0.094	...	...	<1.496	-0.044	...
Q0836 + 11	2.465	20.58	> -0.701	> -0.562	...	0.250	...	<0.283	...	<-0.421	<0.051	<1.296	-0.039	<0.272
Q0841 + 12 <sup>a</sup>	2.375	20.95	...	...	> -0.428	0.406	...	...	...	...	0.129	<0.807	...	0.170
Q0841 + 12	2.476	20.78	...	...	> -0.304	> -0.095	...	...	...	<-0.188	0.142	<0.786	0.075	0.349
BRI 0951 - 04	3.857	20.60	...	...	0.183	>0.462	...	...	...	...	...	<2.084	<0.124	...
BRI 0951 - 04	4.203	20.40	...	...	...	...	...	...	...	...	...	...	...	...
BRI 0952 - 01	4.024	20.55	>0.075	...	...	...	...	...	...	...	...	...	...	...
BRI 0952 - 01	4.203	20.40	...	...	...	...	...	...	...	...	...	...	...	...
BRI 0952 - 01	4.024	20.55	>0.075	...	...	...	...	...	...	...	...	...	...	...
PSS 0957 + 33	3.279	20.32	...	...	> -0.035	0.453	...	...	...	...	...	<2.153	<0.502	...
PSS 0957 + 33	4.178	20.50	...	> -0.155	>0.137	0.367	...	0.563	...	...	...	<1.508	0.201	<0.590
PSS 0957 + 33	3.608	20.50	> -0.259	> -0.381	> -0.052	0.318	...	...	...	...	...	<2.109	<0.031	...
BRI 1108 - 07	1.892	20.60	...	...	> -0.501	0.274	...	...	...	...	...	...	<0.502	...
Q1210 + 17	1.999	20.95	> -1.168	> -0.991	> -0.337	0.222	...	...	...	...	0.122	<0.367	-0.069	0.249
Q1215 + 33	2.466	21.50	> -1.052	> -1.050	...	0.251	<0.696	...	...	<-0.345	0.186	<0.702	0.096	0.412
Q1223 + 17	1.776	21.18	...	...	>0.131	0.607	...	...	...	<-0.222	0.166	<0.064	0.042	0.223
Q1331 + 17	3.736	20.72	> -0.150	>0.063	...	0.302	...	...	<0.507	...	...	<2.264	0.168	0.754
BRI 1346 - 03 <sup>b</sup>	4.224	20.80	> -0.642	> -0.526	> -0.236	0.170	...	...	...	...	...	<0.895	<0.424	...
PSS 1443 + 27	2.625	20.80	> -0.841	> -0.200	...	0.385	> -0.074	0.452	< -0.397	...	...	<0.518	0.137	...
Q1759 + 75	2.844	20.27	...	0.211	...	0.304	...	<0.553	...	...	<-0.050	<0.518	-0.039	> -0.573
Q1946 + 7658	1.920	20.65	...	...	...	0.440	...	...	...	...	...	...	...	...
Q2206 - 19	2.076	20.43	> -0.168	> -0.155	> -0.216	0.440	...	...	...	0.032	0.172	0.254	0.186	0.448
Q2206 - 19	1.864	20.85	...	...	> -0.157	0.297	...	...	...	...	<0.416	...	<0.510	<0.704
Q2230 + 02	2.066	20.56	...	...	...	0.412	...	...	...	<-0.009	0.049	<0.524	0.194	0.446
Q2231 - 002	2.538	20.36	> -0.435	> -0.369	...	0.529	...	...	...	0.380	0.337	<0.748	0.196	0.520
Q2344 + 12	2.426	20.50	...	...	...	0.089	<0.684	<0.471	...	...	...	...	<0.034	...
Q2348 - 01	2.615	21.30	...	...	>0.335	0.691	...	...	...	...	<-0.071	...	-0.014	<0.258
Q2348 - 01 <sup>a</sup>	2.615	21.30	...	...	> -0.294	0.389	...	...	...	...	0.061	...	...	...
Q2348 - 14	2.279	20.56	> -0.221	> -0.343	> -0.155	0.321	...	0.203	...	...	...	...	<0.011	...
Q2359 - 02	2.095	20.70	> -0.448	...	>0.179	0.878	...	...	...	0.345	0.105	<0.873	0.129	0.880
Q2359 - 02	2.154	20.30	>0.018	...	0.252	0.294	...	...	...	...	0.509	...	<0.535	<0.808

<sup>a</sup> Ni is serving as a proxy for Fe.<sup>b</sup> Al is serving as a proxy for Fe.

$\text{Ly}\alpha$  forest cloud. We also report a tentative measurement of  $\text{Ti II } \lambda 1910$  for the system at  $z = 2.095$ . Given the very large  $\text{Zn/Fe}$  ratio for this system, the enhanced  $\text{Ti/Fe}$  ratio is strongly suggestive of Type II SN enrichment. Figures 38 and 39 present all of the new transitions, and Tables 39 and 40 list the column densities.

#### 4. SUMMARY

Tables 41 and 42 present a summary of the absolute and relative abundances of the 38 DLA systems in our complete database. Regarding Table 42, where we present abundances relative to Fe, in a few cases we have considered Ni, Cr, or Al as a proxy for Fe, as noted.

We have presented ionic column density measurements for our complete sample of DLA systems. With the exception of a few important transitions that exhibit blends with other profiles, we have measured each column density with the apparent optical depth method. In general, therefore, all

of the data have been reduced and analyzed with an identical approach. We have used the most up-to-date atomic data and will continue to update the database as new information becomes available. Visit the Web site mentioned in footnote 6 for tables, figures, and updated measurements. A series of companion papers (in particular, Paper II) present new scientific results based on this database.

We thank T. Barlow for providing the HIRES reduction package. We also thank Jim Lawler and Chris Howk for helpful discussions. We acknowledge the Keck support staff for their efforts in performing these observations. We thank R. Carswell and J. Webb for providing the VPFIT software package. J. X. P. acknowledges support from a Carnegie postdoctoral fellowship. A. M. W. was partially supported by NASA grant NAGW-2119 and NSF grant AST 86-9420443.

#### REFERENCES

- Bergeson, S. D., & Lawler, J. E. 1993a, *ApJ*, 408, 382  
 ———, 1993b, *ApJ*, 414, L137  
 Bergeson, S. D., Mullman, K. L., & Lawler, J. E. 1994, *ApJ*, 435, L157  
 Bergeson, S. D., Mullman, K. L., Wickliffe, M. W., Lawler, J. E., Litzen, U., & Johansson, S. 1996, *ApJ*, 464, 1044  
 Djorgovski, S. G., Gal, R. R., Odewahn, S. C., de Carvalho, R. R., Brunner, R., Longo, G., & Scaramella, R. 1998, in *Wide Field Surveys in Cosmology*, ed. S. Colombi & Y. Mellier, (Paris: Editions Frontieres), 89  
 Edmunds, M. G., & Phillips, S. 1997, *MNRAS*, 292, 733  
 Ellison, S. L., Ryan, S., & Prochaska, J. X. 2001, *MNRAS*, in press  
 Fan, X., et al. 1999, *AJ*, 118, 1 (SDSS Collaboration)  
 Fedchak, J. A., & Lawler, J. E. 1999, *ApJ*, 523, 734  
 Fedchak, J. A., Wiese, L. M., & Lawler, J. E. 2000, *ApJ*, 538, 773  
 Grevesse, N., Noels, A., & Sauval, A. J. 1996, in *Cosmic Abundances*, ed. S. Holt & G. Sonneborn (San Francisco: BookCrafters), 117  
 Hagen, H. J., Engels, D., & Reimers, D. 1999, *A&AS*, 134, 483  
 Howk, J. C., Savage, B. D., & Fabian, D. 1999, *ApJ*, 525, 253  
 Howk, J. C., Sembach, K. R., Roth, K. C., & Kruk, J. W. 2000, *ApJ*, 544, 867  
 Kirkman, D., & Tytler, D. 1997, *ApJ*, 484, 672  
 Lanzetta, K. M., Wolfe, A. M., & Turnshek, D. A. 1995, *ApJ*, 440, 435  
 Lu, L., Sargent, W. L. W., & Barlow, T. A. 1999, in *ASP Conf. Ser. 156, Highly Redshifted Radio Lines*, ed. C. Carilli, S. Radford, K. Menten, & G. Langston (San Francisco: ASP), 132  
 Lu, L., Sargent, W. L. W., Barlow, T. A., Churchill, C. W., & Vogt, S. 1996, *ApJS*, 107, 475 (L96)  
 Molaro, P., Bonifacio, P., Centurión, M., D'Odorico, S., Vladilo, G., Santin, P., & Di Marcantonio, P. 2000, *ApJ*, 541, 54  
 Molaro, P., Levshakov, S. A., D'Odorico, S., Bonifacio, P., & Centurion, M. 2001, *ApJ*, 549, 90  
 Morton, D. C. 1991, *ApJS*, 77, 119  
 Mullman, K. L., Lawler, J. E., Zsargo, J., & Federman, S. R. 1998, *ApJ*, 500, 1064  
 Outram, P. J., Chaffee, F. H., & Carswell, R. F. 1999, *MNRAS*, 310, 289  
 Pettini, M., Ellison, S. L., Steidel, C. C., Shapley, A. E., & Bowen, D. V. 2000, *ApJ*, 532, 65  
 Pettini, M., Lipman, K., & Hunstead, R. W. 1995, *ApJ*, 451, 100  
 Pettini, M., Smith, L. J., Hunstead, R. W., & King, D. L. 1994, *ApJ*, 426, 79  
 Pettini, M., Smith, L. J., King, D. L., & Hunstead, R. W. 1997, *ApJ*, 486, 665  
 Prochaska, J. X., Gawiser, E., & Wolfe, A. M. 2001, *ApJ*, 552, 99 (PGW01)  
 Prochaska, J. X., & Wolfe, A. M. 1996, *ApJ*, 470, 403  
 ———, 1997, *ApJ*, 474, 140  
 ———, 1999, *ApJS*, 121, 369 (PW99)  
 ———, 2000, *ApJ*, 533, L5  
 ———, 2001, *ApJ*, submitted (Paper II)  
 Raassen, A. J. J., & Uylings, P. H. M. 1998, *A&A*, 340, 300  
 Savage, B. D., & Sembach, K. R. 1991, *ApJ*, 379, 245  
 Schectman, R. M., Povolny, H. S., & Curtis, L. J. 1998, *ApJ*, 504, 921  
 Storrie-Lombardi, L. J., Irwin, M. J., & McMahon, R. G. 1996, *MNRAS*, 282, 1330  
 Storrie-Lombardi, L. J., & Wolfe, A. M. 2000, *ApJ*, 543, 552  
 Tripp, T. M., Lu, L., & Savage, B. D. 1996, *ApJS*, 102, 239  
 Turnshek, D. A., Wolfe, A. M., Lanzetta, K. M., Briggs, F. H., Cohen, R. D., Foltz, C. B., Smith, H. E., & Wilkes, B. J. 1989, *ApJ*, 344, 567  
 Verner, D. A. 1996, *At. Data Nucl. Data Tables*, 64, 1  
 Verner, D. A., Barthel, P. D., & Tytler, D. 1994, *A&AS*, 108, 287  
 Vogt, S. S., et al. 1994, *Proc. SPIE*, 2198, 362  
 Wiese, L. M., Fedchak, J. A., & Lawler, J. E. 2001, *ApJ*, 547, 1178  
 Wolfe, A. M., Fan, X.-M., Tytler, D., Vogt, S. S., Keane, M. J., & Lanzetta, K. M. 1994, *ApJ*, 435, L101  
 Wolfe, A. M., Lanzetta, K. M., Foltz, C. B., & Chaffee, F. H. 1995, *ApJ*, 454, 698  
 Wolfe, A. M., & Prochaska, J. X. 2000, *ApJ*, 545, 591  
 Wolfe, A. M., Prochaska, J. X., & Gawiser, E. 2001, *ApJ*, submitted  
 Wolfe, A. M., Turnshek, D. A., Smith, H. E., & Cohen, R. D. 1986, *ApJS*, 61, 249